9-7-2012

The Photooxidation of Domoic Acid

Punam K. Parekh
Florida International University, punam15parekh@gmail.com

FLORIDA INTERNATIONAL UNIVERSITY

Miami, Florida

THE PHOTOOXIDATION OF DOMOIC ACID

A thesis submitted in partial fulfillment of

the requirements for the degree of

MASTER OF SCIENCE

in

CHEMISTRY

by

Punam Parekh

2012

To: Dean Kenneth G. Furton
College of Arts and Sciences

This thesis, written by Punam Parekh, and entitled Photooxidation of Domoic Acid, having been approved in respect to style and intellectual content, is referred to you for judgment.

We have read this thesis and recommend that it be approved.

_____
Kathleen Rein

_____
John Landrum

_____
Kevin O'Shea, Major Professor

Date of Defense: July 23, 2012

The thesis of Punam Parekh is approved.

_____
Dean Kenneth G. Furton
College of Arts and Sciences

_____
Dean Lakshmi N. Reddi
University Graduate School

Florida International University, 2012

DEDICATION

I would like to dedicate this work to Shri Ramchandra Bhagavan. Thank you for everything. I love you. Hridaye basahu sur bhoop.

ACKNOWLEDGMENTS

I would like to thank Dr. O'Shea for providing the necessary resources for my research. His encouragement, compassion and suggestions were valuable in accomplishing my goals. I am thankful to my committee members, Drs. Rein and Landrum, for their guidance in helping me develop proper background knowledge. I am also grateful to YaLi for his NMR training and advice. Additionally I am thankful to my lab members for offering me their knowledge and experience. Furthermore I am appreciative of the FIU chemistry department for providing me with the necessary financial aid for completion of my project and a chance to experience teaching chemistry. I would also like to extend a thank you to my family and friends for their love and support.

ABSTRACT OF THE THESIS

THE PHOTOOXIDATION OF DOMOIC ACID

by

Punam Parekh

Florida International University, 2012

Miami, Florida

Professor Kevin O'Shea, Major Professor

Domoic acid (DA) is a naturally occurring cyanotoxin, which upon ingestion, is responsible for amnesic shellfish poisoning (ASP) in both humans and animals. Produced by the marine diatom, *Pseudonitzschia*, DA is accumulated by a number of marine organisms including shellfish, clams and mussels which upon consumption can lead to headaches, nausea and seizures. Possessing a variety of functional groups the structure of DA contains three carboxyl groups, a pyrrole ring and a potent conjugated diene region allowing for binding to glutamate receptors in the dorsal hippocampus of the brain causing the described detrimental effects. Although limitations have been placed regarding the amount of DA that may be contained in seafood no limitations have been placed on the amount present in drinking water. Natural degradation of the toxin may occur through reactive oxygen species such as the hydroxyl radical and singlet oxygen at the conjugated diene region. In this work the photooxidation of DA via singlet oxygen has been studied using sorbic acid as a model compound. The three major reaction pathways observed during the photooxdiation process for both acids include 2 + 4 cycloaddition to produce endoperoxides , 2 + 2 reaction to afford aldehydes and ketones or an ene reaction to generate hydroperoxides.

Under similar reaction conditions for SA and DA, the endoperoxide has been seen to be the major product for photoxidation of SA while the hydroperoxide has been seen to be the dominant product during photooxidation of DA.

TABLE OF CONTENTS

LIST OF TABLES

TABLE PAGE

LIST OF FIGURES

LIST OF ABBREVIATIONS AND ACRONYMS

ASP: Amnesic Shellfish Poisoning

ATP: Adenosine Triphosphate

COSY: Correlation Spectroscopy

DA: Domoic Acid

D_2O: Deuterium Oxide

GA: Glutamic Acid

HABS: Harmful Algal Blooms

HPLC: High Performance Liquid Chromatography

Hz: Hertz

J: Coupling Constant in Hz (NMR)

KA: Kainic Acid

LC: Liquid Chromatography

MHz: Megahertz

mL: Milliliter

MS: Mass Spectroscopy

nm: Nanometers

NMR: Nuclear Magnetic Resonance

ppm: Parts per Million

PSP: Paralytic Shellfish Poisoning

RB: Rose Bengal

ROS: Reactive Oxygen Species

SA: Sorbic Acid

UV: Ultraviolet

Chapter 1

General Introduction

1.1 Causes of Harmful Algal Blooms

When an abundance of algal growth occurs, in marine environments as a consequence favorable environmental conditions, the event is known as a harmful algal bloom (HAB) (Buralge, 2011). A number of causes of blooms are known. One such cause is a spike in nutrients which can trigger increased unisexual algal reproduction (Kalluri, 2007). The nutrients phosphorus and nitrogen have been shown to be key promoters of algal growth (Conley et al., 2009). Certain physical forces including wind, storms, tides and currents also influence HABs through leaching of terrestrial nutrients into coastal environments (Sims, 2009). Temperature also plays a major role in contributing to HABs as elevations in temperature, as a result of global warming, have led to favorable conditions such as longer seasons of warm temperatures with less ice, increased evaporation rates and droughts thereby increasing algal productivity (Paerl et al., 2010). Another known factor contributing to HABs is salinity fluctuations (Pande, 2008). Research has revealed that low salinity offer optimal environments for algal growth (Round, 1984).

Generally a beneficial occurrence, HABs provide a means of survival and livelihood of marine life, however, they have also been known to produce detrimental effects (Soumya et al., 2012). Such negative consequences of blooms include toxicity, clogging of fish gills, a reduction in water quality, and oxygen depletion (Graneli et al., 2007). Most HABs involve dinoflagalettes or cyanobacteria but other classes of algae also exhibit blooms such as diatoms (Glibert et al., 2005).

1.2 Diatoms

Diatoms, a group of eukaryotic algae (Hedges e. al., 2009), which produce carbohydrates, are a key source of food for zooplankton in the marine food chain (Seckbach et al., 2011). These algae are also responsible for recycling organic matter and nutrients in marine environments (Allen, 1934; Allen, 1936). Although they are believed to have appeared during the Creatceous period, they have been studied for about 200 years and are most notable for their use as environmental indicators (Smol et al., 2010; Cholnoky, 1968; Lowe, 1974). Although all members of the radiation are characterized by a siliceous cell wall known as the frustule, different species are characterized by different morphologies and occupy several aquatic habitats (Smol et al., 2010). Diatoms are found to have a global distribution (Gregory, 1892). Classification of diatoms is primarily determined by pore structure and the positioning of organelles into the cell wall (Round et al., 1990). The order consists of three famalies, the Coscindiscophyceae (centric diatoms), Fragilcriophyceae (araphid diatoms), and Bacillariophyceae (raphid pennate diatoms). Bacillariophyceae diatoms are those that contain a raphe, a slit opening in the cell wall used in locomotion (Hedges et al., 2009). The centric diatoms contain round valves and have ribs which radiate out from a central ring known as the annulus (Round et al., 1990). In regards to the simple pennate or araphid diatoms, the ribs extend out from both sides of a sternum whereas in the raphid diatoms the ribs again extend out from the sternum but the sternum contains one or two raphe slits (Round et al., 1990). Some examples of the genera of centric diatoms include *Thalassiosira, Stephanodiscus, Skeletonema* and *Cyclotella* (Stoermer, 2003). Examples of araphid diatoms include *Centronella, Fragilaria, Diatoma* and *Synedra* whereas examples of raphid diatoms

include *Achnatnthes, Karayevia, Planothidium*, *Rossithidium and Pseudonitzschia* (John et al., 2002; Falkowski, 2007).

1.2.1 Diatom Blooms

There are at least eight different known methods in which harmful phytoplankton can cause fatality (Smayda, 1997). The eight methods can be divided into two groups including non-chemical effects that cause physical damage and chemical effects which lead to metabolite production and physical-chemical reactions (Smayda, 1997). Phytoplankton use such methods during blooms for nutrient acquisition. The most common type of blooms include HABs or harmful algal blooms. In these types of blooms, algal toxins produced by algae accumulate in both predators and prey thereby moving the effects up the food web (Backer et al., 2006). Although these blooms occur quite frequently, they are not the only type of blooms present in marine environments. Diatoms are commonly known to produce harmful effects by an allelopathic method in which specific areas of the human body are targeted by toxins and may be impaired, stunned, repelled or experience avoidance reactions including death (Smayda, 1997). When certain macronutrients, such as nitrate (NO_3^-), phosphate (HPO_4^{2-}) and silicic acid (H_4SiO_4), occur in abundance, rapid growth of diatoms ensues (Bruland et al., 2001). In general it is seen that spring diatom blooms are more extensive than autumn blooms; pennate diatoms dominant during the spring blooms and the centric diatoms dominant during the autumn blooms (Chandler, 1940).

1.3 *Pseudonitzschia*

Most diatoms are considered to be harmless however some are known to cause harm via oxygen depletion, physical injuries and phycotoxin production (Graneli et al.,

2006). Diatoms known to cause such harmful effects are members of the genus *Pseudonitzschia* which are able to produce the neurotoxin, domoic acid (DA); responsible for causing amnesic shellfish poisioning (ASP) in humans (Sun et al., 2011). There are a total of 27 species that comprise the genus with members producing chains of various sizes by linking their cells end to end (Hasle et al., 1997; Lundholm et al., 2002; Lundholm et al., 2003; Prisholm et al., 2002). Currently ~12 species of the genus *Pseudonitzschia* are known to produce DA (Graneli et al., 2007) with some of these members being *Pseudonitzschia australis, P. cuspidate, P. galaxiae, P. pungens and P. fradulenta* to name a few (Thessen et al., 2008). Most of these species have been found to be coastal although some have been found to lie as far as 150 km offshore (Graneli et al., 2007). Typical characteristics of species from this genus include elongated cells with a rectangular shape and arrangement of cells in a stepped chain fashion (Tomas, 1997). Energy needs of the organism are met through ATP production via photosynthesis, as the species contain chloroplasts. *Pseudonitzschia* has a global distribution including the coasts of California, Japan and New Zealand (Horner et al., 1996); Kotaki et al., 1996; Rhodes et al., 1996) as well as along the coasts of Denmark, Portugal, Italy, Spain and other European countries (Miguez et al., 1996; Vale et al., 1998; Bates et al., 1998). Although the genus seems to be ubiquitous there seems to be only limited knowledge regarding species identification. Proper identification of species requires a great amount of time as well as the need to discern morphological differences which can only be accomplished via scanning or transmission electron mircroscopy (Egmond et al, 2004). In regards to reproduction of the genus, species undergo sexual reproduction during events known as blooms.

1.3.1 *Pseudonitzschia* Blooms

From the needle shaped genus *Pseudonitzschia* some species are capable of contributing significantly to both open-ocean and coastal blooms (Schmidt, 2011). Prediction of the timing of *Pseudonitzschia* blooms is difficult. However, a positive correlation has been established between blooms and an escalated amount of certain nutrients including Fe (III), PO_4^{3-} and NO_3^- (Fisher et al., 2006). Heavy rains, winds, and high turnovers of the water column facilitate bloom events as they provide a means of the species of *Pseudonitzschia* to gather necessary nutrients (Thessen, 2007; Puschner et al., 2002). During blooms some species of the genus are able to produce the neurotoxin, domoic acid which has proven to be detrimental to many living beings including humans.

Although the exact reason for the production of DA is unresolved, one theory is DA complexes iron to enhance nutrition as well as copper to remove toxic trace metals (Bruland et al., 2001).

1.3.2 Monitoring Blooms

Many techniques have been utilized and many more have been proposed in monitoring harmful algal blooms. This is a result of the fact that occurrence of algal blooms is dependent on a variety of factors including nutrient concentrations and temperature (Wong et al., 2009). Nutrient concentrations have increased in recent decades as a consequence of several factors including urban runoff, wastewater treatment plants, agriculture and fossil fuel use (CENR, 2000; NRC, 2000). Increases in nutrient levels lead to a decline in water quality as well as a decrease in the size of wildlife populations (Summer et al., 2005). Online monitoring can be used for nutrient

monitoring, for example nitrate concentrations in wastewater are measured via the sequential fiber optic spectrometer (Summer et al., 2005).

Created by the U.S. Global Ocean Observing System (GOOS) Program a method for forecasting algal blooms has been developed (Fisher et al., 2002). The subdivision of the program referred to as the Harmful Algal Blooms Observing System (HABSOS) has been specifically designed to observe bloom events in the Gulf of Mexico (Pennock et al., 2004). Initially focusing on *Karenia brevis* (red tide) the project is expected to be expanded to study other bloom events (Melzian et al., 2002). Data on the evolution and location of *K. brevis* blooms were used to forecast future blooms by using satellite imagery capable of detecting the increased concentrations of chlorophyll a present during blooming events (Melzian et al., 2002). To date researchers found that there is no way to determine a *K. brevis* bloom 2-3 days before hand since the regional environmental data needed to predict a bloom were not available (Pennock et al., 2004). Scientists have also concluded that the satellite coverage system known as SeaWIFS cannot alone be used to monitor red tide blooms but instead depends on the use of many methods including knowledge of wind vectors and currents as well as SeaWIFS (Pennock et al., 2004).

Harmful algal blooms are a worldwide problem affecting many nations. Countries of the European Union have joined to form EUROHAB (European initiative on Harmful Algal Blooms) which has engaged in the funding of research conducted on harmful algal blooms (Anderson, 2005). The main goal of EUROHAB includes the changes in environmental conditions in European coastal ecosystems due to human related activities (Graneli et al., 2000). The creation of EUROHAB and ECOHAB

(Ecology and Oceanography of Harmful Algal Blooms), a similar organization in the US, has led to the birth of multilateral monitoring agencies created to incorporate international collaboration (Anderson, 2005). These include GEOHAB (Global Ecology and Oceanography of Harmful Algal Blooms) and SCOR (Scientific Committee on Oceanic Research) (Anderson, 2005).

1.4 Domoic Acid

Significant effort and resources have been dedicated to monitoring HABs, but detection of the cyanotoxins is critical to environmental health. Domoic Acid (DA) (3-carboxymethyl-4-(2-carboxy-1-methylhexa-1,3-dienyl) proline) [$C_{15}H_{21}NO_6$] with molecular weight 311 (Nemoto et al., 2007) and (Bell, 2003), is a harmful algal toxin produced by the species in the marine diatom, *Pseudonitzschia*. The toxin is produced during harmful algal blooms and has led to numerous intoxications of both animals and humans. Domoic acid belongs to a group of neurologically active amino acids known as the kainoids, for which kainic acid is the parent (Lefebvre et al., 2002). The toxicity of domoic acid and kainic acid results from their common structural features and their affinity for glutamate receptors as illustrated in Figure 1. (Lefebvre et al., 2002). Domoic acid and kainic acid however, are potent agonists of glutamate receptors in the dorsal hippocampus of the brain (Scholin et al., 2000). Acting as an agonist, domoic acid binds to specific glutamate receptors mimicking the typical action of glutamic acid. The dorsal hippocampus contains neurons that are responsible for the encoding of past experiences (Work et al., 1993). When domoic acid binds to glutamate receptors, excitatory responses throughout the central nervous system are initiated. Hippocampal neurodegeneration results from binding to 2-amino-3-hydroxy-5-methyl-4-

isoxazolepropionate (AMPA)– type (AMPARs) and kainate (KA)-type GluRs (KARs) (Fritz et al., 1992).

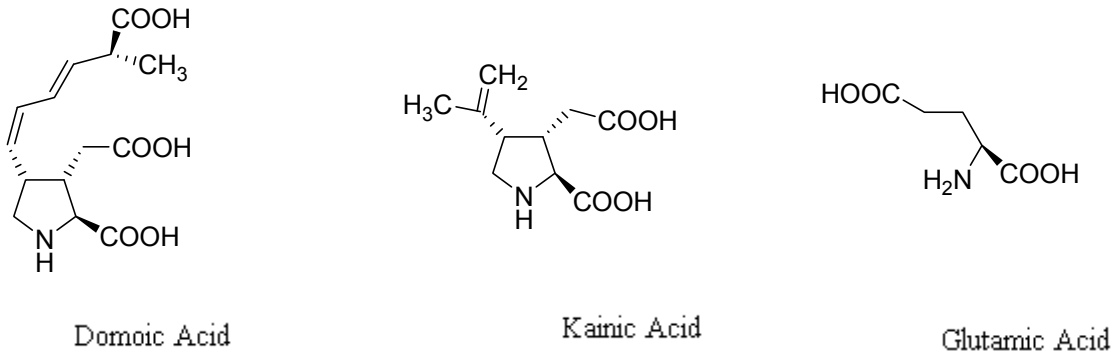

Figure 1: Structures of Domoic Acid (DA), Kainic Acid (KA) and Glutamic Acid

The structure of domoic acid contains four chiral centers and three carboxyl groups as well as an electron rich conjugated diene region believed to be the center of most reactions. At least nine geometrical isomers of domoic acid exist which can be created through irradiation of domoic acid via UV light (He et al., 2010). These isomers are shown in Figure 2.

1.4.1 Photoisomerization of Domoic Acid

Isomerization of domoic acid can occur either thermally or photochemically (Wilson et al., 2000). Because there are four chiral centers in DA there are a total of 16 stereoisomers each with four geometric isomers resulting in a total of 64 isomers. Currently there are at least nine known isomers of domoic acid with six of the isomers being constitutional isomers (Zhao et al., 1997). These isomers are isolated from mussel tissue and separated via the employment of SAX-SPE for LC analysis followed by the use of the basic background electrolyte (BGE), ß- cyclodextrin for increased efficiency

(Zhao et al., 1997). Domoic acid can photoisomerize to isodomoic acids D, E and F, with a greater production of acids D and E over F, under stimulated sunlight (Bouillon et al., 2008). These three acids can interconvert by cis-trans isomerization of the conjugated diene (Wright et al., 1990). Studies have shown that photoisomerization requires UV light with wavelength in the range of 280-400 nm and can occur in natural waters (Bouillon et al., 2006). Exposure of domoic acid to UV light (250 nm) for 9-12 minutes leads to the production of three geometric isomers (Clayden et al., 2005). On the basis of the findings of Zhao, DA is also seen to epimerize through deprotonation and reprotonation at reverse ends of a planar intermediate (Zhao et al., 1997; Soderberg, 2012). The resulting intermediate is an enolate anion which is stabilized by resonance (Soderberg, 2012).

The three isomers produced under UV irradiation exhibit toxic effects similar but less potent to domoic acid (Wright, 1995). The differences in toxicity of DA and its isomers lies in the configuration of the double bond in the hexadienyl side chain extending from the ring structure (Sawant et al., 2010). The Z configuration on the first double bond of DA allows for an increased binding strength and biological activity of the toxin to kainic acid receptors, characteristic of the binding site (Hampson et al., 1992).

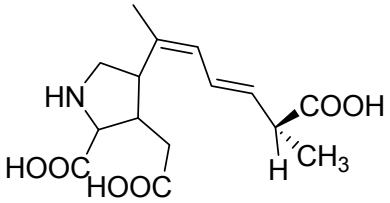

Domoic Acid

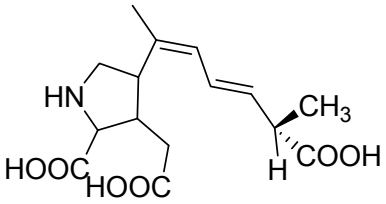

5'-Domoic Acid

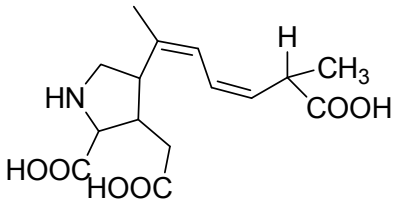

Isodomoic Acid D

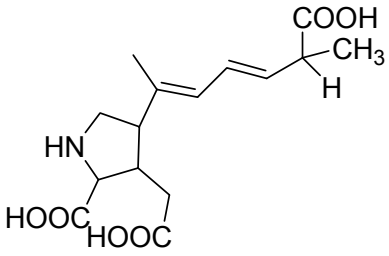

Isodomoic Acid E

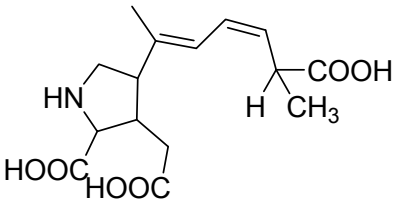

Isodomoic Acid F

Figure 2: Isomers of Domoic Acid

Rue et al., have proposed synthesis of domoic acid by *Pseudonitzschia* as a means of preventing the iron deficiency that occurs during HABs (Rue et al., 2001). The main reason for this lies in DA's structural similarity to iron-complexing agents, such as mugineic acid, generated by terrestrial plants and shown in Figure 3 (Takagi et al., 1993). Mugineic acid, generated by the roots of barley plants, is capable of solubilizing iron through the formation of a stable acid-metal complex (Sugiura et al., 1981). Similarities between mugineic acid and DA are found in the size, overall structure, especially the carboxylic acid functionality, as metal-binding sites are major factors leading to the belief of DA as an iron-binding chelator (Rue et al., 2001). Another possible function of DA is the removal of the toxic cuprate ion which may hinder the reproduction of *Pseudonitzschia* phytoplankton (Brand et al., 1986). It is believed therefore that in order to combat this potential problem; domoic acid is created to remove free cupric ions to prevent their entrance into cells while enhancing the cell's resistance to toxicity caused by the ion (Rue et al., 2001).

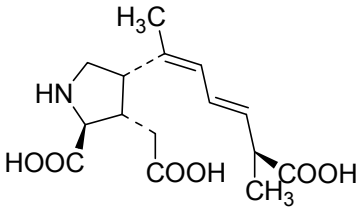

Domoic Acid

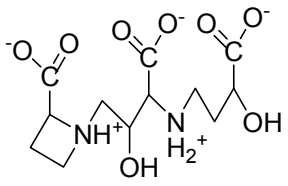

Mugineic Acid

Figure 3: Structures of Domoic Acid and Mugenic Acid

1.4.2 Toxicity of DA

Domoic acid is the toxin responsible for causing amnesic shellfish poisioning (ASP) (Sun et al., 1999). Although used as an ascaricide and first discovered to be produced in 1958, in Japan, by the red microalga, *Chondria armata* Okamura, DA production has seen to occur mainly in *Pseudonitzschia* (Work et al., 1993; Bell, 2003). Potency of the toxin occurs when contaminated shellfish are consumed by humans (Smith et al., 1995). Shellfish are able to feed on phytoplankton and concentrate DA to the point where consumption of contaminated shellfish becomes toxic to humans (Duxbury, 2000). Several major incidences involving DA toxicity have occurred in the past. One major incident occurred in Prince Edward Island, Canada during December 1987 when a domoic acid outbreak occurred in cultured blue mussels (Smith et al., 1995). A total of 153 people suffered acute intoxication and three elderly people died (Sun et al., 1999). It was later discovered that deaths were the result of a combination of preexisting conditions such as renal disease and hypertension along with domoic acid intoxication (Scallet et al., 2005). The symptoms people suffered included cardiovascular fluctuations, gastrointestinal distress, seizures and respiratory secretions (Scallet et al., 2005). Other symptoms of those intoxicated were vomiting, loss of balance, short term memory loss, confusion, nausea, diarrhea and coma (Duxbury, 2000). Additionally, damage to the hippocampus and amygdale have been seen to occur in those affected by ASP through post-mortem evaluations (Scallet et al., 2005). Those most severely affected were seen to still have memory loss after 5 years (Todd, 1993). During this Canadian poisoning it was discovered that the amount of DA in affected shellfish was around

300g/μg (Duxbury, 2000). Domoic acid has not only harmed Canadians but Americans as well when in November 1991 consumption of razor clams and crabs raised in Washington D.C. and Oregon caused illness to consumers (Todd, 1993).

Domoic acid affects humans and animals. When marine diatoms are ingested by creatures such as oysters, mussels, sardines, clams, scallops, crabs and anchovies, DA becomes concentrated in their gill structures (Scallet et al., 2005). When various marine lives consisting of dolphins, pelicans, sea lions, loons, grebes and cormorants feed on the intoxicated seafood the result is often disorientation followed by death (Lefebvre et al., 1999; Lefebvre et al., 2002; Scholin et al., 2000).

One major incident involving ingestion of DA by brown pelicans and Brandt's cormorants occurred in Monterey Bay California in September 1991 (Work et al., 1993). A great number of birds died following exposure to DA (Fritz et al., 1992). The poisoned animals experienced vomiting and loss of balance and also showed unusual head movements (Duxbury, 2000). It was shown that the pelicans in particular endured hemorrhages and necrosis of the skeletal muscle (Work et al., 1993). Another similar incident of pelican poisoning through domoic acid occurred in Cabo San Lucas, Mexico in 1996, causing hundreds of pelicans to die (Beltran et al., 1997). Domoic acid was found in the stomachs of the deceased animals as a result of their feeding on contaminated anchovies (Work et al., 1993).

Sea lions are another species which have been victims to DA intoxication. The incident arose in May 1998 along the central beaches of California (Gulland, 1999). Forty-seven sea lions died and an additional twenty-three required rehabilitation before being released into the wild (Gulland, 1999). Examination via autopsy

demonstrated for sea lions that died, shortly after exposure to DA, detectable levels of DA in the urine and blood and also lesions and necrosis in the hippocampus were observed (Scholin et al., 2000; Silvagni et al., 2005). Currently it has also been speculated that domoic acid exposure to a developing fetus may cause detriments leading to long-term cognitive impairment (Ramsdell et al., 2008; Tiedeken et al., 2010). Domoic acid has not only shown to distress to wildlife but also has shown to influence lab animals such as mice, rats and monkeys who have dealt with acute intoxication subsequent to exposure of domoic acid (Lefebvre et al., 1999).

To ensure food safety, limits have been placed on the amount of DA seafood can contain. In Canada, since the domoic acid limit in mussels was ≤ 20 μg/g, there have been no major episodes of DA poisoning in humans (Truelove et al., 1994). The 20 μg/g of DA in seafood has been enforced in other countries as well including the United States, New Zealand, Australia and the European Union (He et al., 2010). One current method of detecting domoic acid in shellfish is through use of LC-tandem mass spectrometry, a specialized technique that provides the sensitivity needed for indisputable evidence of domoic acid (Tor et al., 2003). Other methods that have been used include surface plasmon resonance biosensors, receptor binding assays, and a modified version of the paralytic shellfish poisoning (PSP) mouse bioassay (Van Dolah et al., 1997; Beani et al., 2000). However as receptor binding assays and PSP mouse assays use radioisotopes and animals for domoic acid identification they have limited usage (Tsao et al., 2007).

As a member of the kainoid class of amino acids, domoic acid closely resembles both kainic acid and glutamic acid as seen in Figure 3 (Bell, 2003). The kainoid class

is one comprised of excitatory neurotransmitters (He et al., 2010). Domoic acid specifically works by acting as an agonist of glutamate receptors in the dorsal hippocampus of the brain (Todd, 1993; Mos, 2001). When DA enters the body the toxin attaches to *N*-methyl-D-aspartate (NMDA) receptors, located in the central nervous system (CNS), which in turn causes depolarization of the neurons (Berman et al., 1997). As these neurons are located in the dorsal region of the brain, many infected persons experience short term memory loss (Yu et al., 2004). Brain damage associated with both intoxication of DA and kainic acid has been found to be similar in humans and animals (Teitelbaum et al., 1990). Neuronal fatalities have been discovered to be a result of apoptosis when a lower concentration of DA has been consumed (100 nM) (Giordano et al., 2007). Fatalities are seen to occur due to the fact that only the AMPA/kainite receptors are affected (Giordano et al., 2007). Another form of neuronal death is through necrosis (Berman et al., 1997; Giordano et al., 2006). Necrosis occurs when a high concentration of domoic acid (10 μM) is consumed (Berman et al., 1997; Giordano et al., 2006). In the case of cell death by necrosis, domoic acid attaches to both AMPA/kainite and NMDA receptors (Giordano et al., 2006).

1.4.3 Monitoring DA

After the major domoic acid poisoning incident in Canada, a number of methods have been developed for the detection of domoic acid in marine organisms. Currently the accepted methods for DA detection in biological samples are via liquid chromatography with ultraviolet absorbance (LC-UV) and mass spectrometric (LC-MS) detection

(Quillam et al., 1989; Holland et al., 2003). The detection limit of DA using LC-UV is around 0.1-1.0 mg /g of tissue, depending on the sensitivity of the UV detector (He et al., 2010). The low detection limit is attributed to the diene chromophore in DA to absorb sufficient light absorbing at 242 nm (Lawrence et al., 1991). The United States, Canada, Peru, New Zealand, Mexico, Chile as well as countries in the European Union monitor domoic acid levels via LC-UV all with a tolerance level of 20 mg/kg (Botana, 2008). Although LC-UV has proven to be a simple technique in detecting trace amounts of the toxin, false positives occur commonly due to interferences from crude extracts (Hess et al., 2001). Specifically the amino acid tryptophan and its derivatives, commonly found in shellfish, in some chromatographic conditions, elute closely to DA resulting in incorrect analysis (He et al., 2010). Additionally operation of HPLC methods demand highly trained personnel, sufficient sample clean up as well as expensive equipment (Yu et al., 2004). Therefore a number of other methods for DA detection have been developed.

Use of LC-electrospray-tandem MS for DA detection has provided unambiguous results for both the quantification and identification of the neurotoxin (Wang, 2007). Such a method allows for the monitoring of DA in biological samples thus giving pertinent epidemiological information needed to monitor certain species of marine organisms in order to protect and maintain human health (Tor et al., 2003). A particular method centering on LC-MS, created by Wang et al., focuses on domoic acid detection in seawater and phytoplankton (Wang, 2007). More specifically detection is achieved via use of SPE under an acidic condition followed by the employment of LC-MS using a Luna C18(2) column giving an unequivocal way of identifying both domoic

acid and its isomers in both seawater and phycoplankton (Wang, 2007). Another method created by Tor et al., aimed to detect DA in marine organisms, utilizes LC-MS.

A number of bioassays have been developed for DA detection such as the mouse bioassay, hippocampal slice preparations and receptor binding bioassay (He et al., 2010). Derived from a modification of the mouse bioassay for PSP toxins, a corresponding assay for the ASP toxin DA has been developed to detect concentration levels of 40 μg/g (Yu et al., 2004). With this method monitoring of DA occurs when shellfish tissue is boiled in HCl, cooled and injected using serial dilutions (Botana, 2008). The toxicity symptoms based both on time and dosage are then recorded over a four hour time period and used to determine concentration via extrapolation with calibration curves (Botana, 2008). Other than having a DA limit of detection higher than the standards of most countries, the mouse bioassay also presents a host of other problems. Such problems are the ethical issues surrounding the treatment and sacrifice of the mice, lack of specificity in determination of the toxin and a high rate of both false positives and negatives (Sauer, 2005; Holland, 2008; Combes, 2003).

As antibodies produced against DA have led to the production of enzyme linked immunoabsorbent assays for DA, use of certain antibodies have led to the synthesis of another detection method, direct competitive enzyme-linked immunosorbent assay (cELISA) (Smith et al., 1994; Garthwaite et al., 1998; Kleivdal et al., 2007). The assay has now been commercialized and serves mainly for the detection of DA in shellfish (Kleivdal et al., 2007). In a study conducted by Hesp et al., research has shown results of close correlation between use of LC-MS and cELISA in the detection of DA in

mammalian tissues (Hesp et al., 2005). cELISA has also been demonstrated as being an effective method for the quantification of DA in mammalian tissues (Maucher et al., 2005). Through a study performed by Maucher et al., biomonitoring of DA was accomplished in female mice (Maucher et al., 2005). More specifically the mice, after being injected with known concentrations of DA, were bled after 48 hours and extraction of DA was carried out via cELISA demonstrating that DA was quantifiable after 4 hours of exposure and was still quantifiable even after 24 hours thus proving to be a potential technique of rapid biomonitoring of DA (Maucher et al., 2005). These assays and antibodies provide a possible means of monitoring levels of DA during different times in the photooxidation process thus allowing the establishment of rate of DA degradation.

1.4.4 DA Degradation

Over the past, a number of both natural and chemical methods for degradation of DA have been investigated. In a study conducted by Mok et al. (2009), the effects of temperature and pH on DA degradation were monitored through the use of HPLC (Mok et al., 2009). Extracts in methanol were derived from oyster, blue mussels and neck clams and results demonstrated that DA was very stable for up to a month in -18 º, 4 º and room temperature. Results also showed that DA was stable when adjusted to a pH range of 3-9 and heated to a temperature of 121 º for a period of up to 30 minutes (Mok et al., 2009).

Natural degradation in a variety of different water matrices has demonstrated DA is mostly photodegraded through a direct photochemical pathway (Bouillon et al., 2006). Using light of a wavelength range of 280-400 nm, Bouillon et al., discovered that the rate of DA degradation decreased with increasing wavelength and that the optimum range for

DA degradation was 280-300 nm with no effect through use of visible light (Bouillon et al., 2006). Studies have also shown temperature to be an important environmental factor of DA degradation as an increase in temperature has led to an increased rate of degradation (Bouillon et al., 2006).

Other studies have also shown that immediate degradation of DA can occur when it is complexed by Fe III in natural sunlit waters (Fisher et al., 2006; Rue et al., 2001; Wells et al., 2005). Through a study conducted on the environmental degradation of mixtures of KA and DA in seawater with and without the addition of transition metals, almost all of the KA used was seen to bind to a transition metal, either Cu II or Fe III in the employed photodegradation conditions. Binding of KA to these metals was monitored using an ^{1}H NMR titration technique in which KA as most other amino acids most likely binds to Fe III in the deprotonated form and that as pD increased the line width broadened thus indicating the presence of an Fe III-KA complex (Burns et al., 2007). Since the binding constants for the Fe III- KA complex were the same order as those found for the complexation of Fe III and DA, competitive binding experiments were performed and illustrated that KA took four times as long to degrade in the presence of DA than when photodegraded alone (Burns et al., 2007). The acid-metal complexes are believed to become labile after photoreduction of Fe III thus allowing for catalytic cycling of the transition metal (Burns et al., 2007). Although scarce, DA has also been shown to undergo microbial degradation through a limited variety of bacteria present in shellfish tissues (Stewart et al., 1998). A recently explored avenue for DA degradation is the use of reactive oxygen species (ROS). In a study conducted by Djaoued et al. (2008), UV degradation of DA was catalyzed through use of TiO_2 thin films prepared by a sol-

gel dip coating method using UVA light (~350 nm). Titanium dioxide was used as it provides a method for the production of $O_2^{-\bullet}$ upon the abstraction of an electron from the conduction band of TiO_2 (Djaoued et al., 2008). The $O_2^{-\bullet}$ radical then in turn reacts with a proton to give the hydroperoxide radical ($HO_2^{\bullet}$) another species along with $O_2^{-\bullet}$ that is capable of degradation of organic pollutants (Djaoued et al., 2008). Initially during photocatalytic degradation several isomers DA were formed including isodomoic acids D, E, F as well as C5 'epidomoic acid which upon continued exposure led to degradation of DA and its isomers (Djaoued et al., 2008).

1.5 Reactive Oxygen Species

Reactive oxygen species (ROS) are highly reactive species that contain one unpaired electron in an outer orbital (Avner et al., 2009). Examples of ROS include free radicals such as hydroxyl ($OH^{\bullet}$), superoxide ($O_2^{-\bullet}$), perhydroxyl ($HO_2^{\bullet}$) as well as hydrogen peroxide (H_2O_2), singlet oxygen ($^1O_2$) and perferryl ions (FeO_2^{2+}) (Afanas-ev, 1991). Although ROS occur naturally in the body overproduction can lead to oxidative damage via the alteration of both chemical structure and function of critical biological macromolecules such as sugars, proteins, lipids and nucleic acids (Houdy et al., 2011).

Environmentally, the ROS, $OH^{\bullet}$ is produced by the Fenton process which involves the catalyzed decomposition of H_2O_2 by Fe II under acidic conditions (Chen et al., 2010). The Fenton process has been used by Bandala et al. (2009) as a means of DA degradation in order to supply water with reduced toxicity to desalination plants. In the study both Fenton processes involving the use of Co and peroxymonosulfate (PMS) and the photo-Fenton process resulted in DA oxidation with use of UV light (365 nm) (Bandala et al., 2009). The photo-Fenton reaction leads to 85% degradation of DA after

60 minutes due to inhibition by the Cl ion in salt water while almost complete degradation is achieved using Co, PMS and UVA light after 5 minutes of irradiation (Bandala et al., 2009). Another potential ROS which may lead to DA degradation is singlet oxygen which is also produced in water where pigments function as photosensitizers (Kohn et al., 2007). Naturally occurring sensitizers, waste stabilization pond constituents (WSP), Fluka humic acid (FHA) and Suwannee River Humic Acid (SRHA) (Kohn et al., 2007) produce singlet oxygen on the order of 10^{-13} M using WSP and 5×10^{-14} M when using FHA and SRHA (Kohn et al., 2007).

1.5.1 Singlet Oxygen Generation

The overall reaction scheme for generation of singlet oxygen is illustrated in Figure 4. The first step in the generation of singlet oxygen occurs when a photosensitizer absorbs enough light energy to transition to an excited singlet state (Kadish et al., 2003). Upon excitation the singlet state can either return to the ground state or undergo intersystem crossing to produce the triplet excited state (Nyokong et al., 2012). The excited triplet state can then undergo an energy transfer reaction with molecular oxygen to generate singlet oxygen (Kadish et al., 2003).

$$\text{Sens}^0 \xrightarrow{h\nu} \text{Sens}^1$$

$$\text{Sens}^1 \xrightarrow{\text{ISC}} \text{Sens}^3$$

$$\text{Sens}^3 + {}^3O_2 \longrightarrow \text{Sens}^o + {}^1O_2$$

Figure 4: Production of Singlet Oxygen using a Photosensitizer

As seen in the Figure 5 one of two types of processes can occur during the photosensitization process. Under the Type I mechanism the excited state of the

sensitizer reacts with the substrate to either undergo hydrogen abstraction or an electron transfer process (Kadish et al., 2003). In the Type II mechanism the excited photosensitizer undergoes energy transfer with molecular oxygen first to produce singlet oxygen (Calzavara-Pinton et al., 2001). The type of process that occurs during photosensitization depends on the solvent, the chemical nature of the sensitizer and also the presence of other substrates in the solution (Rhodes, 2000). In regards to the solvent, a number have been studied for singlet oxygen generation showing that deuteration of solvents increases the lifetime of singlet oxygen significantly (Anslyn et al., 2006). A number of dyes including Rose Bengal and erythrosine B are excellent photosensitizers for the production of $^1O_2$ (DeRosa et al., 2002).

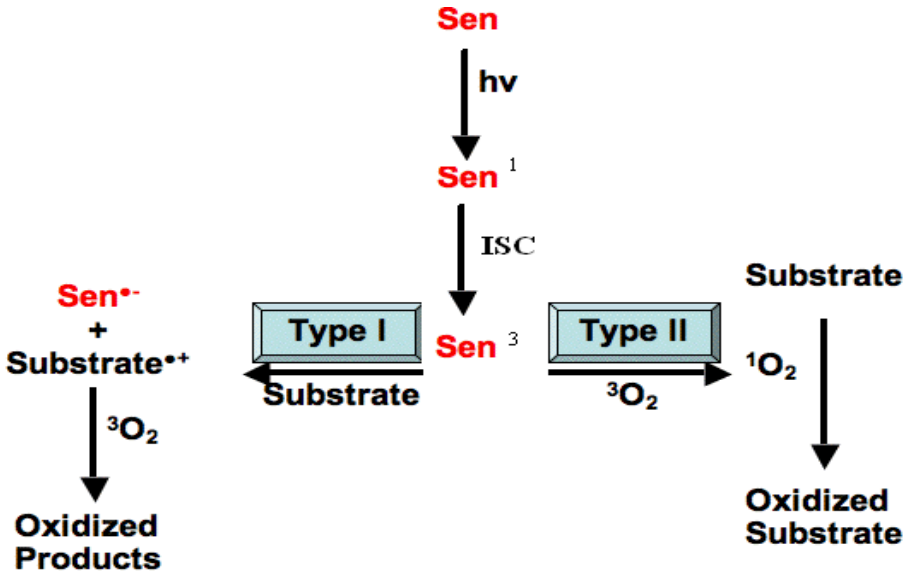

Figure 5: Type I and Type II Photosensitization Reactions (Olenick, 2011)

1.5.2 Rose Bengal

The vegetable dye Rose Bengal (RB), Figure 6, (4,5,6,7-Tetrachloro-2′,4′,5′,7′-tetraiodofluorescein disodium salt) [$C_{20}H_2Cl_4I_4Na_2O_5$] serves a variety of purposes

including tissue welding, use as an opthamological agent, a photobacteriocide and a photosensitizer (Wainwright, 2009). Operation as a $^1O_2$ sensitizer occurs when there is energy transfer between the triplet excited state of the sensitizer and the oxygen molecule to generate singlet oxygen (Kruk, 1998). Effectiveness of the sensitizer arises from its possession of the halogen, I, which allows for greater intersystem crossing because of the heavy atom effect and thus an increased production of the triplet excited state of the sensitizer (Nyokong, 2012). As RB is a polar molecule it can be used in polar solvents however the dye can also be used in non polar solvents when attached to a polystyrene bead which acts as a non-polar polymer support (Paczkowski et al., 1984). Studies have shown that in polar solvents the salt form of RB follows Beer's law indicating that the dye does not aggregate and therefore results in no change in the maximum absorption in spectral analysis but as the solvent is changed to a non polar one, aggregation may occur (Neckers et al., 1987).

Although demonstrated to be an effective sensitizer, RB and all other dyes undergo a process known as photobleaching, with some dyes more susceptible than others (Whitaker, 2010). The amount of photobleaching relies predominantly on three factors including the dye, the amount of oxygen or the amount of extinction light (Pawley, 2006). In order to reduce bleaching and other problems presented by RB several derivatives of RB have been synthesized.

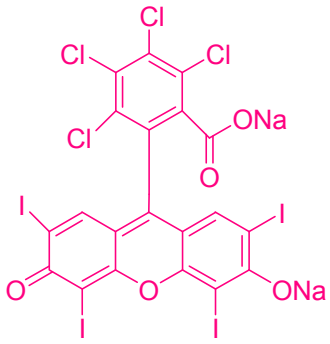

Rose Bengal

Figure 6: Structure of Rose Bengal (RB)

1.6 Reactions of Singlet Oxygen with Dienes

Singlet oxygen commonly reacts with 1, 3 conjugated diene functionalities, such as that present in domoic acid, in three specific ways: the ene reaction, the 2+2 reaction and the Diels-Alder or 4+2 reaction (Pattenden, 1980). Figure 7 below depicts the general reactions of dienes and singlet oxygen. Presence of these reaction products forms a complex mixture for which product distribution is influenced by reactant confirmation, geometry and substituents. Some of these products are unstable and difficult to isolate and purify. Therefore in order to gain a better understanding of product formation and stability the reaction of a simpler model compound, sorbic acid, with singlet oxygen is explored in chapter two.

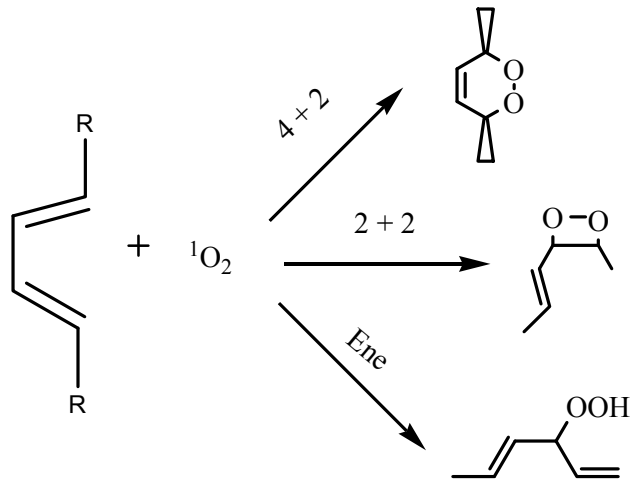

Figure 7: Possible Reactions of Conjugated Dienes and Singlet Oxygen

Chapter 2

Photooxidation of Sorbic Acid (SA), a Model Compound for Domoic Acid

2.1 Introduction

The reactions of singlet oxygen with DA may play an important role in the environmental fate of DA and also may be attractive for treatment of waters contaminated with DA. Domoic acid contains amine, carboxylic acid and diene functional groups. The carboxylic acid group is unreactive towards singlet oxygen because of the resonance present between the carbonyl and hydroxyl groups (Macomber, 1996). The resonance effect results in a decreased electrophilicity of the carbonyl carbon making it less susceptible to attacks from incoming nucleophiles (Patrick, 2004). As for the pyrrolidine ring on DA, it is known that amine groups can quench singlet oxygen. (Matysik et al., 2002). The pyrrolidine ring causes quenching of singlet oxygen via DA (Matysik et al., 2002). In addition, it has a number of chiral centers and thus synthesis of DA for my photoxidation studies is not practical. While DA can be isolated from cell cultures or purchased both options are expensive.

While DA contains a number of functional groups, the conjugated diene functional group is most susceptible to singlet oxygenation. With this in mind I chose to use the potassium salt of SA as a model compound for DA to study the reactions with singlet oxygen, as seen in Figure 8. Sorbic acid is less complicated structurally and spectroscopically than DA allowing for product studies with easier optimization of the reaction conditions. Despite the simple structure of SA compared to DA both compounds are expected to react with $^1O_2$ at the diene and in an analogous fashion.

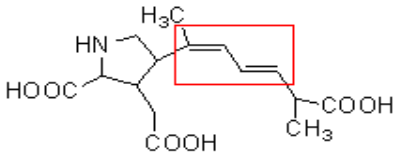

Domoic Acid

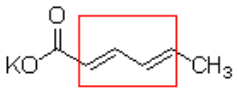

Potassium Sorbate

Figure 8: Structures of DA and SA Highlighting the Reactive Diene Region

Given the presence of the diene and CO_2H functionality, aqueous solubility and preference for $^1O_2$ to react at the diene, SA is an excellent and inexpensive model for studying reactions of $^1O_2$ of DA. The high costs of DA seriously limit my ability to run detailed product studies. The price of DA is found to be $154.50 for 1 mg of the compound while the price of SA is seen to be only $21.50 for 100 g (Aldrich, 2012). The solubility of the salt form of SA, potassium sorbate, is found to be as soluble as DA (Luck, 1990; Falk et al., 1991).

2.2 Sorbic Acid

While I employed SA as a model compound for DA, the reactions of $^1O_2$ with SA have yet to be studied in detail and are of significant interest. Sorbic Acid (SA) (2,4-hexadienoic acid) [$CH_3CH=CHCH=CHCOOH$] with molecular weight 112.13 (Aldrich, 2012) is a commonly used food additive that was discovered to possess antimicrobial properties in the 1930s (Naidu, 2000). Synthesized through the heating of parasorbic acid found in rowan berries, sorbic acid has a variety of uses including food preservative, cosmetics, pharmaceuticals, animal feeds and industrial processes (Davidson et al., 2005). Chemically, the structure of sorbic acid consists of a short chain trans –trans

conjugated diene and is classified as a fatty acid (Fennema, 1996). The antimicrobial activity of SA is believed to rest on a number of factors including changes in cell transport functions as well as changes in cell membranes, enzyme inhibition, and changes in genetic composition (Naidu, 2000). Numerous derivatives of SA, which also function as food preservatives, have been synthesized including esters, amides, alcohols, amine salts and alkaline salts (Naidu, 2000). One such salt includes potassium sorbate which is favored in certain foods over sorbic acid because of its greater water solubility (Pearson et al., 1996).

2.2.1 Photoisomerization of SA

SA, its potassium salt, and its ester form undergo isomerization when exposed to UV irradiation (Cigic et al., 2001). There exist a total of four geometrical isomers of SA produced by cis-trans isomerization just as in DA (Grebel et al., 2011). The wavelength shown to isomerize SA is 248 nm (Waldron et al., 1996). An UV irradiation time of 120 minutes has been found to be ideal leading to the greatest production of isomers without product degradation (Cigic et al., 2001). Photoisomerization of potassium sorbate with UV light also gave the four geometrical isomers (E, E), (E, Z) and (Z, E) (Cigic et al., 2001). The cis isomers exhibit lower microbial activity as the permeability across cell membranes was decreased subject to steric hindrances (Xiang et al., 1998). Figure 9 displays the geometrical isomers of potassium sorbate.

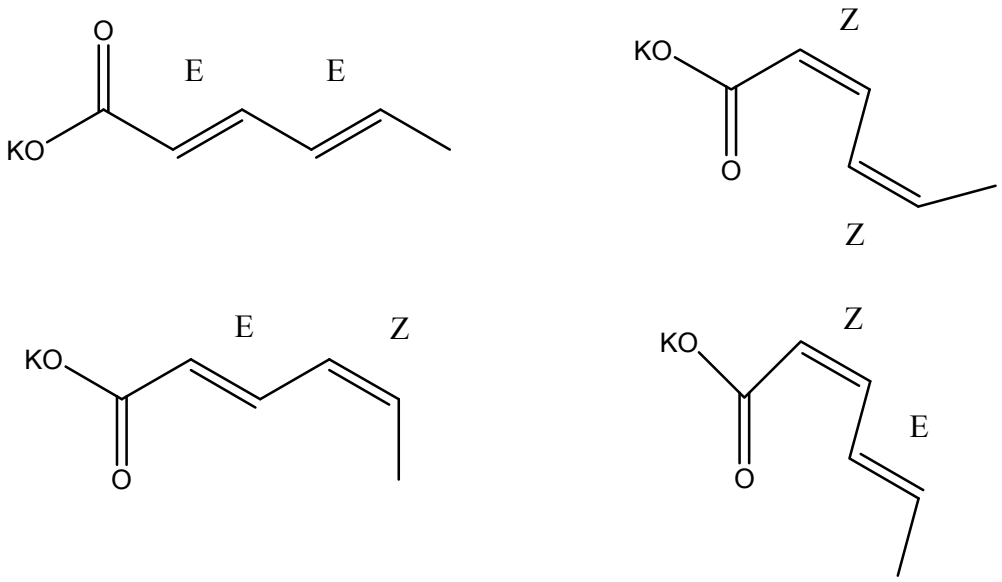

Figure 9: Geometrical Isomers of Potassium Sorbate

2.2.2 Toxicity of SA

Although when SA is metabolized by the human body it is considered non-toxic; acute toxicity is exhibited at 10g kg^{-1} of body weight (Hornsey, 2007). As a consequence of these findings, the WHO has set the daily guideline of SA to 25 mg kg^{-1} (Hornsey, 2007). Acute toxicity of SA has been studied in rats. After a feeding period of 120 days, the animals experienced increases in growth rate and liver weight when exposed to SA (Davidson et al., 2005). A prolonged SA intake for rats, up to a life span of one or more generations, has shown to induce chronic toxicity resulting in increased weights of the liver, ovary and kidney as well as a decrease in body weights (Maga et al., 1995). Occurrence of toxicity may be the result of reaction between SA and sodium nitrates or sulfur dioxide to produce mutagenic products (Naidu, 2000). It is likely that biological and environmental transformation involves reactive oxygen species, such as $^1O_2$.

2.3 Reactions of SA with Singlet Oxygen

As a 1,3-conjugated diene, SA is expected to react with singlet oxygen in three specific ways: the [4 + 2] or Diels-Alder reaction to form endoperoxides, the [2 + 2] reaction to give 1,2-dioxetanes and the Schenck or ene reaction to afford hydroperoxides (Ramamurthy et al., 2001). These reactions are shown in Figure 10.

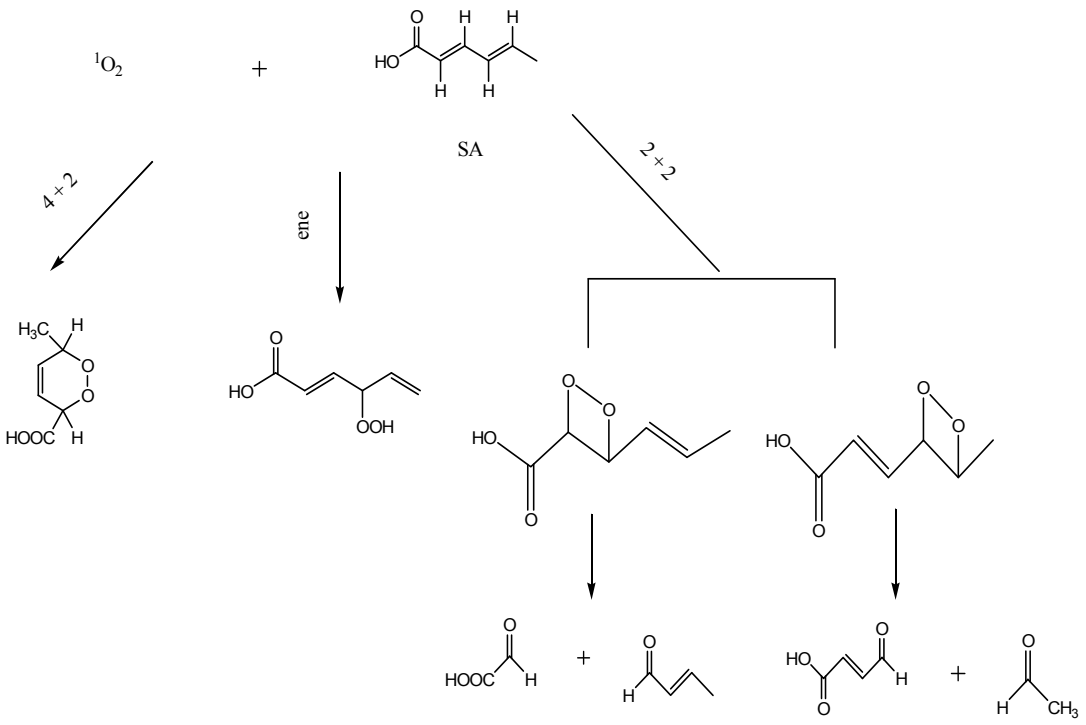

Figure 10: Possible Reactions and Products of SA Photooxidation

2.4 Experimental

2.4.1 Materials

Potassium Sorbate (MW = 150.22) was purchased from Aldrich and used without further purification. Deuterium oxide (D_2O) the NMR solvent, was purchased from Cambridge Isotope Laborotories Incorporated. Rose Bengal was purchased from Aldrich and had a purity of 95%. The NMR tubes (OD 5 mm) were purchased from Kimble Chase.

2.4.2 Stock Solutions

A stock solution of (1×10^{-4} M) Rose Bengal and D_2O was prepared using volumetric glassware and stored in a glass vial (O.D. 3 cm) for future use. The vial was tightly capped and wrapped with parafilm.

2.4.3 Sample Preparation

For a typical experiment, a specific amount of SA was weighed out and added to 0.7 mL of stock D_2O/RB solution. Each sample run was transferred to a clean dry NMR tube (O.D. 5 mm) and stored prior to irradiation in the refrigerator. The NMR tube was placed in a windowed Dewar containing an ice bath for irradiation.

2.4.4 Photoxidation

Photooxidation was conducted via a Xenon lamp (Oriel), model 68806, equipped with a heat filter containing deionized water and connected to a lamp housing, model 7240, outfitted with a cooling fan positioned on an adjustable jack. The xenon lamp contained inside possessed a rating of 15 W and was set to a current of 7.5 Amps. The NMR tube containing the sample was placed in a windowed Dewar filled with water and a thin layer of ice. The liquid level was marked on the NMR tube for extended

photooxidation. The RB/D_2O stock solution was added to the mark to compensate for photobleaching of the RB and/or loss of solvent. At specific reaction times the NMR tube was removed from the windowed Dewar and excess water on the outside of the tube was cleaned off prior to NMR analysis

2.4.5 NMR Analysis

The ^1H NMR (Bruker, 400 MHz) was used for the majority of 1D NMR and 2D NMR experiments involving SA, but the 600 MHz was instead used for product confirmation. Spectra were analyzed and integrated with a TMS peak centered at 0 parts per million. The integration of SA and products were used to determine the relative ratios of starting material and products as a function of irradiation time.

2.4.6 Photooxidation Experiments

For a typical experiment 3 mg of SA was transferred to an NMR tube with 0.7 mL of the RB/D_2O stock solution. The NMR tube was irradiated using the Xe lamp and the reaction monitored by ^1H NMR. Under these experimental conditions the reaction was run for up to 7 hours until most of the SA was reacted in order to determine the percentage of products through ^1H NMR. In order to establish the reaction profile, samples were analyzed at intermediate times, i.e., after two hours of irradiation. 2D COSY were taken of the sample. For better resolution and lower detection limits select samples were run at 600 MHz.

2.4.7 Variable Temperature NMR

To probe the presence of equilibrating confirmations variable temperature ^1H NMR was performed. The sample was gently heated and ^1H NMR spectra collected of

the sample and measurements were equilibrated for 10 minutes at each temperature 24, 35, 45, 55 and 65 ºC. A total of 80 scans were collected at each temperature.

2.5 Results and Discussion

Through the graph seen below in Figure 11, evidence shows that oxygen gas, as well as RB are necessary to ensure the photooxidation of SA. Through the control involving oxidation without use of RB results confirm that there is no direct photolysis. Through the control involving oxidation without use of O_2 gas evidence demonstrated there was no direct energy transfer from RB to DA.

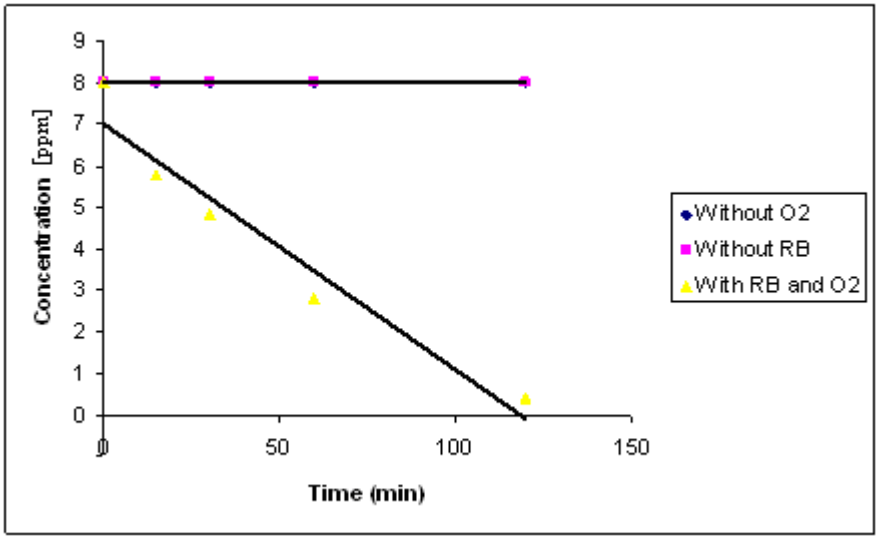

Figure 11: Graph of SA Controls

The time plot for the photooxidation of SA in Figure 12 shows that starting material is still present after two hours of reaction. However the reaction is proven to occur due to the presence of the methyl peak at ~1.7 ppm as a result of a proposed

product. The time plot shows that although the rate of product formation is quick, as products are evidenced as early as 15 minutes of photooxidation, the rate of SA degradation seems very slow as a significant amount still remains after the two hour oxidation time. Upon an oxidation of 7 hours the starting material is still seen to remain in the reaction mixture as shown in Figure 13. However the dominant product seems to be the endoperoxide followed by the hydroperoxide and then the aldehydes. The percents of products formed are ~78% endoperoxide, 1.5% crotonaldehyde, 1% fumaraldehydic acid and 0.2% acetaldehyde.

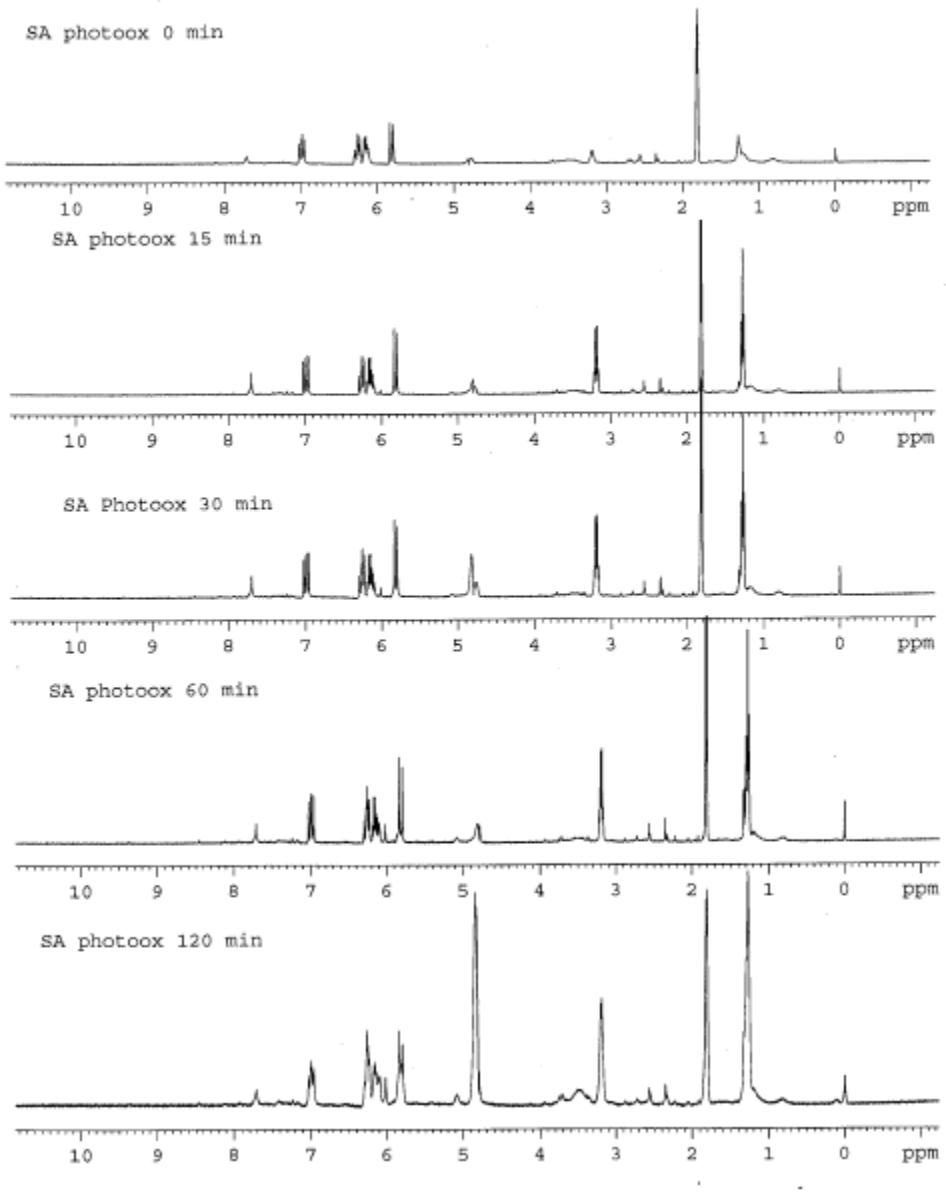

Figure 12: Time Plot of the Photooxidation of SA

Sorbic Acid: ^{1}H NMR (400 MHz, D_2O, δ): 1.7; 5.7; 5.9; 6.2; 6.9. From the above figure it is noted that SA is still present after two hours of photooxidation when starting with 3 mg of SA.

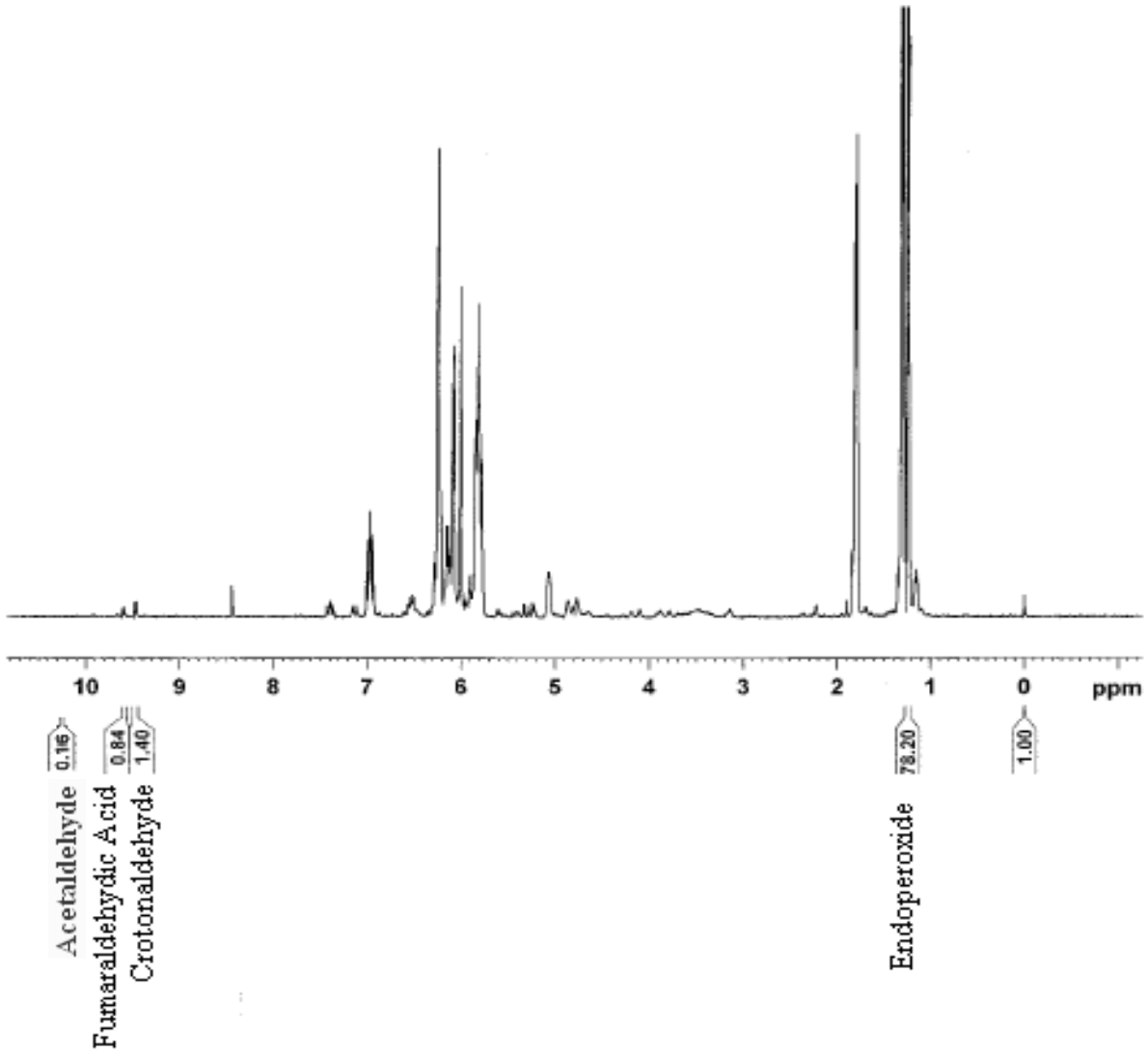

Figure 13: Integration values of SA Photooxidation Products

Clearly the ^{1}H NMR show the disappearance of SA with the formation of several sets of new peaks. Control experiments established that the reaction involves singlet oxygen which generally reacts by 2 + 2, 4 + 2 and ene reactions. I will attempt to assign and evaluate the different reaction products by reaction type first 2 + 2, second ene and last 4 + 2. 2 + 2 reactions of singlet oxygen are known to produce dioxetanes which readily collapse to the corresponding carbonyl compounds. In the case of SA, the 2 + 2 addition of $^1O_2$ can occur at C2-C3 and C4-C5 double bonds resulting in two sets of products. The double bonds are labeled in the figure below. Upon reaction at the C2-C3 the anticipated products from collapse of the dioxetane are glyoxylic acid and crotonaldehyde shown below. The two products produced at reaction of the C4-C5 and collapse of the corresponding dioxetane are fumaraldehydic acid and acetaldehyde shown below. The 2 + 2 reaction pathways are summarized in Figure 14.

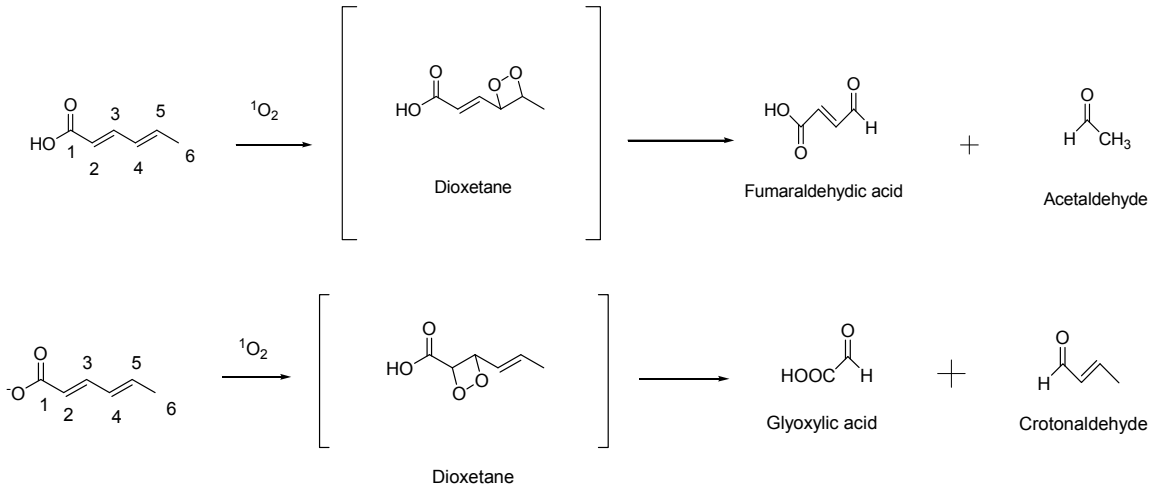

Figure 14: 2 + 2 Reactions between SA and Singlet Oxygen

The ^{1}H NMR of the reaction products from $^1O_2$ and SA, Figure 15, has four peaks in the aldehyde region 9-10 ppm (Pavia et al., 2001) indicating a number of aldehydes are produced. Product confirmation has been attained through use of both

COSY and ^{1}H NMR as depicted in the spectra below. The products expected from collapse of the dioxetane are fumaraldehydic acid, acetaldehyde, glyoxylic acid and crotonaldehyde. To confirm their presence I consulted the literature, ^{1}H NMR values and/or reaction NMR spectra of authentic samples.

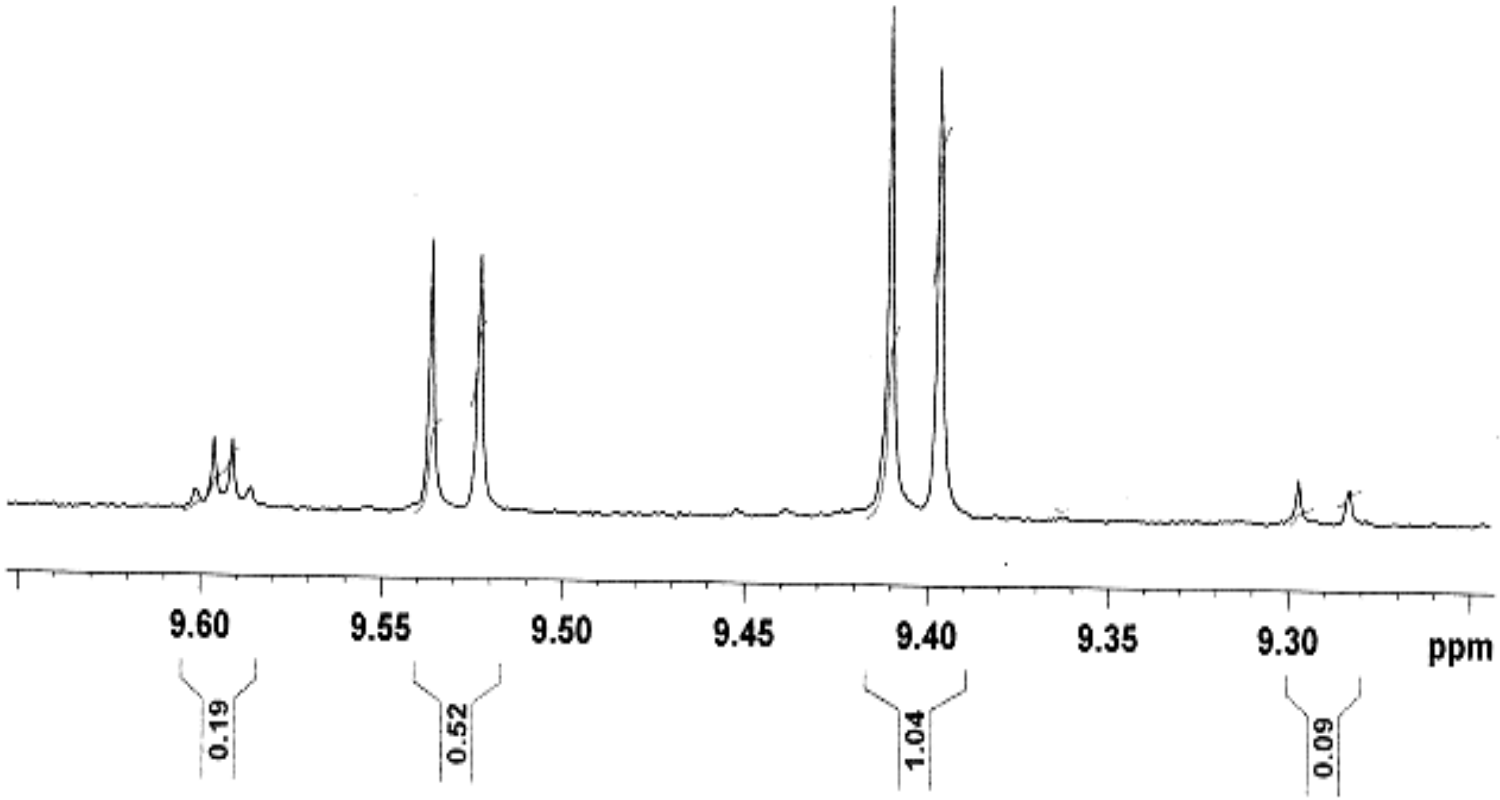

Figure 15: Aldehyde Products from 2 + 2 Reaction Pathway between SA and Singlet Oxygen

Reaction at the C4-C5 bond is expected to produce fumaraldehydic acid and acetaldehyde. Assignments of both products were based on the structures shown in Figure 16.

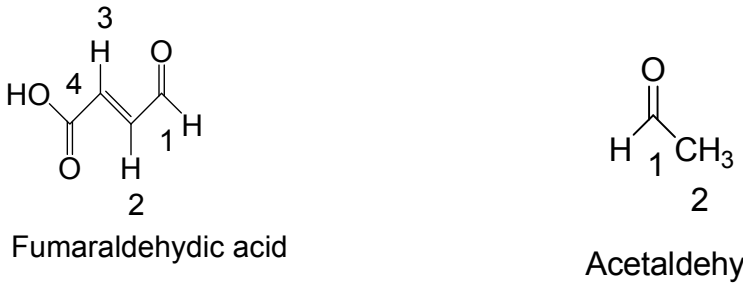

Figure 16: Numbered Structures of Fumaraldehydic Acid and Acetaldehyde

Literature reference regarding ^{1}H NMR of fumaraldehydic acid, in acetone-d_6, gave values of chemical shifts of 10.0 ppm, 6.70 ppm, 6.70 ppm and 11.2 ppm for H1, H2, H3 and H4 respectively (Scharf et al., 1978). The COSY spectra for the fumaraldehydic acid peaks are displayed in Figure 18. The aldehydic peak at ~9.40 ppm was assigned as H1 of fumaraldehydic acid with an integration value of 0.86. The coupling constant is 7.98 Hz which is in agreement with the range of 5-8 Hz (Silverstein et al., 1991). Even in the COSY the exact peak assignment for H2 is unclear, because of overlap. However the splitting pattern for H2, a doublet of doublets peak at ~ 6.23 ppm with an integration of 0.64 was further considered. While the chemical shift and multiplicity are consistent with fumaraldehydic acid, the small coupling constant of ~1.7 Hz suggests the peak is not associated with fumaraldehydic acid. With this in mind the peak representing H2 is assigned to ~6.18 ppm for which the coupling constant and integration values are not definitive. Upon inspection of the COSY and crosspeaks for

H2, I observed coupling to a peak at 6.90 which I assigned as H3. The splitting pattern for H3 is only expected to be a doublet with a trans coupling constant, but it is masked by the large doublet of doublets. Although acetaldehyde and fumaraldehydic acid are produced in a 1:1 ratio upon collapse of the dioxetane the integration of ^{1}H NMR indicate a ratio of 0.16: 0.86 of acetaldehyde to fumaraldehydic acid. I explain the inequity as a result of the evaporation of volatile acetaldehyde during bubbling of solution with O_2. The trans geometry of the olefin is retained in the reaction with singlet oxygen as the process is believed to be a one step concerted mechanism involving antarafacial attack of singlet oxygen and suprafacial attack of the alkene (Olah et al., 2003). The mechanism expected to occur via formation of a dioxetane showed no signs of the intermediate in the ^{1}H NMR spectra of any of the reactions performed. A summary of the chemical shifts, multiplicities and coupling constants is displayed in Figure 17.

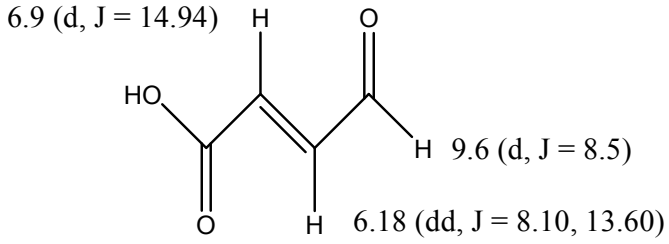

Figure 17: Structure of Fumaraldehydic Acid Showing Chemical Shifts, Multiplicities and Coupling Constants

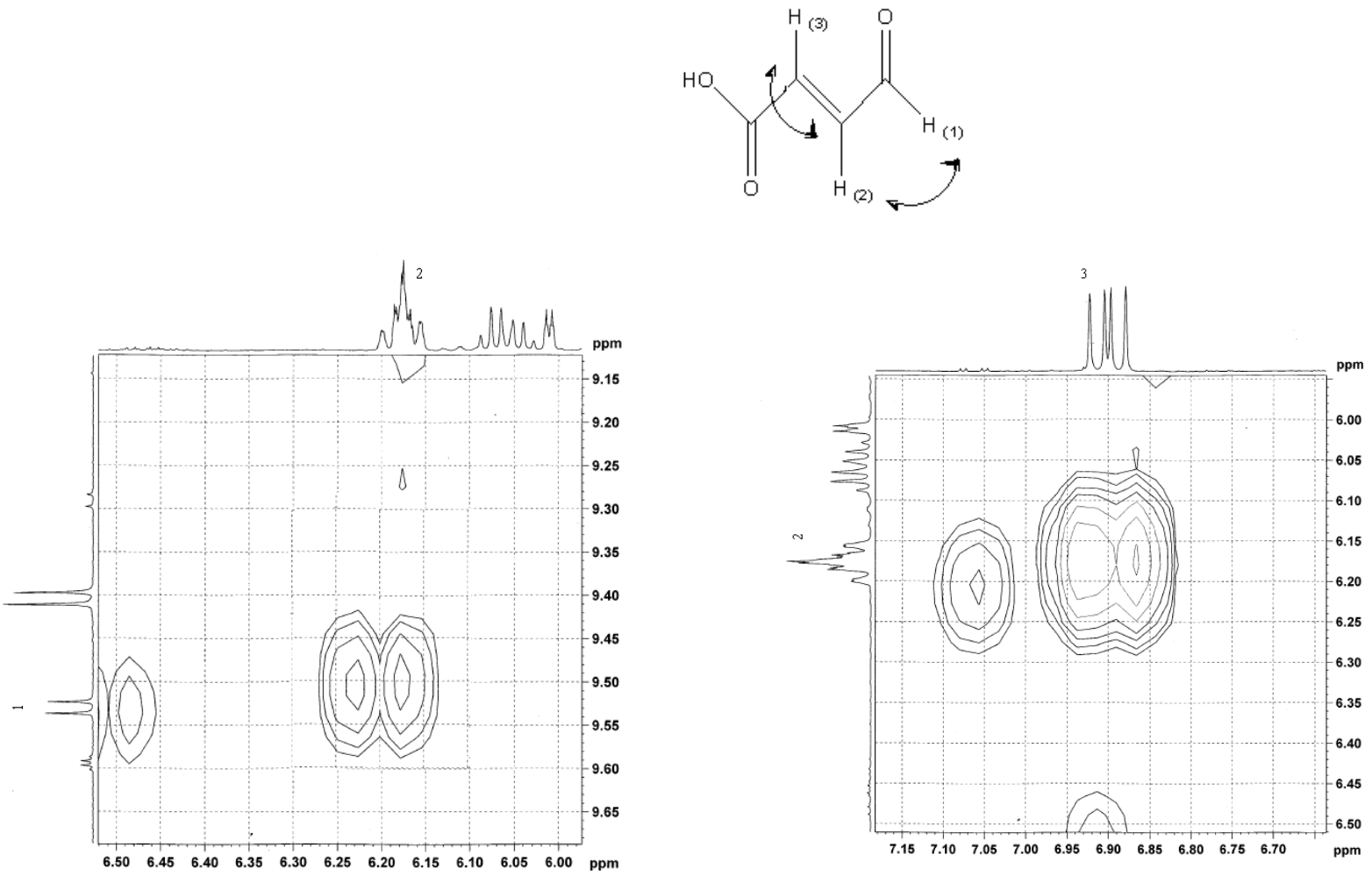

Figure 18: COSY of Fumaraldehydic Acid Peaks

The complementary product to fumaraldehydic acid is acetaldehyde. The ^{1}H NMR of the product mixture exhibits a peak at ~ 9.60 ppm as a quartet with a coupling constant of 2.7 Hz which is assigned to acetaldehyde.

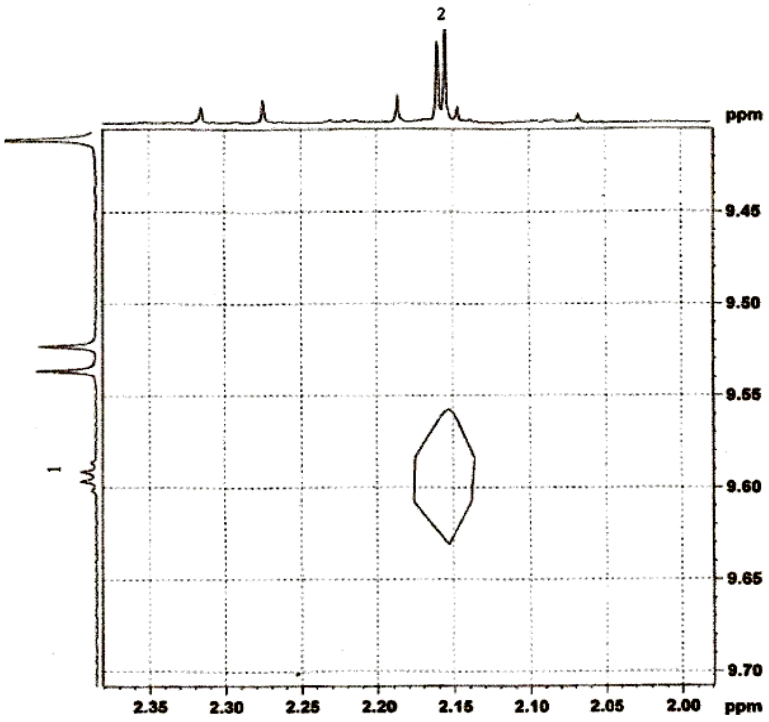

Figure 19: COSY of Acetaldehye Peaks

As shown in Figure 19, the COSY spectrum shows coupling with the aldehyde peak, H2 is found at ~2.15 ppm is a doublet with a coupling constant of 2.8 Hz. For the peaks at 9.60 ppm and 2.15 ppm the ratio of integration values is 1:3 further supporting the acetaldehyde assignment. The integration value for this peak is 0.59 which about three times that of the aldehydic proton. Chemical shifts, coupling constants and integrations for acetaldehyde are summarized below in Table 1 and match with literature values.

Table 1: ^{1}H NMR Chemical Shifts and Coupling Constants and Integration Values for Acetaldehyde

Position	1H, δ (ppm)	J (Hz)	Integration
1	9.60	2.70	0.16
2	2.15	2.88	0.59

Singlet oxygen can also form a dioxetane by 2 + 2 reaction at the C2-C3 bond. Since these dioxetane products tend to collapse to the corresponding carbonyl products at room temperature glyoxylic acid and crotonaldehyde, seen in Figure 20, are indicative of 2 + 2 addition at C2-C3.

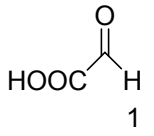

Glyoxylic acid

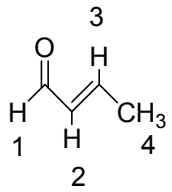

trans-Crotonaldehyde

Figure 20: Structures of Glyoxylic Acid and Crotonaldehyde

From the structure and ^{1}H NMR chemical shift for aldehydes one may expect to have a singlet peak for glyoxylic acid between 9-10 ppm. However the literature chemical shift for this aldehydic proton is 5.2 ppm. Upon acquisition of ^{1}H NMR spectrum of an authentic sample of glyoxylic acid there was no peak in the aldehyde region, thus none of the peaks observed between 9-10 ppm for the reaction mixture can be assigned to glyoxylic acid. The aldehydic peak for glyoxylic acid occurs at ~5.20 ppm due to the hydration of the carbonyl group. As C1 of the carbonyl group is electrophilic, and can hydrolyze to the acetal product (Anslyn et al., 2006) the result is in an upfield shift for H1. I was unable to confirm a peak assignment for the glyoxylic acid peak in the SA photooxidation reaction because of overlap with the water (HOD) peak from the NMR solvent.

Crotonaldehyde is the other product expected from collapse of the C2-C3 dioxetane intermediate. Chemical shifts and peak assignments were made using ^{1}H and COSY spectra and confirmed with literature and/or authentic samples (Balci, 2005). ^{1}H

NMR analysis authentic on crotonaldehyde performed in D_2O was compared to the SA photooxidation reaction mixture for peak assignments as shown in Figure 21. The aldehydic peak present at ~9.30 ppm represents a very minor product and is consistent with the cis-crotonaldehyde product allowing for possible research in the future. Comparison of the integration value for fumaraldehydic acid and crotonaldehyde as a measure for reaction at C2-C3 indicates reaction of SA does not occur predominantly at the double bond further away from the acidic electron withdrawing group.

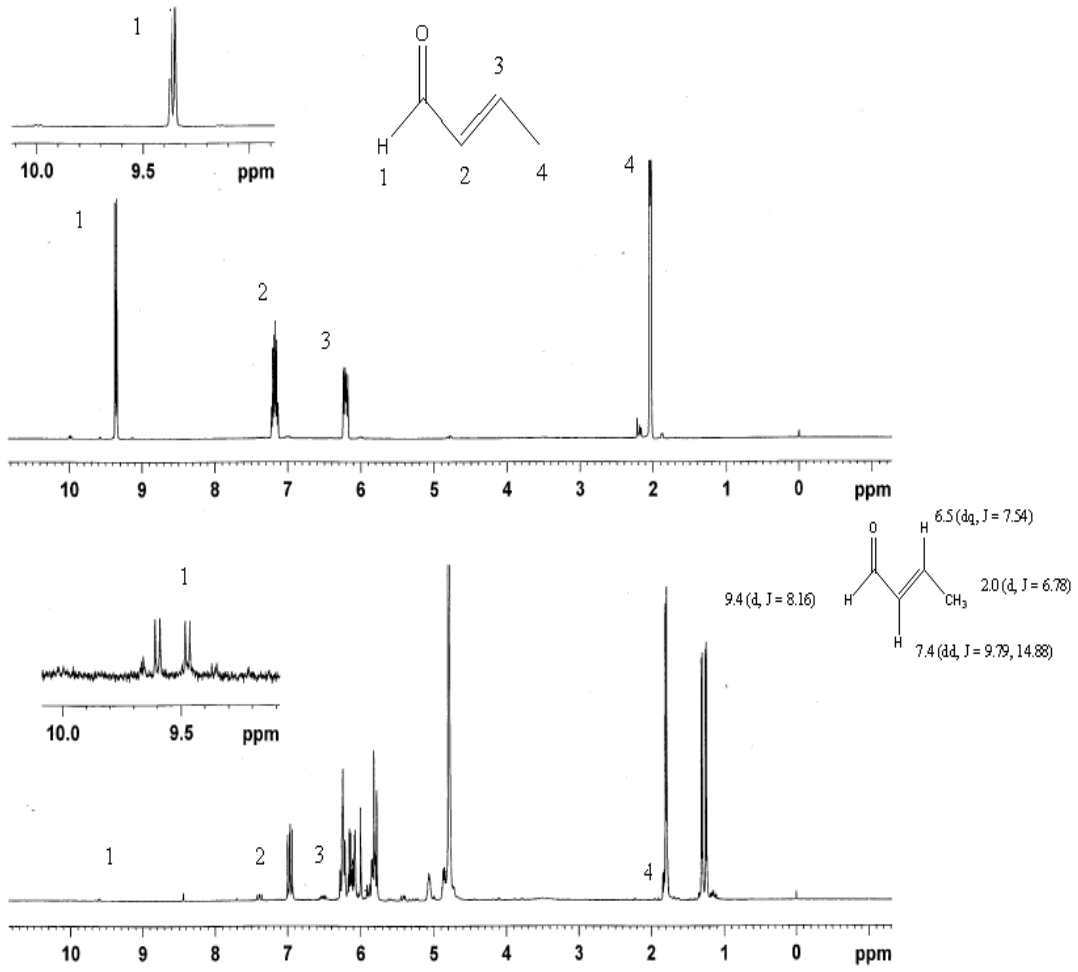

Figure 21: Stacked Plot of Crotonaldehyde (top) and SA Photooxidation Reaction Mixture (bottom)

The reaction of singlet oxygen with an allylic hydrogen via ene reaction yields the hydroperoxide shown in Figure 22. The chemical shifts for many of the peaks representing the protons of the hydroperoxide product appear in regions overlapping with other products and the starting material. With this in mind COSY experiments were run to try and distinguish and assign peaks from the hydroperoxide product. Only one hydroperoxide product is possible from the singlet oxygenation of sorbic acid.

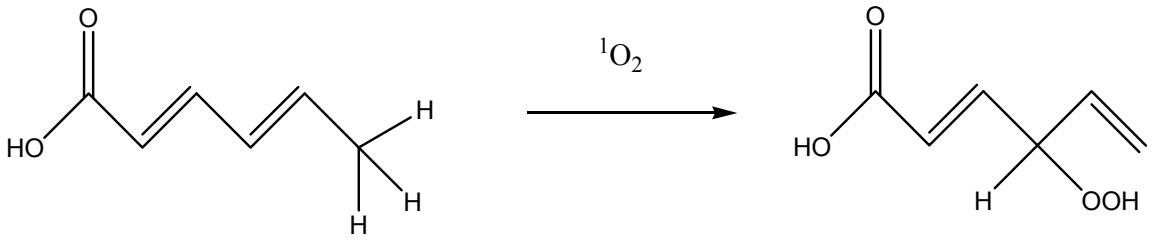

Figure 22: Ene Reaction of SA

The hydroperoxide product is expected to show up to six individual peaks in the ^{1}H nuclear magenetic resonance. The acid and hydroperoxide protons will not be observed because of exchange with the D_2O solvent. Five of these six protons are olefinic and expected to appear between 5-7 parts per million, the sixth proton is aliphatic but doubly allylic and α to an oxygen and may appear ~ 4-5 parts per million. With this in mind, I began my assignments for the hydroperoxide. The proton attached to the C2 should be a doublet with a characteristic trans-coupling constant. Using the ^{1}H NMR the doublet at 5.80 ppm (J = 15.6) is assigned to H1. Although the chemical shift for H1 appears to be lower than the expected value the chemical shift values for the other protons are in good agreement with expected ones. The H2 proton should couple to H1 (COSY, Fig. 23) and appear as a doublet of doublets and have 1:1 integration with H1.

The doublet of doublets around 6.96 ppm matches expectations for H2, 1:1 integration and J = 15.6, 10.9. Coupling of H2 is observed in the COSY with a peak at ~ 6.24 ppm, which in an area with several overlapping peaks, but the assignment is made at 6.24 ppm (J = 15.1, 10.2 Hz) determined by the coupling constants and the integration value. From the COSY, Figure 22 the peak for H3 couples to another peak at ~6.12 ppm which is assigned to H4. The splitting pattern is a complex multiplet because of coupling to H3 and cis and trans orientations to the terminal olefinic protons. Because of overlapping peaks and a complex splitting pattern I was unable to obtain accurate coupling constants and integration values. However crude integration value of 40.25 is consistent with expectations for a single proton. The peak assigned to H4 exhibits coupling to a set of peaks at ~5.10 ppm. The HOD peak for D_2O also occurs in this region. It is difficult to make the proper assignments for these geminal protons but the COSY crosspeaks and chemical shifts are consistent with geminal olefin protons. A summary of the chemical shifts, coupling constants and integration values are displayed in Table 2.

Table 2: ^{1}H NMR Chemical Shifts, Coupling Constants and Integration Values for SA Hydroperoxide

Position	1H, δ (ppm)	J (Hz)	Integration
1	5.8	15.6	46
2	6.97	10.9, 15.6	37
3	6.24	10.2, 15.1	61
4	6.12	*	40
5	5.1	*	*
6	5.1	*	*

*Not all coupling constants and integration values could be determined due to overlap of peaks.

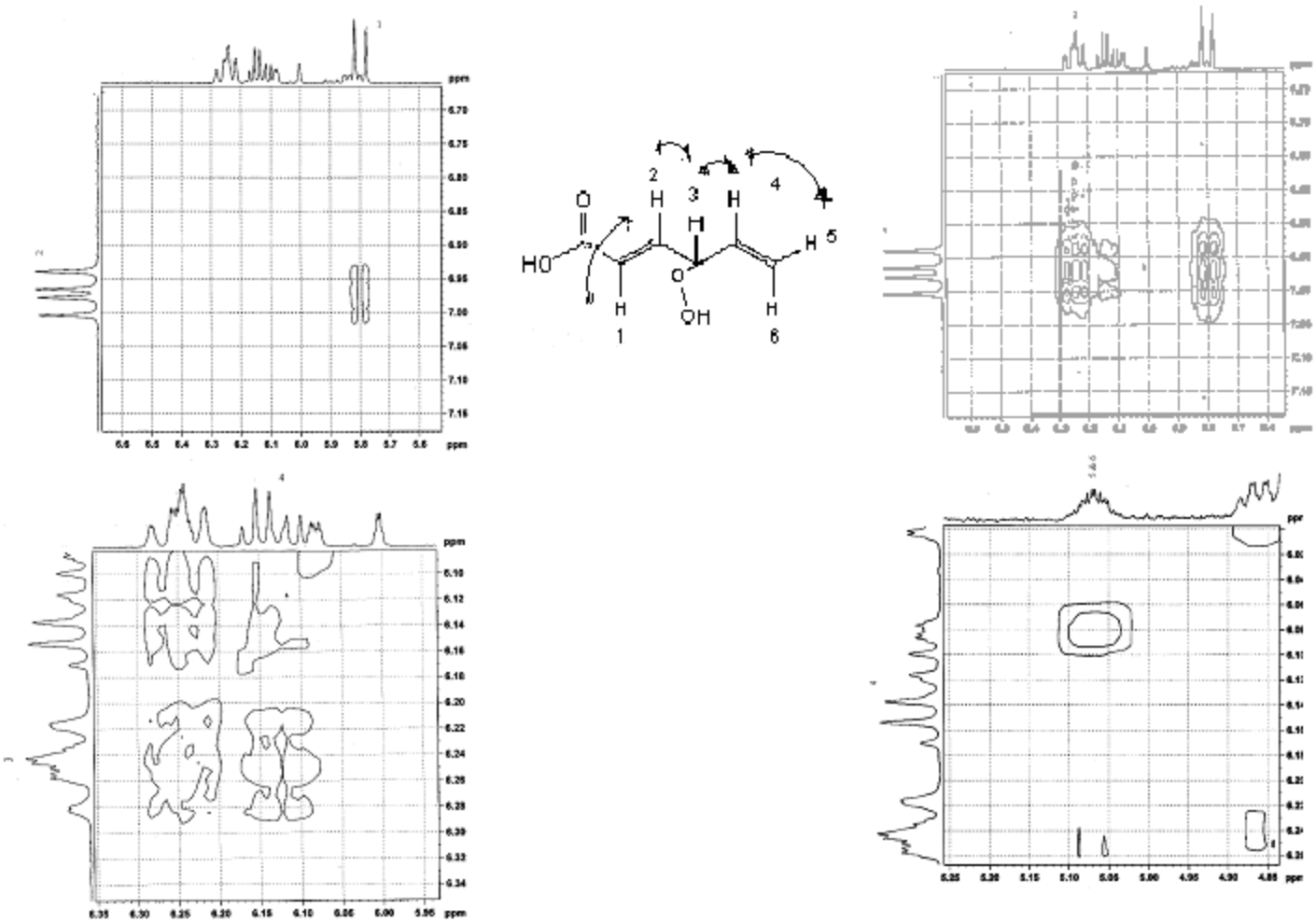

Figure 23: COSY of SA Hydroperoxide Product

The final product expected from singlet oxygenation of SA is the 4 + 2 or endoperoxide shown in Figure 24.

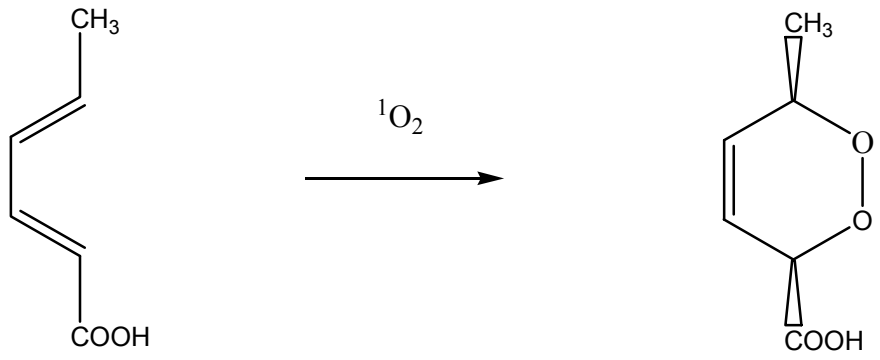

Figure 24: Diels-Alder Reaction of SA with Singlet Oxygen

The endoperoxide is expected to exhibit 5 different signals in ^{1}H nuclear magnetic resonance. The carboxylic acid group will not be observed because of exchange with D_2O. Aliphatic protons H1, H2 and H5, are expected to have multiplicities and chemical shifts: H1, d, ~3 ppm, H2, multiplet, ~ 4 ppm, H5, d, 4 ppm. H3 and H4 will appear as doublet of doublets in the olefinic region ~4 parts per million. The exact chemical shifts are listed in Table 3 below. Confirmations of the endoperoxide peaks were assigned through use of COSY, Figure 30, using the assignments seen below in Figure 25.

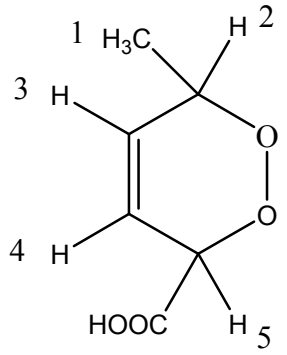

Figure 25: Numbered SA Endoperoxide Product

From these expectations and elimination of ^{1}H NMR peaks assigned to 2 + 2 and ene products I began my assignment of peaks for the endoperoxide.

Table 3: ^{1}H NMR Chemical Shifts for SA Endoperoxide

Position	1H, δ (ppm)
1	3.10
2	4.87
3	6.08
4	6.25
5	4.65

**Coupling constants and integration values could not be determined due to overlap of peaks*

Primary identification of the endoperoxide product is determined by the upfield methyl peak of the compound.

Notable is the presence of two doublets assigned to the methyl group, initially assumed the result of long range coupling may exist between the methyl group and the vinyl proton. However upon closer inspection the coupling constant between the two methyl peaks is 23.65 Hz, a value too large to be attributable to normal coupling constants (Silverstein et al., 1991). A reasonable explanation could involve slow conformational equilibria as shown in Figure 26.

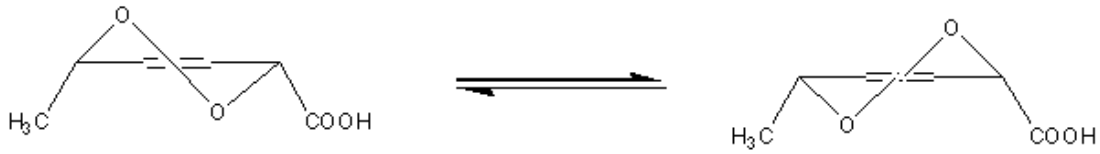

Figure 26: Half-Chair-Half-Chair SA Endoperoxide Interconversion

Peroxides are known to adopt a gauche conformation to reduce the Coloumb repulsion between the lone pairs in oxygen (Rappoport, 2007). However in most medium to small endoperoxides such energetically favorable conformations are not formed because of ring strain (Rappoport, 2007). As a result of this knowledge, temperature control experiments using ^{1}H NMR were explored to seek potential interconversions of the endoperoxide. It is known that two conformers are likely depending on whether the hydrogen is either in the axial or equatorial position (McMurray, 2009). Using the work of Drago temperature control performance ^{1}H NMR experiments were considered. Drago noted that at room temperature the conversion between the axial and equatorial positions is so rapid that there is no contribution to the observed line width resulting in the observance of only one peak. However upon a series of temperature control experiments involving ^{1}H NMR, the line width is observed to broaden and eventually separate into two distinct peaks (Drago, 1992). Thus for the DA endoperoxide product at room temperature the conversion between positions is so slow two sets of peaks are observed. These peaks, upon warming, may coalesce into a single peak if the equilibrium becomes faster than the NMR time scale. As peaks for the endoperoxide were observed, higher temperatures were employed to see if the two peaks would merge. Using temperatures of

24 º, 35 º, 45 º, 55 º and 65 º the two methyl peaks were seen to converge as the temperature rose with coalescence taking place at 65 º. Existing as the E, E geometrical isomer, SA is expected to give a cis-endoperoxide upon the Diels Alder reaction with singlet oxygen (O'Shea et al., 1988).

Research focused on the conformational analysis of 3,6-dihydro-1,2-dioxin generated through the photooxidation of 1-3 butadiene with singlet oxygen has been investigated by Kondo et al. (1978). On the basis of findings, explanations have been provided in support of half-chair-half-chair interconversions of such endoperoxide products (Kondo et al., 1978). The formula expressed as $\Delta G_c^{\ddagger} = 4.56 \text{ X } 10 \text{ -3 } T_c(9.97 + \log T_c/\delta v)$(kcal/mol) allows for the calculation of the free energy of activation for conformational equilibria represented by $\Delta G_c^{\ddagger}$ through the coalescence temperature denoted by T_c and the chemical shift difference between the two peaks given by δv (Kondo et al., 1978).

Figure 27 displays the ^{1}H NMR peaks representative of the methyl group of the endoperoxide product at a series of different temperatures. Two separate peaks are observed until a coalescence temperature of 65 º is reached. The temperature dependence ^{1}H NMR confirms half-chair-half-chair interconversions for the endoperoxide product. Using the above equation, a coalescence temperature, T_c, of 343.15 K and a chemical shift difference, δv, of 22.97 Hz a Gibbs energy of activation, ΔG_c value of 15.8 kcal/mol was obtained.

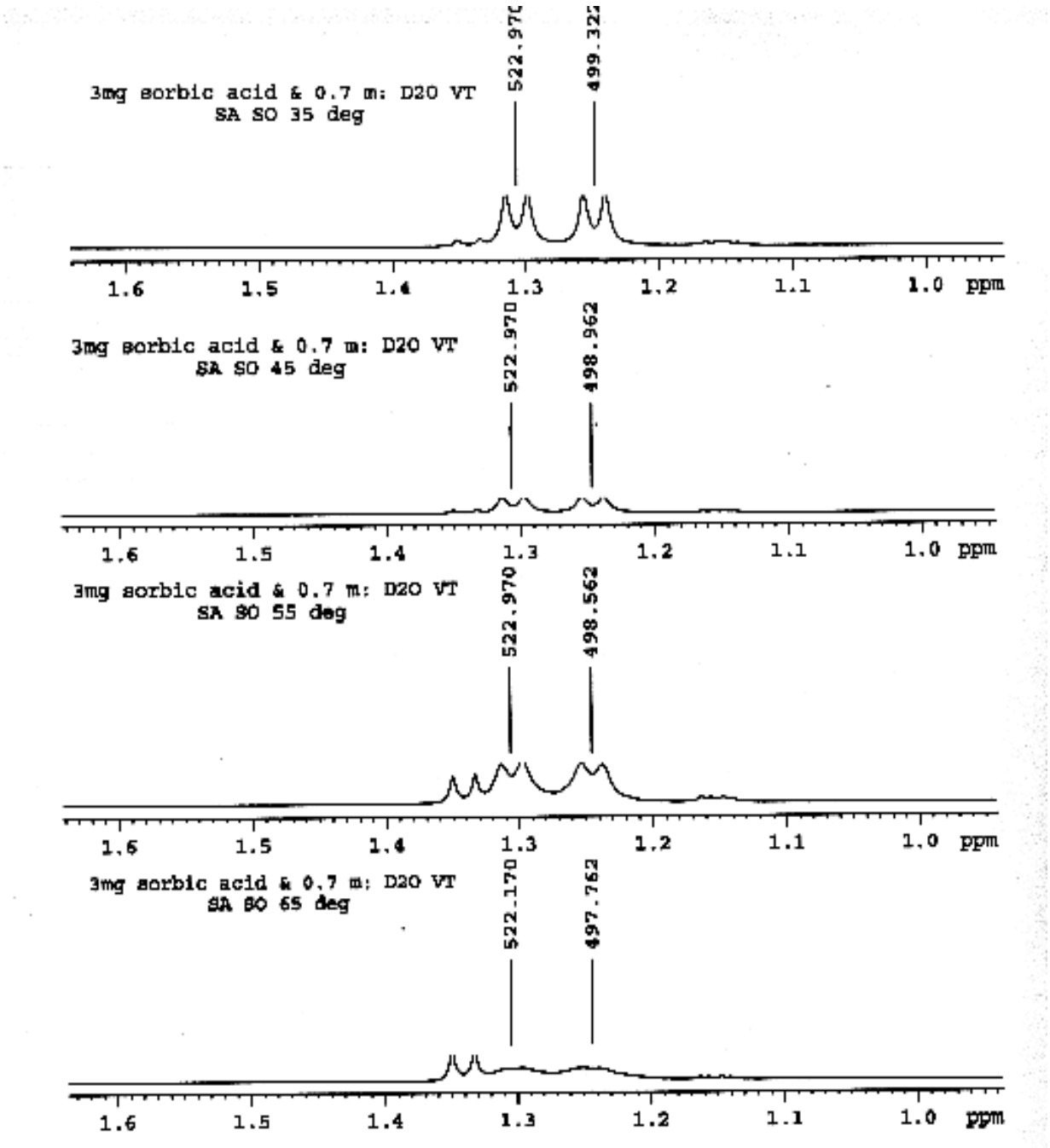

Figure 27: Temperature Control Experiments of the Endoperoxide Product

In order to confirm the structure of the endoperoxide, I used Co(II)TPP as a catalyst to convert the endoperoxide to the highly stable furan. Confirmation of the endoperoxide isomerization was endeavored through the work of O'Shea et al. (1988) which involved the application of Co(II)TPP to produce a furan product upon reaction with the endoperoxide. Cobalt (II) tetraphenylporphyrin Co(II)TPP, is a macrocyclic metal complex with cobalt II coordinated to 4 nitrogen atoms (Kadish et al., 2003). The structure for the compound is shown in Figure 28 (Aldrich, 2012).

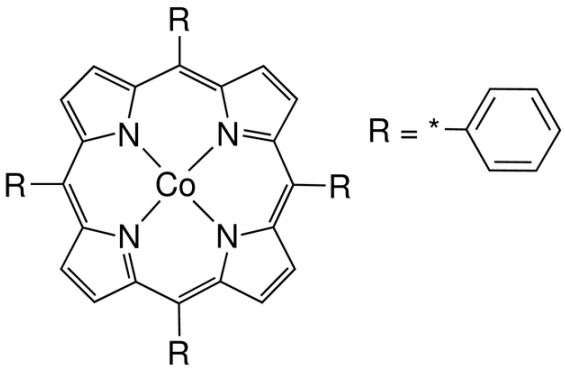

Figure 28: Structure of Co(II)TPP

As a porphyrin, Co(II)TPP is expected to produce a furan upon reaction with an endoperoxide (O'Shea et al., 1988). A proposed mechanism for the reaction involves the catalytic cleavage of the peroxide bond followed by a hydrogen shift, expulsion of Co(II)TPP and closure to form a furan product (O'Shea et al., 1988). The overall reaction scheme is exhibited in Figure 29. Progress of such a reaction was monitored by ^{1}H NMR however no change in the methyl peaks were observed as the peaks remained as two separate doublets. Peaks of the endoperoxide were assessed using COSY for each conformer.

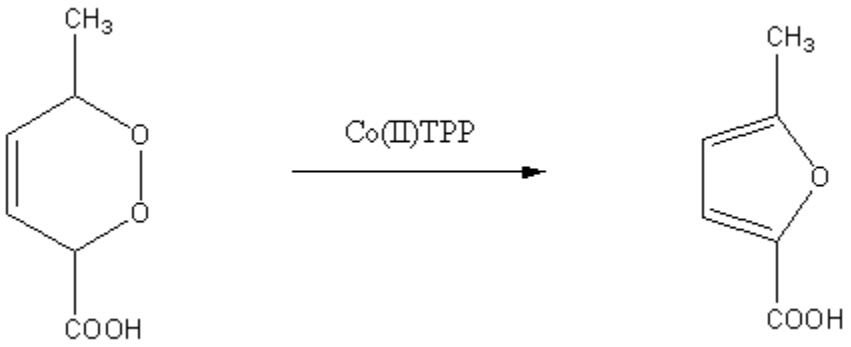

Figure 29: Co(II)TPP Catalyzed Rearrangement of DA Endoperoxide Product to Give a Furan

The chemical shifts of the endoperoxide product for SA are summarized in Table 4 as seen below.

Table 4: ^{1}H NMR Chemical Shifts for SA Endoperoxide Conformers

Position	1H, δ (ppm)	1H, δ (ppm)
1	2.50	3.10
2	5.07	4.87
3	5.81	6.08
4	6.25	6.25
5	4.63	4.65

**Coupling constants and integration values could not be determined due to overlap of peaks*

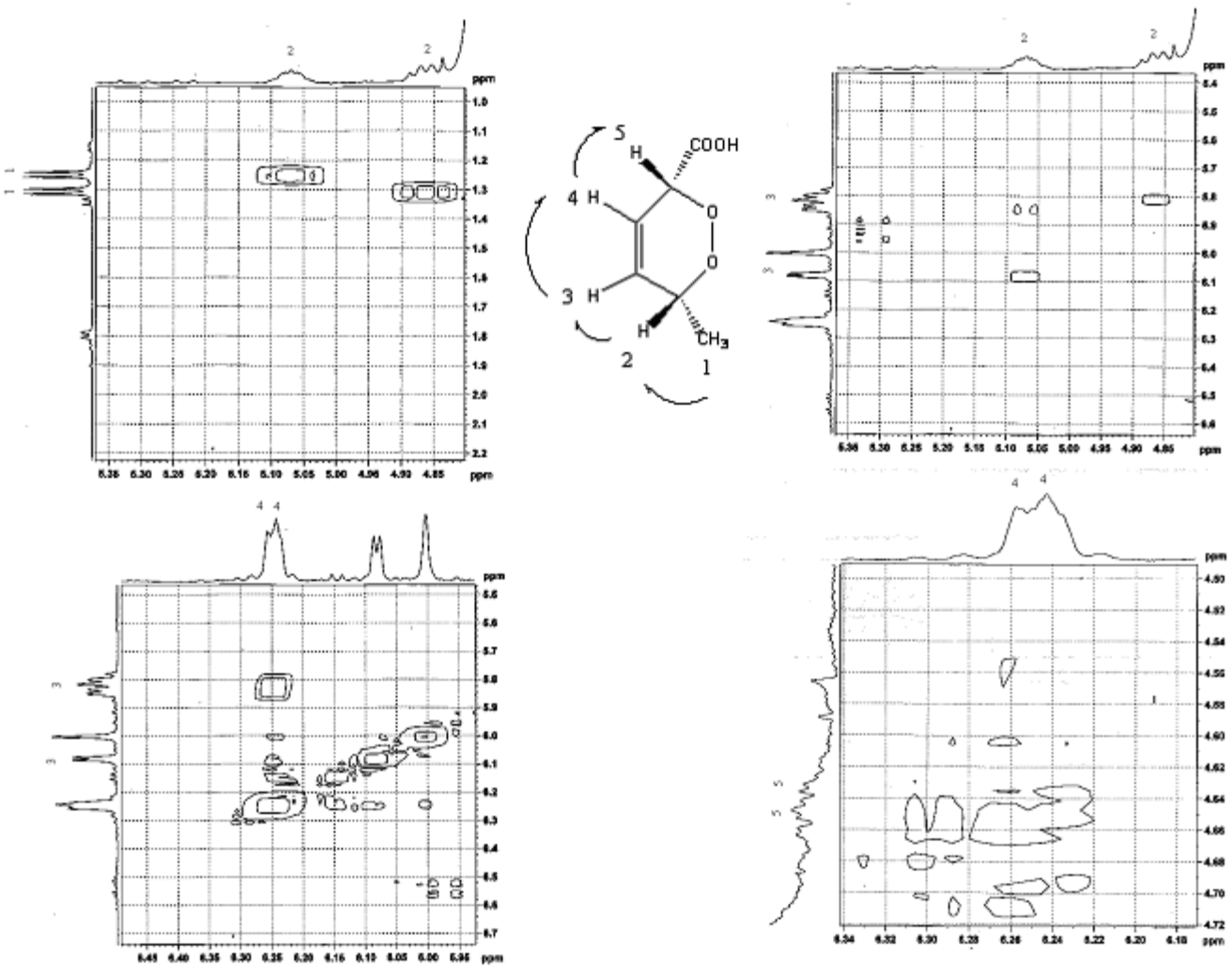

Figure 30: COSY of Endoperoxide Products

Conclusion

Sorbic acid was used as a model compound to investigate the photooxidation products for DA. Upon reaction of singlet oxygen, products resulting from 2 + 2 and Diels Alder reaction were determined. Although the ene reaction was also expected to occur the peaks representing the hydroperoxide product were masked by the starting material and also other products. Neither of the two expected dioxetane intermediates afforded by the 2 + 2 reaction were observed. However three of the four aldehydes expected upon cleavage of the dioxetanes were confirmed. Reaction at the C4-C5 olefin led to generation of the confirmed fumaraldehydic acid and acetaldehyde while reaction at the C2-C3 olefin led to the confirmed crotonaldehyde and the unconfirmed glyoxylic acid.

Two peaks were observed in the methyl region for the endoperoxide product. Upon conducting a temperature controlled ^{1}H NMR experiment the two methyl peaks coalesced at 65 º indicating slow half-chair-half-chair interconversions of the endoperoxide. Through use of 1D and 2D NMR techniques the peaks for both conformers were identified.

Out of the verified products, the endoperoxide was produced in the greatest yield followed by crotonaldehyde, fumaraldehydic acid and then acetaldehyde. Although crotonaldehyde and acetaldehyde were expected to occur at a 1:1 ratio the generation of acetaldehyde was much less than that of crotonaldehyde due to the bubbling off of acetaldehyde. The percents of these products after 7 hours of oxidation of the 3mg SA sample were seen to be ~78% for the endoperoxide, ~1.4% for crotonaldehyde, ~0.84% for fumaraldehydic acid and ~0.2% for acetaldehyde. As no definitive peak could be

identified for the hydroperoxide, the percent composition of the product could not be determined.

Chapter 3

Photooxidation of DA

3.1 Introduction

Domoic Acid (DA), Figure 31, (3-carboxymethyl-4-(2-carboxy-1-methylhexa-1,3-dienyl) proline) [$C_{15}H_{21}NO_6$] with molecular weight 311 (Nemoto et al., 2007; Bell, 2003), is a harmful algal toxin produced by a marine diatom in the genus, *Pseudonitzschia*. Toxicity of DA and its isomers varies depending on the geometry of the double bond in the hexadienyl side chain (Sawant et al., 2010). Research has indicated that the Z configuration on the first double bond of DA shows the highest biological activity because of an increased binding strength of the toxin to KA receptors (Hampson et al., 1992). Until now not much research has been conducted on the toxicity of DA oxidation products and degradation. One possible solution to reduce or eliminate the toxicity of DA is through degradation via photooxidation. I reported the singlet oxygen initiated degradation of my DA model compound, SA occurs at the diene in chapter 2. I expect similar reaction pathways for the singlet oxygenation of DA. The possible reaction pathways are 4 + 2, 2 + 2 and ene processes leading to the products shown in Figure 32. In this chapter, I will first discuss the 2 + 2 reaction followed by the ene reaction and concluded with discussion on the Diels Alder reaction.

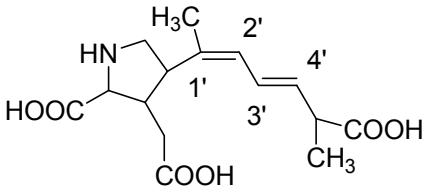

Domoic Acid

Figure 31: Structure of DA

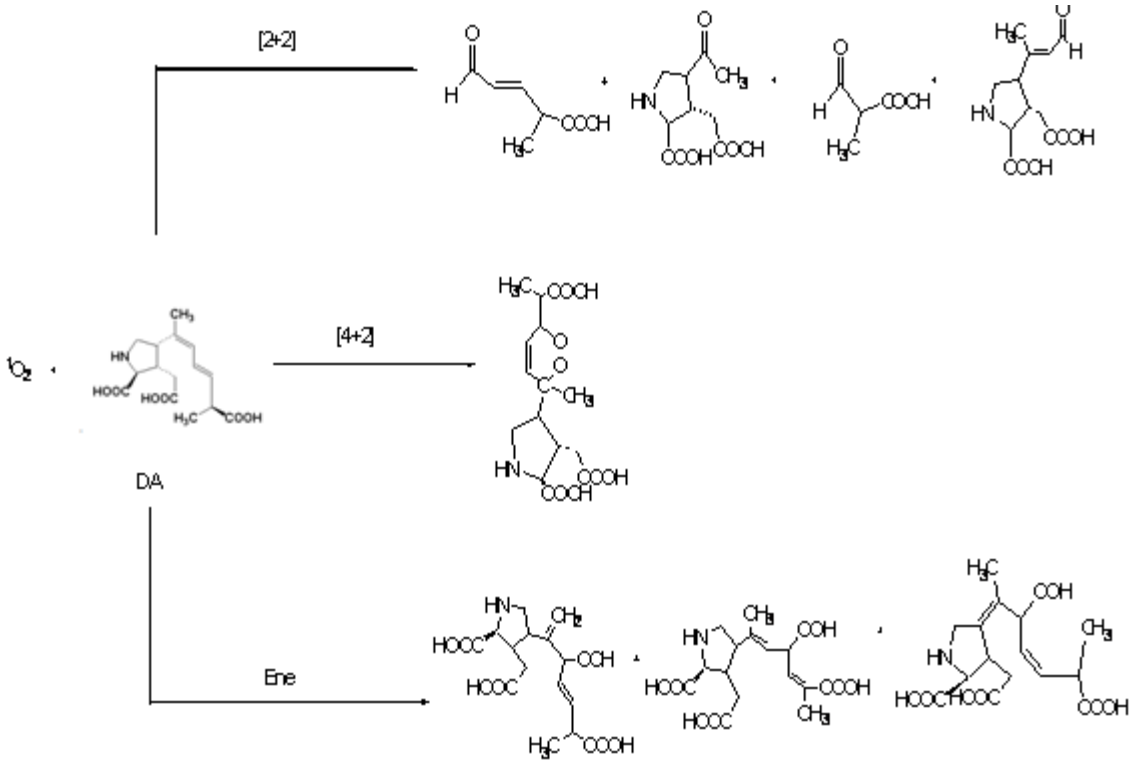

Figure 32: Possible Products of DA Photooxidation

3.2 Experimental

3.2.1 Materials

Domoic acid (MW = 311 g/mol) was purchased from Aldrich and Ascent Scientific based on costs and availability. Deuterium oxide (D_2O), the NMR solvent, was acquired from Cambridge Isotope Laboratories Incorporated. Rose Bengal was purchased from Aldrich. NMR tubes (OD 5 mm) were purchased from Kimble Chase. Kainic acid (MW = 231.25 g/mol) was purchased from Aldrich.

3.2.2 Stock Solutions

The stock solution of 1 mg/1 mL, domoic acid and D_2O was prepared using volumetric glassware, stored in the glass vial containing the original DA and stored in the refrigerator for further use. A stock solution of (1×10^{-4} M) RB and D_2O was also prepared and stored in a glass vial in the refrigerator until used. The glass vial (O.D. 3 cm) containing the RB was sealed to avoid contamination with moisture. A stock solution of 10 mg/ 3 mL, kainic acid and D_2O was prepared using volumetric glassware, stored in the glass vial containing the original KA and stored in the refrigerator for further use.

3.2.3 Sample Preparation

For each experiment 0.1 mL or 0.2 mL of DA/D_2O stock solution was transferred to the NMR tube with 0.7 mL of the Rose Bengal and D_2O stock solution using glass pipets. To ensure complete mixing the sample was sonicated for a minimum of 2 minutes. All NMR tubes were cleaned with acetone and stored in the oven for a minimum time of 8 hours before use. In specific cases, the samples were stored in the refrigerator for further experiments or characterization. Purging of the solution with O_2

gas took place before and during the photooxidation process. Unless indicated otherwise the solution was purged prior for 2 minutes and throughout the irradiation.

3.2.4 Photooxidation

Photooxidation was conducted via a Xenon lamp (Oriel), model 68806, equipped with a heat filter containing deionized water and connected to a lamp housing, model 7240, outfitted with a cooling fan positioned on an adjustable jack. The xenon lamp contained inside, possessed a rating of 15 W and was set to a current of 7.5 Amps. The NMR tube containing the sample was placed in a windowed Dewar filled with water and a thin layer of ice. After one hour of photooxidation, more RB/D_2O solution was added in all cases to compensate for photobleaching of the RB photosensitizer.

3.2.5 Sample Workup

After photooxidation, the NMR tube was removed from the windowed dewar and excess water on the outside of the tube was cleaned off. The tube was kept outside until room temperature was reached before NMR analysis ensued.

3.2.6 NMR Analyses

Oxidation of DA was monitored using NMR (Bruker, 400 MHz and 600 MHz). Magnetic field strengths of 400 and 600 MHz were applied for sample analysis using two different NMR instruments. Both proton and COSY NMR spectra were obtained.

3.2.7 Control Experiments

Prior to commencing any experiments ^1H NMR was taken of the DA/RB solution to identify starting material peaks as shown in Figure. 33. To ensure that both RB and O_2 gas were necessary for the production of singlet oxygen and photooxidation two control experiments were run. The first involved the creation of a DA/D_2O sample with 0.7 mL

of D_2O solution without RB. The sample was gently purged with O_2 gas. As for the second case, another sample was prepared using the RB/D_2O stock solution but the solution was purged with Argon (without O_2). Both samples were irradiated (Xe lamp) for a time of 2 hours and then analyzed via NMR 400 megahertz.

3.2.8 Singlet Oxygenation Experiments

Photooxidation with another DA/D_2O sample followed next with the addition of the RB/D_2O stock. The sample was subject to a slow purging of O_2 gas for 2 hours. The sample was aligned with the beam of the Xe lamp so that the light hit the center of the sample. Such alignment resulted in optimal results as there was no starting material present after the 2 hours.

3.2.9 Montioring of Photooxidation

^{1}H NMR (600 MHz) of a DA/D_2O sample was taken at specific intervals to monitor product formation and identify intermediate products. The sample was irradiated for a total time of 2 hours. The ^{1}H NMR spectra were obtained at 0, 15, 30, 60 and 120 minutes of irradiation. The NMR sample was allowed to equilibrate to room temperature for ease of optimization of shimming and tuning parameters.

3.3 Results and Discussion

3.3.1 Structure Confirmation

Before commencing photooxidation, a proton NMR of DA was taken to identify starting material peaks. Preparation of the sample occurred immediately before NMR analysis to avoid any degradation. A sample was prepared using 0.7 mL of D_2O without RB and spectrum was obtained using the 400 MHz NMR. Peak assignments were made

and then verified by comparison with literature (Kotaki et al., 1996). A sample of DA in RB/D_2O solution was also run to assign the RB peaks in the ^1H NMR spectrum prior to the photooxidation, as shown in Figure 34. However the spectrum in Figure 34 showed additional peaks besides those present for DA and RB. As a result an ^1H NMR was taken of just the RB/D_2O stock solution which showed the same additional peaks shown in Figure 35. These peaks seen to occur at 1.25 ppm, 2.1 ppm and 3.1 ppm are the result of the presence of impurities in the RB stock.

Control experiments were conducted to assess the significance of direct photolysis and energy transfer from RB to DA as shown in Figure 33. Irradiation of the DA sample using the Xe lamp in the presence of RB under Ar purge (no O_2) showed no reaction eliminating the possible involvement of energy transfer induced transformation of DA. To probe the role of direct photolysis a solution purged with O_2 gas without addition of RB was photolyzed. I observed no change in the spectra demonstrating that direct oxidation does not occur under my experimental conditions. Irradiation of a solution with RB, O_2 and DA resulted in rapid transformation producing a complex reaction mixture. These experiments confirm photooxidation processes are occurring.

Further confirmation of the occurrence of photooxidation is shown in Figure 36. Through comparison of Figures 34 and 36 the presence of new peaks can be observed. These new peaks have been assigned to 3 major products including an aldehyde, a hydroperoxide and an endoperoxide. With better alignment and a more consistent flow of oxygen gas to the sample the maximum yield of products obtained was roughly 0.49% of the endoperoxide, 0.62% of the hydroperoxide and 0.24% of the aldehyde. The

analysis performed for assignment of these peaks to the above mentioned products will be discussed in this chapter.

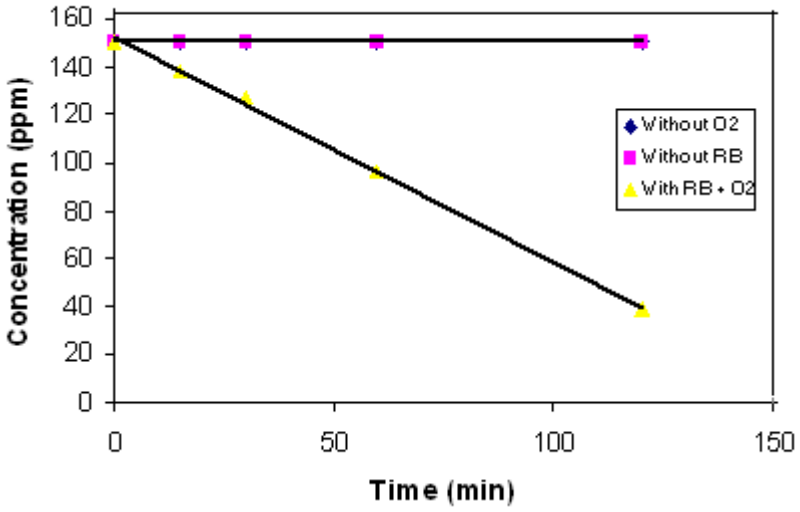

Figure 33: Control Experiments for Photooxidation of DA

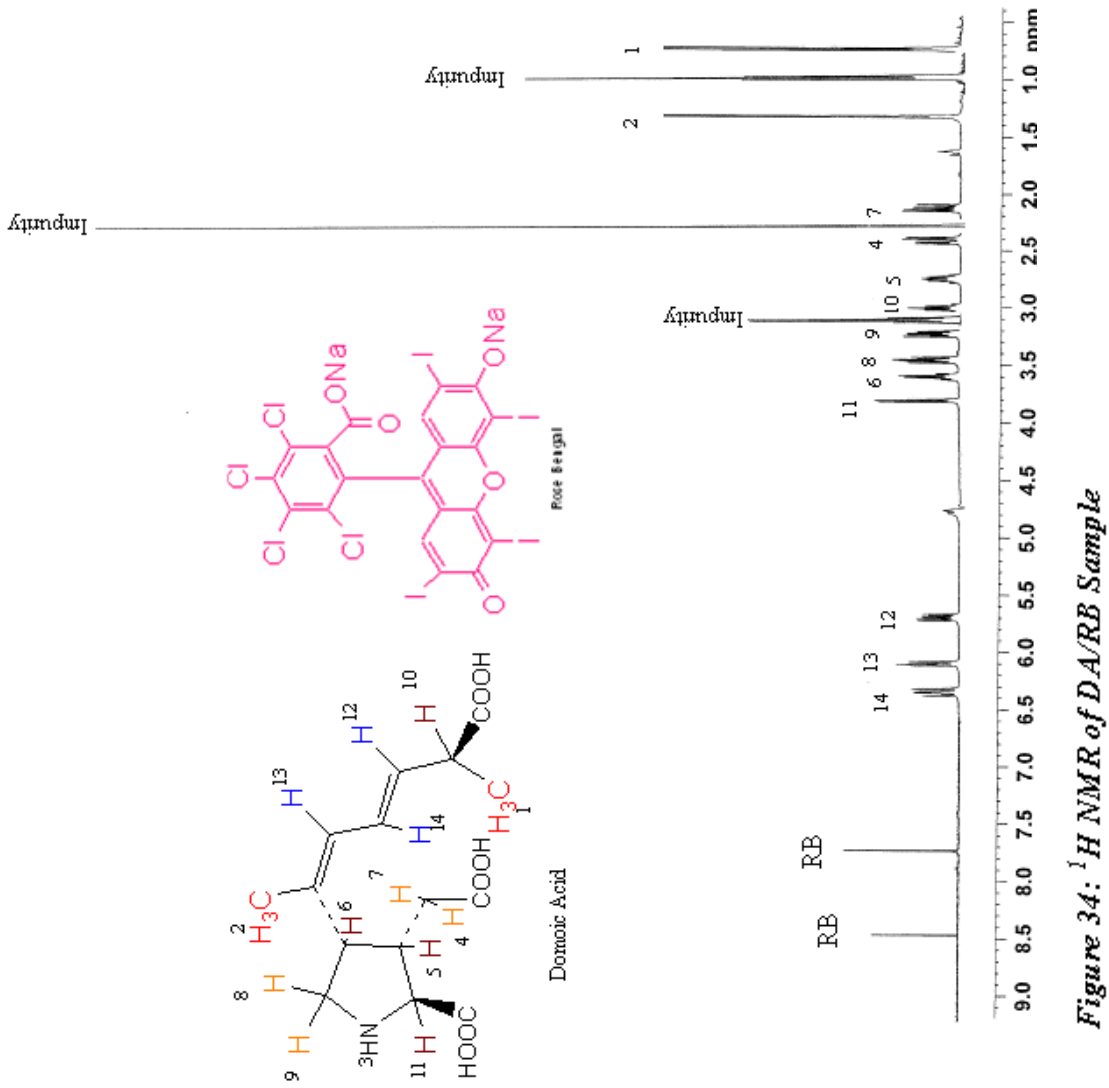

Figure 34: ^{1}H NMR of DA/RB Sample

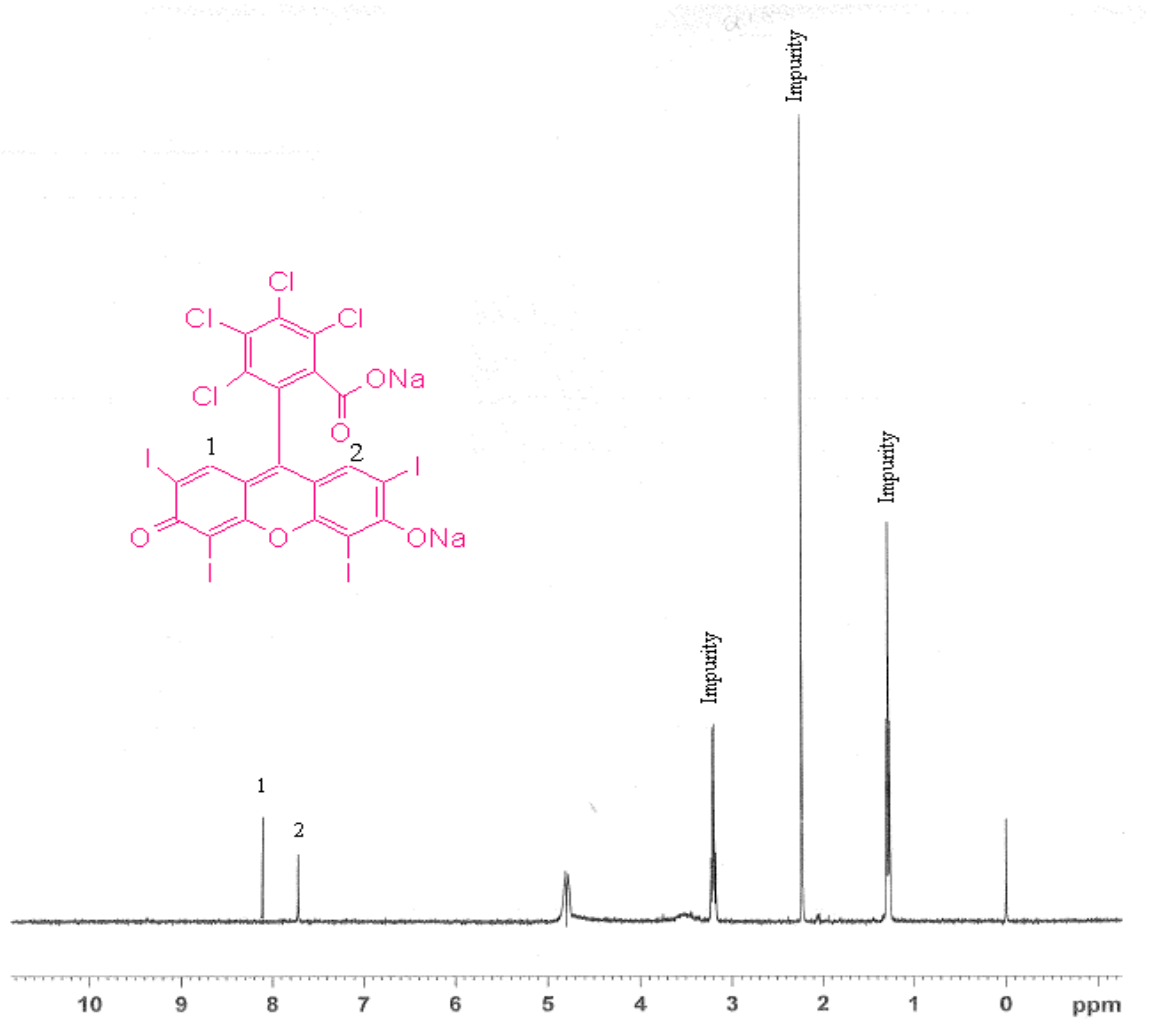

Figure 35: ^{1}H NMR of RB/D_2O Stock Solution

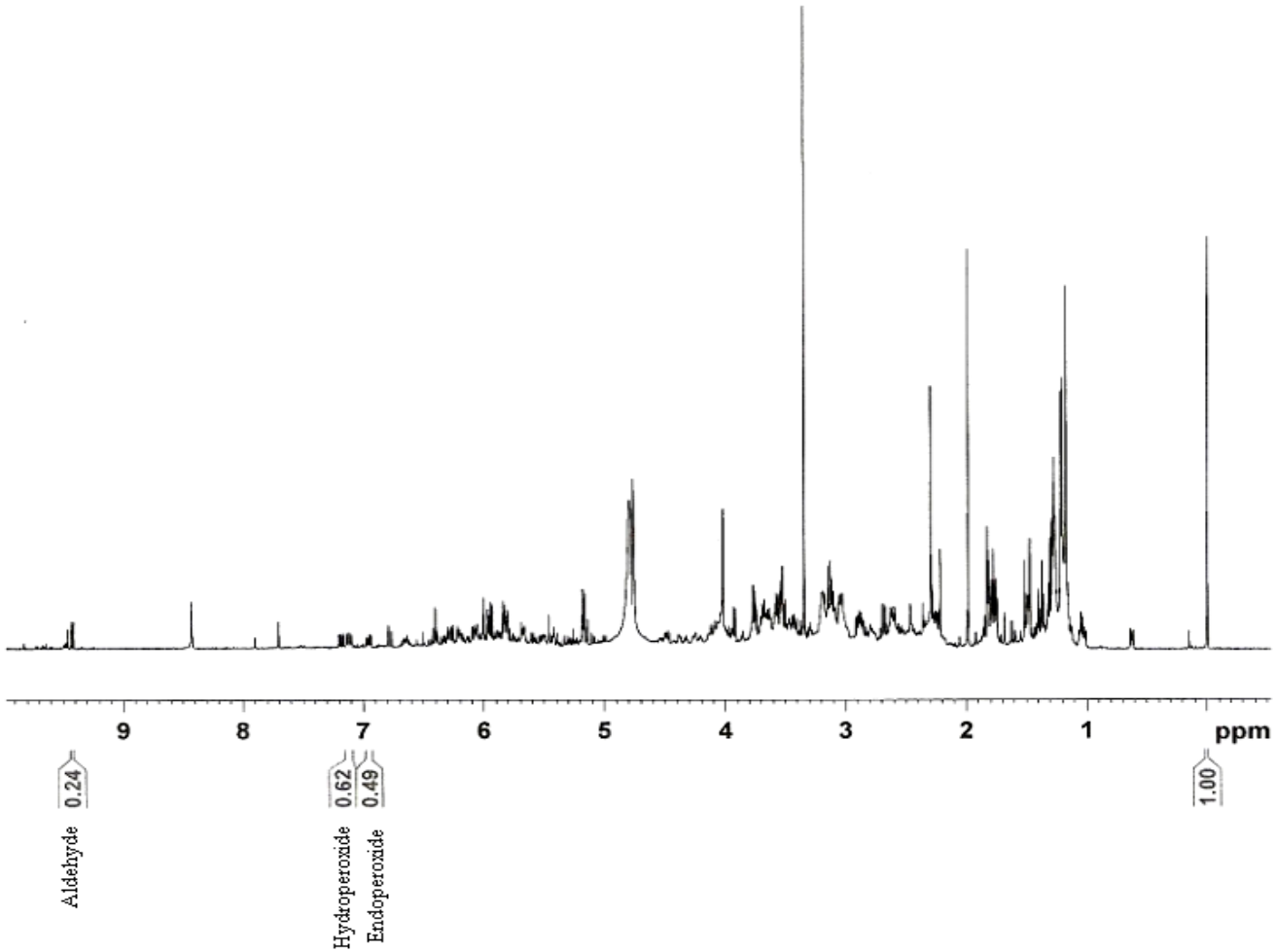

Figure 36: Integration values of DA Photooxidation Products

The photooxidation of DA, as a function of time was monitored at 0, 15, 30, 60 and 120 minutes using the NMR (400 MHz) as illustrated in Figure 37. The reaction times are strongly dependent on sample alignment in the light beam, sample concentration and O_2 purge. Results demonstrate that there is still starting material present after a total reaction time of 2 hours however appearance of additional peaks in the aldehyde and diene regions indicate reaction has occurred. Reaction times were varied based on desired results, product formation was significant after 30 minutes of irradiation and among the initial products are characteristic peaks indicating aldehyde products. As the aldehyde peak was easily observed, the corresponding product was analyzed first.

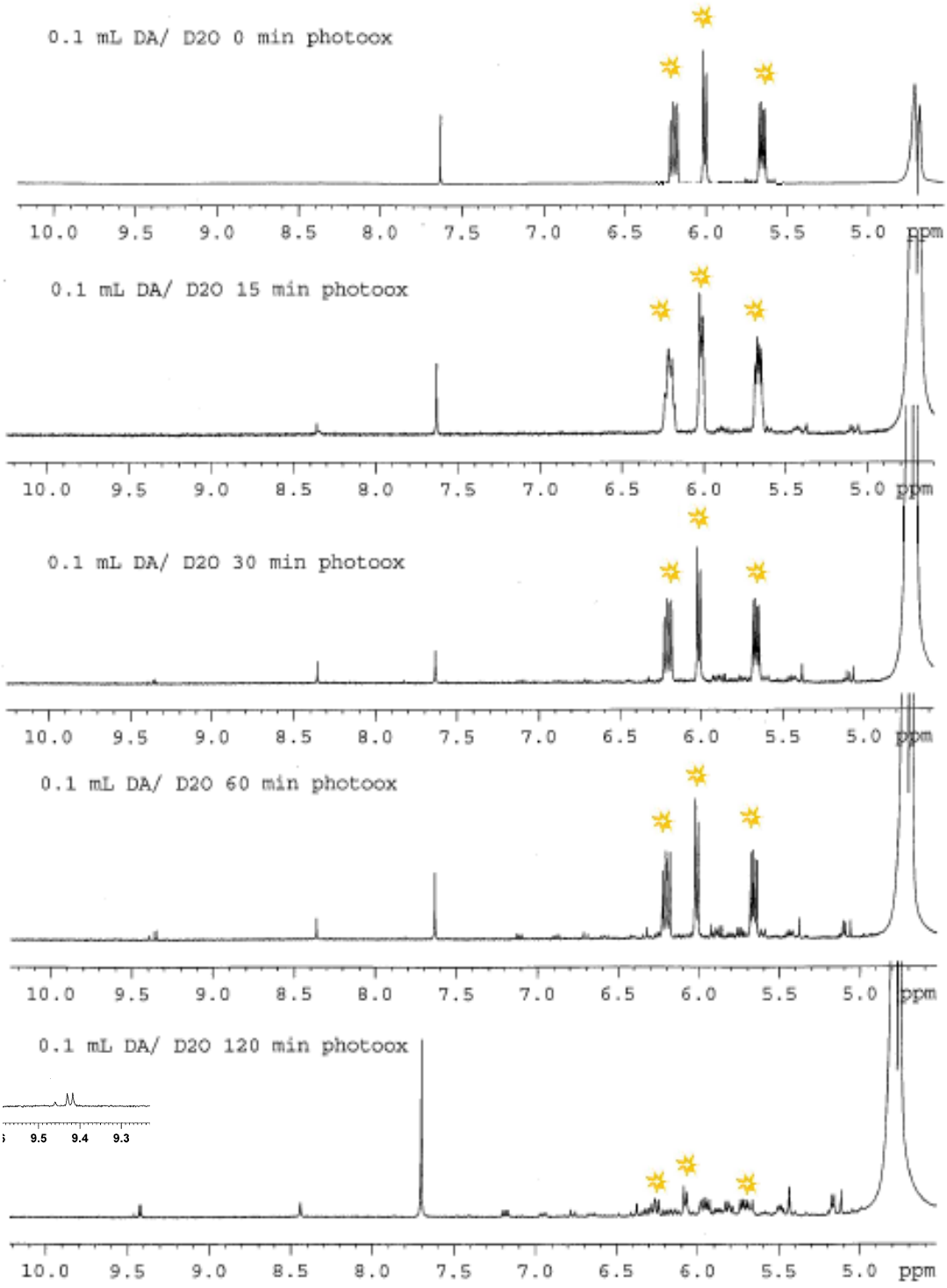

Figure 37: Time Profile for DA Photooxidation

First I attempted to assign peaks and compounds resulting from the 2 + 2 addition. While the 2 + 2 yields a dioxetane it readily collapses to the corresponding carbonyl compounds at room temperature. With this in mind, I begin my assignments in the 9-10 ppm region characteristic of aldehyde peaks. Reaction of DA and $^1O_2$ at the C1'-C2' bond affords the aldehyde product denoted A and the methyl ketone product represented as A' as depicted in Figure 38. The C1-C2 bond is more substituted and thus more electron rich and expected to be more reactive towards $^1O_2$. Reaction at the C3'-C4' bond would produce the aldehyde products labeled B and B'.

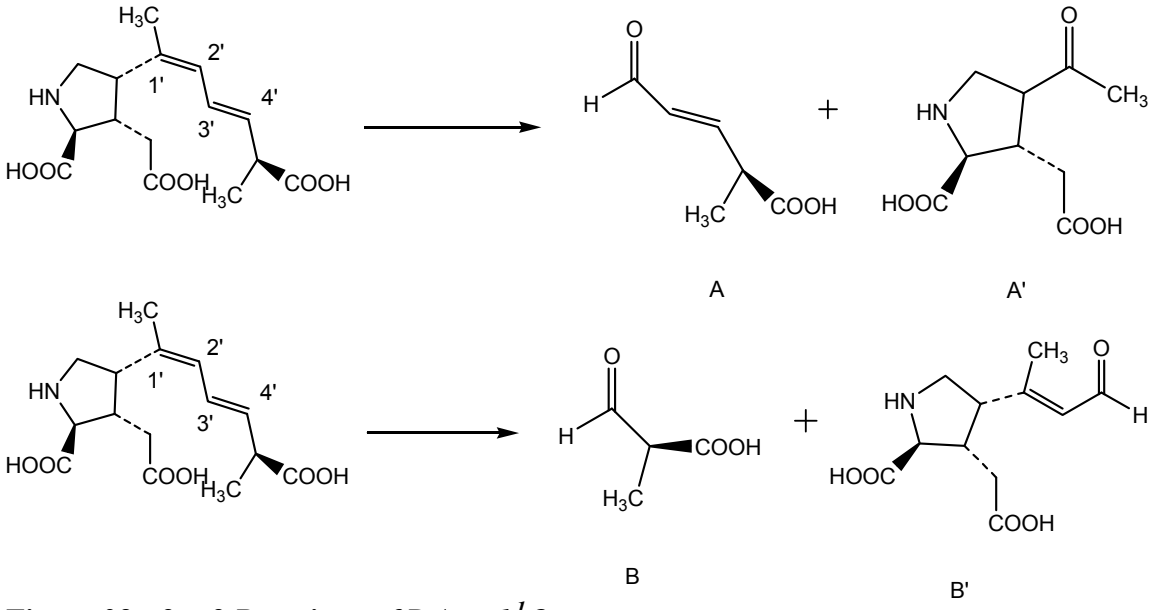

Figure 38: 2 + 2 Reactions of DA and $^1O_2$

The ^{1}H NMR spectra obtained for the reaction mixture of DA and $^1O_2$ products exhibits only a doublet peak in the aldehyde region. Reaction at the C3-C4 bond yields two aldehyde products which would show two doublets in the aldehyde region. Such peaks were not observed indicating no measurable reaction via 2 + 2 at the C3-C4 bond. Unlike SA in which only aldehydes are formed at reaction with both double bonds a

ketone is made as the C1'-C2' bond in DA is trisubstituted instead of disubstituted. The aldehyde peak at 9.35 ppm indicates "A" as a reaction product. Analysis of the aldehyde product has been conducted through COSY NMR spectra shown in Figure 40. Assignments have been made using the numbered structure for the aldehyde below in Figure 39.

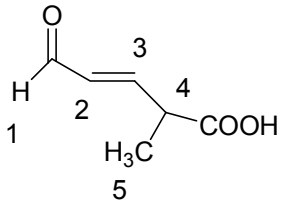

Figure 39: Numbered Structure of DA Aldehyde Product

The NMR spectra indicate only one aldehydic doublet at 9.35 ppm proposed as the product from collapse of the C1'-C2' dioxetane and labeled as H1 in Figure 39. The measured coupling constant for H1 of 8.40 Hz is in good agreement with the literature values for such a proton. In the COSY spectrum, H1 is coupled to a peak at 6.13 ppm which I assign as H2. Although identification of the chemical shift can be established via COSY accurate integration values and coupling constants cannot be made due to overlap of peaks. The H2-H3 coupling occurs at a chemical shift value of 7.11 ppm. However the peak shows an integration value which indicates overlapping peaks in this region. Continuing with my assignment from the COSY spectrum confirmation of the methine proton H4 is seen through COSY via coupling to H3. The H4 peak shows at 3.3 ppm and couples to a peak at 1.23 ppm assigned to H5. All the peaks of this aldehyde product, except for the aldehyde peak at 9.35 ppm, are masked by other peaks based on complex sets of peaks. The chemical shifts for the respective peaks are listed in Table 5.

Table 5: ^{1}H NMR Chemical Shifts for the DA Aldehyde Product

Position	1H, δ (ppm)
1	9.36
2	6.13
3	7.11
4	3.30
5	1.23

* Integration values and coupling constants were not given due to overlap of peaks for some protons

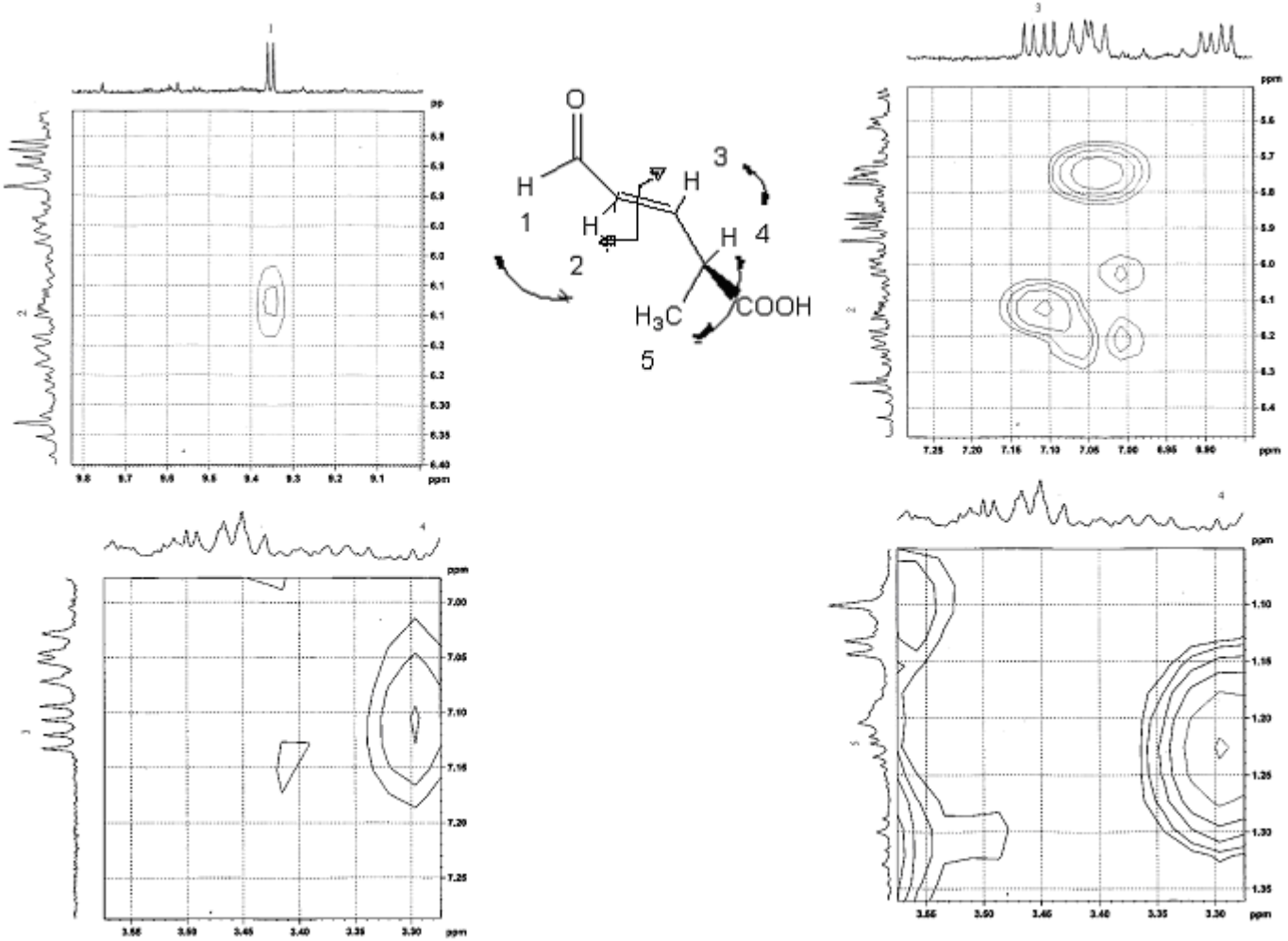

Figure 40 : COSY Spectra of the DA Aldehyde Product (E)-2-Methyl-5-Oxopent-3-enoic Acid

Complementary to this aldehyde product was the methyl ketone labeled A' in Figure 38. Identification of the product proved difficult because of the complex nature of the ^{1}H NMR coupling expected for the compound and the heavy overlap of peaks in the aliphatic region (1.5-2.5 ppm). An authentic sample of the methyl ketone would help confirm its presence in the reaction solution. The methyl ketone is not commercially available, but could be produced by oxidation of DA or kainic acid (KA). Given that the cost of KA is half of DA I chose to employ KA for my initial attempts to synthesize a methyl ketone.

3.3.2 Kainic Acid

Kainic acid (KA), Figure 41, (2-Carboxy-3-carboxymethyl-4-isopropenylpyrrolidine) [$C_{10}H_{15}NO_4$] with molecular weight 231.25 (Aldrich, 2012) is a compound that may also be used as a model for DA. KA is an amino acid that contains a pyrrolidine ring with three stereogenic centers (Anderson et al., 2003).

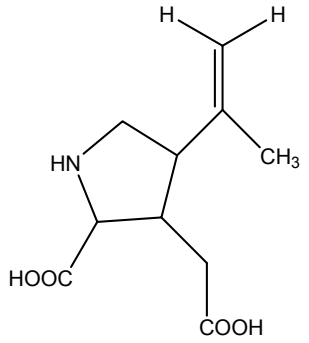

Kainic Acid

Figure 41: Structure of KA

3.3.3 Oxidation of Kainic Acid

Two methods were attempted to oxidize KA. The conjugated diene region of KA should be subject to oxidative cleavage by ozonolysis to yield the desired methyl ketone adduct, shown in Figure 42 (Hart et al., 2011). There are a number of ways to generate O_3, I employed an ozone generator which operates via the passing of O_2 through a high voltage spark created by a Tesla coil (Millar, 1998). Although a definite possibility, the final reductive step of the ozonolysis procedure offers complications for product purification (Isobe et al., 1977; Dai et al., 2004). A solution proposed by Schiaffo et al. (2008) entailed the use of water with a water-miscible organic solvent to act as a nucleophile for carbonyl oxides based on the idea of a phase transfer catalyst (PTC).

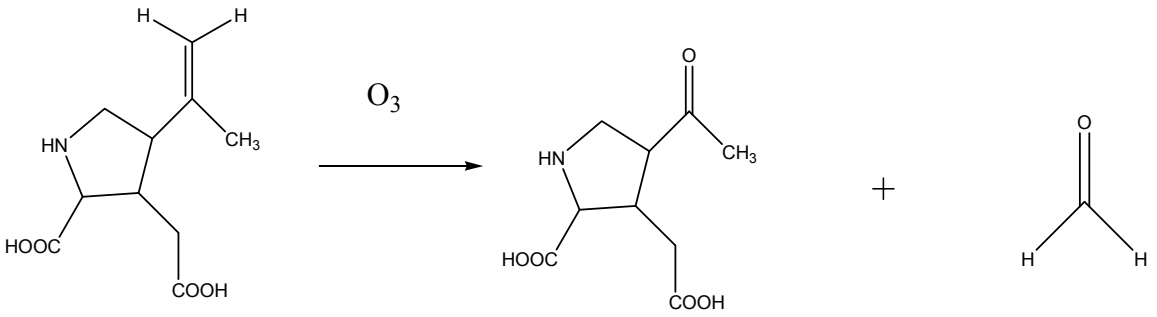

Kainic Acid

Figure 42: Reductive Ozonolysis of KA

An alternative method for the oxidation of KA involves the use of $KMnO_4$. When used as an oxidizing agent for alkenes $KMnO_4$ is reduced to manganese dioxide (Morse, 1905). As a strong oxidizing agent, $KMnO_4$ first reacts with alkenes to produce

diols which then oxidize to form the corresponding carbonyl compounds (Fox et al., 2004).

3.3.4 Ozonolysis of Styrene to Confirm Production of O_3

Styrene was used as an initial compound for establishing the oxidation conditions. Styrene should produce benzaldehyde and formaldehyde through cleavage of the double bond as seen in Figure 43.

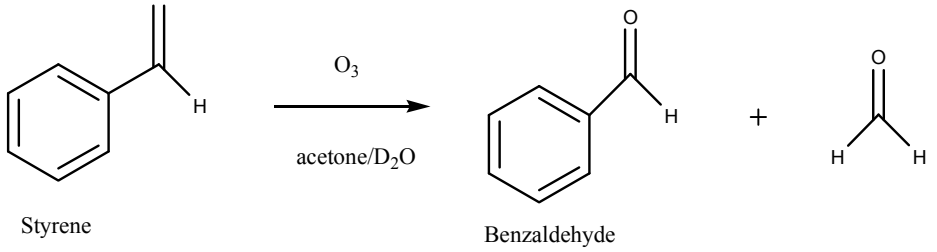

Figure 43: Reductive Ozonolysis of Styrene to form Benzaldehyde and Formaldehyde

Styrene (5.52 μL) was transferred into a glass test tube along with 4.75 mL of acetone and 0.25 mL of D_2O. The reaction solution was then purged with O_2 gas for two minutes and prior to turning on the ozone generator. The reaction ran for 75 minutes. After 75 minutes, the ozone generator was turned off and the reaction mixture was purged with O_2 gas for another 2 minutes. The reaction solution was diluted with 5 mL of water and the mixture extracted twice with CH_2Cl_2 (5 mL) and once with hexanes (5 mL). The organic layers were combined and then dried with Na_2SO_4. The Na_2SO_4 was then gravity filtered off and the resulting solution was rotovapped to remove CH_2Cl_2 and hexanes. Analysis of the mixture by ^1H NMR (400 MHz) resulted in a spectrum without the aldehyde peak (9-10 ppm) expected for the benzaldehyde product. Subsequent repeat of the experiment gave similar results without any indication of oxidative cleavage.

Failure to observe peaks in the aldehyde region led to the trial of a new oxidation technique and may be a result of the lack of significant ozone production as a result of the generator.

3.3.5 Oxidation of KA with $KMnO_4$

Given the inability to achieve oxidative cleavage using the available O_3 in our laboratory, I chose to use $KMnO_4$ as an oxidant to KA to make the desired methyl ketone following a procedure described in Laboratory Manual Organic Chemistry I & II (Keller et al., 2010). A KA/D_2O stock solution (0.2 mL) was placed in an NMR tube. The tube was capped with a needle pierced through the top for ventilation and placed in a hot water bath set at approximately 60 º for 2 hours. After heating, the hot solution was gravity filtered using Whatman 4 filter paper to remove MnO_2 solids. Several attempts were made with the utilization of higher temperatures and longer reaction times. Unfortunately repeated attempts to obtain clean spectrum of the desired compound were unsuccessful. Difficulties with the procedure included small scale reactions (1-2 mg), work-up and interference from MnO_2, relatively messy spectra including starting material and undesired by-products.

3.3.6 Refining Conditions for MnO_4 Oxidation

Crotonic acid as a model to establish conditions for oxidative cleavage of double bonds, was oxidized to produce glyoxylic acid and acetaldehyde as a side product as seen in Figure 44.

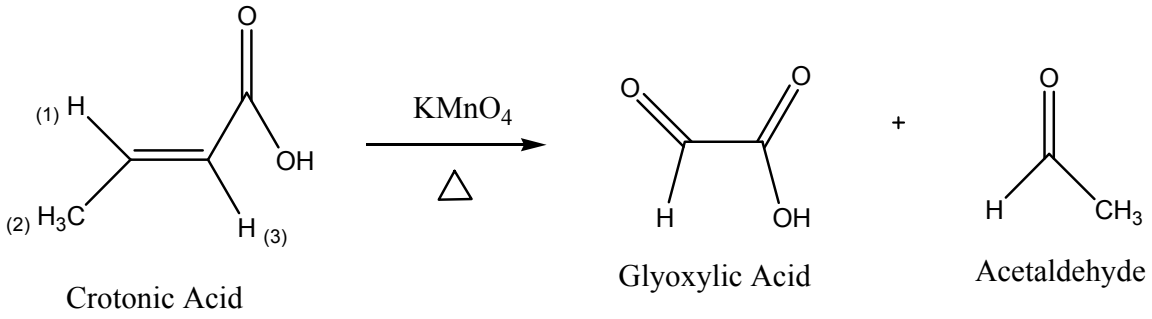

Crotonic Acid

Glyoxylic Acid

Acetaldehyde

Figure 44: Oxidation of Crotonic Acid Using $KMnO_4$ to Produce Glyoxylic Acid and Acetaldehyde

Crotonic acid (0.00538 g) was placed inside an NMR tube followed by the addition of D_2O (0.7 mL) and ^1H NMR (400 MHz) was taken of this starting material. Another sample was prepared with crotonic acid (5 mg) with the addition of Millipore water (432.7 μL) and $KMnO_4$ (0.200 g). The reaction mixture was heated in a hot water bath at approximately 70 º for 1 hour using the high heat setting of the heating mantle. After allowing the solution to equilibrate to room temperature, CH_2Cl_2 (0.75 mL) was added and extraction was performed once. Crotonic acid established clean oxidation. Analysis of the resulting mixture was performed via ^1H NMR (400 MHz) glyoxylic acid δ: 5.3; acetaldehyde δ: 2.1, 9.7.

3.3.7 KA Oxidation (Revisited)

On the basis of the success from the oxidation of crotonic acid, an attempt was made to obtain the methyl ketone oxidation product of kainic acid. Kainic acid stock solution (0.2 mL) was placed in an NMR tube. Deuterium oxide (0.6 mL) was also added to the NMR tube followed by addition of potassium permanganate (0.0012 g). The NMR tube was then kept in a hot water bath at approximately 70 º for 2 hours. Work up of the reaction involved extraction using CH_2Cl_2 (0.2 mL) followed by ^1H NMR (400 MHz)

analysis of the organic layer however a product could not be identified. However no product was detected likely the result of the inability of the methyl ketone to dissolve in dichloromethane.

Alternatively kainic acid (0.2 mL) was placed inside an NMR tube along with the appropriate amounts of D_2O and $KMnO_4$ as before. Heating of the NMR tube took place in a water bath set at 75 º for a time of 2 hours. After heating, the solution was filtered through a pipet and extra amounts of unreacted $KMnO_4$ were quenched by adding a small amount of sodium bisulfite resulting in a clear solution. The resulting solution was analyzed via ^1H NMR (400 MHz). While numerous variations in reaction conditions and workup were attempted the isolation of the methyl ketone was unsuccessful. I did not pursue this further.

The next set of products I attempted to identify were hydroperoxides. The ene reaction of $^1O_2$ can yield the three hydroperoxides depicted in Figure 45. The least likely product is "C" since tertiary hydrogens are the least likely to be abstracted (Kurti et al., 2005). Through comparison of the reactions leading to products "A" and "B" greater formation of product A is predicted by the fact that the proton that is abstracted to produce "B" is more hindered than that needed to produce "A". There are three equivalent protons that may be abstracted to give product "A".

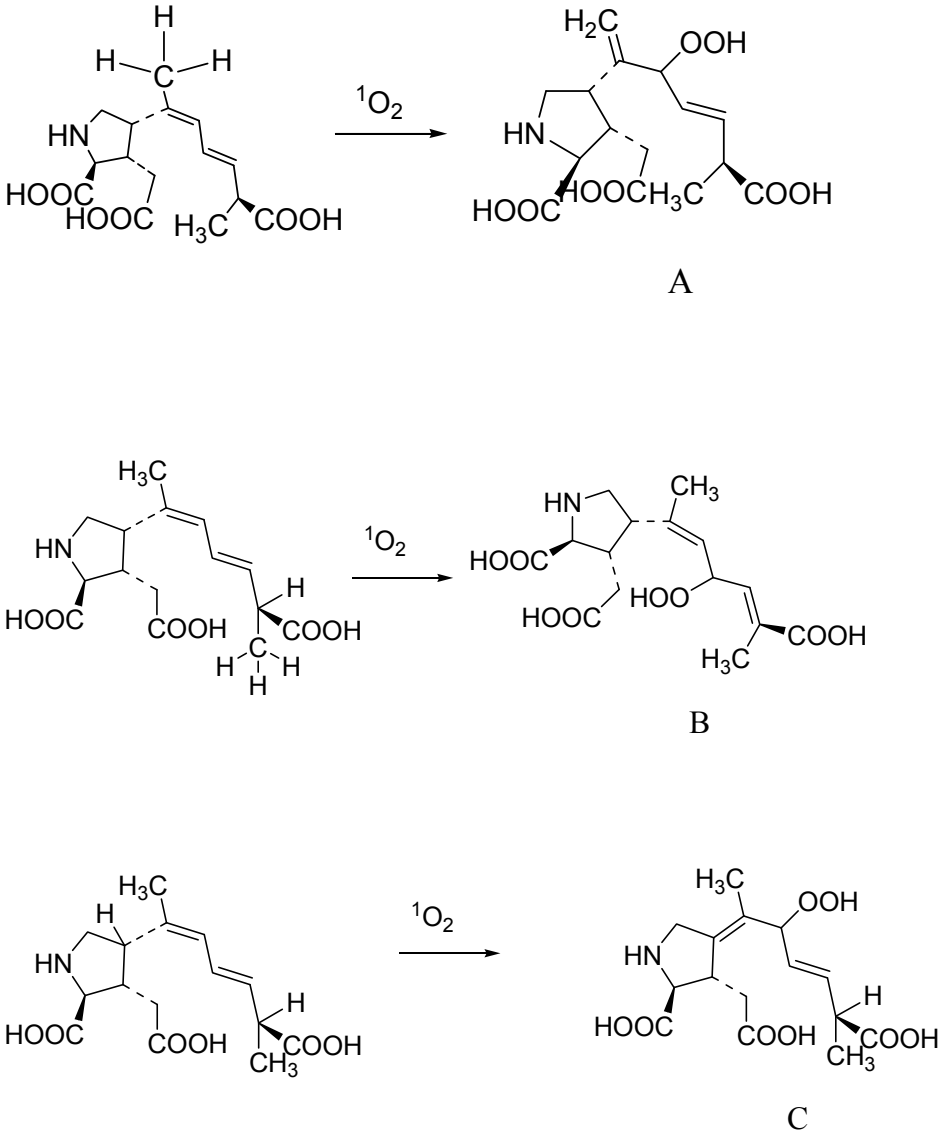

Figure 45: Possible Ene Reactions for DA

Although three hydroperoxide products are possible, using the ^{1}H NMR, I was able to assign peaks consistent with the one expected major hydroperoxide. Peak assignments of the hydroperoxide product were made using the numbered structure shown in Figure 46.

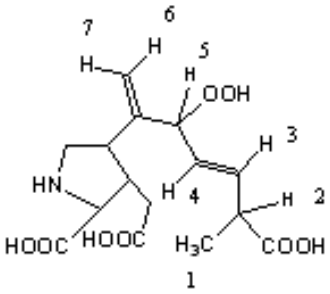

Figure 46: Numbered Structure of Hydroperoxide Product

Observation of the ^{1}H NMR in Figure 48 reveals H1 to have an upfield shift of 1.15 ppm and a coupling constant of 7.7 Hz. Using COSY in Figure 47, H1 is seen to couple to a peak at 3.10 ppm which is assigned as H2. The coupling constants for H2 are 6.8 Hz and 6.5 Hz which are consistent of coupling to a methyl group and an olefinic proton respectively. Further confirmation of peak assignments is provided through integration values. The ratio of integration values for H1/H2 is 1.12/0.38 which falls in near proximity to the expected 3/1 ratio. COSY shows H2 couples to a peak with a chemical shift value of 6.95 ppm assigned to H3. As H3 couples with both a methine proton and an olefinic proton the multiplicity of the peak is expected to be a doublet of doublets. The coupling constants of 7.3 Hz corresponding to coupling with a methine proton and a trans coupling constant of 15.1 Hz based on coupling with an olefinic proton confirm this. The integration ratio of 0.38/0.31 is close to the expected ratio of 1/1 for H2/H3. The H3 proton couples to a peak seen at 5.80 ppm assigned to H4 which is

predicted to have a doublet of doublets splitting pattern. The coupling constants for H4 are 9.1 Hz and 15.5 Hz due to coupling with a methine proton and an olefinic proton respectively. The integration ratio of 0.31/0.43 fits near the expected integration ratio of 1/1 for H3/H4. Via the COSY it is observed that H4 couples to a peak at 5.15 ppm assigned as H5. With a splitting pattern of a doublet H5 shows a coupling constant of 8.2 Hz, which is in good agreement with coupling to an olefinic proton. The integration ratio for H4/H5 is 0.43/0.32 which is close to the expected 1/1 ratio. From the COSY it seems as though H5 may couple other protons at around 5.00 ppm. This may be a result of long range coupling with the geminal protons H6 and H7. The coupling constants and integration values for these protons however could not be determined as a result of overlap with other product peaks. These values have all been summarized in Table 6.

Table 6: ^{1}H NMR Chemical Shifts, Coupling Constants and Integration Values for DA Hydroperoxide Product

Position	1H, δ (ppm)	J (Hz)	Integration
1	1.15	7.7	1.12
2	3.10	6.8, 6.5	0.38
3	6.95	7.3, 15.1	0.31
4	5.80	15.5, 9.1	0.43
5	5.15	8.2	0.32

** Not all coupling constants and integration values could be obtained due to overlap of peaks*

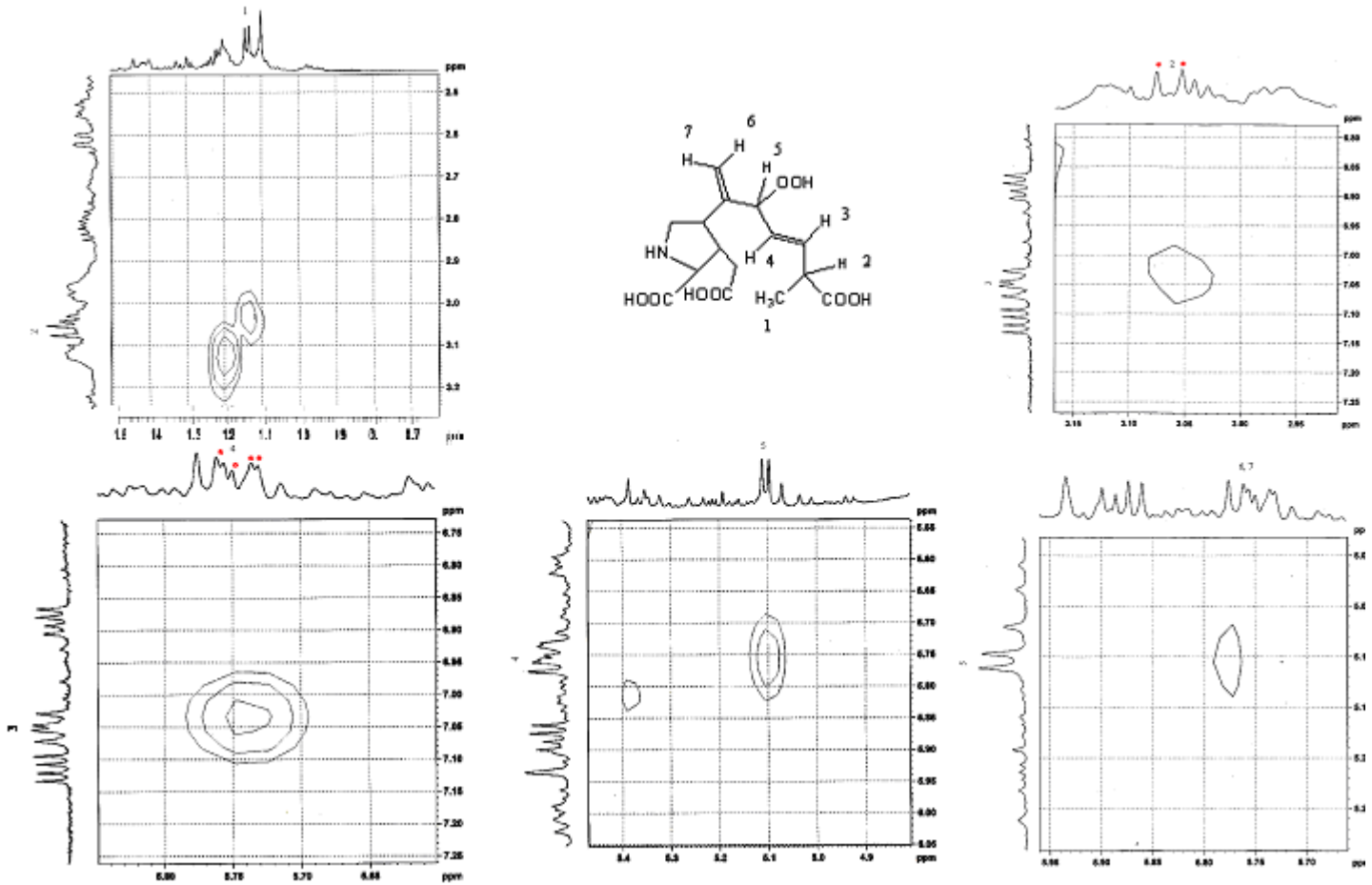

Figure 47 : COSY for DA Hydroperoxide Product

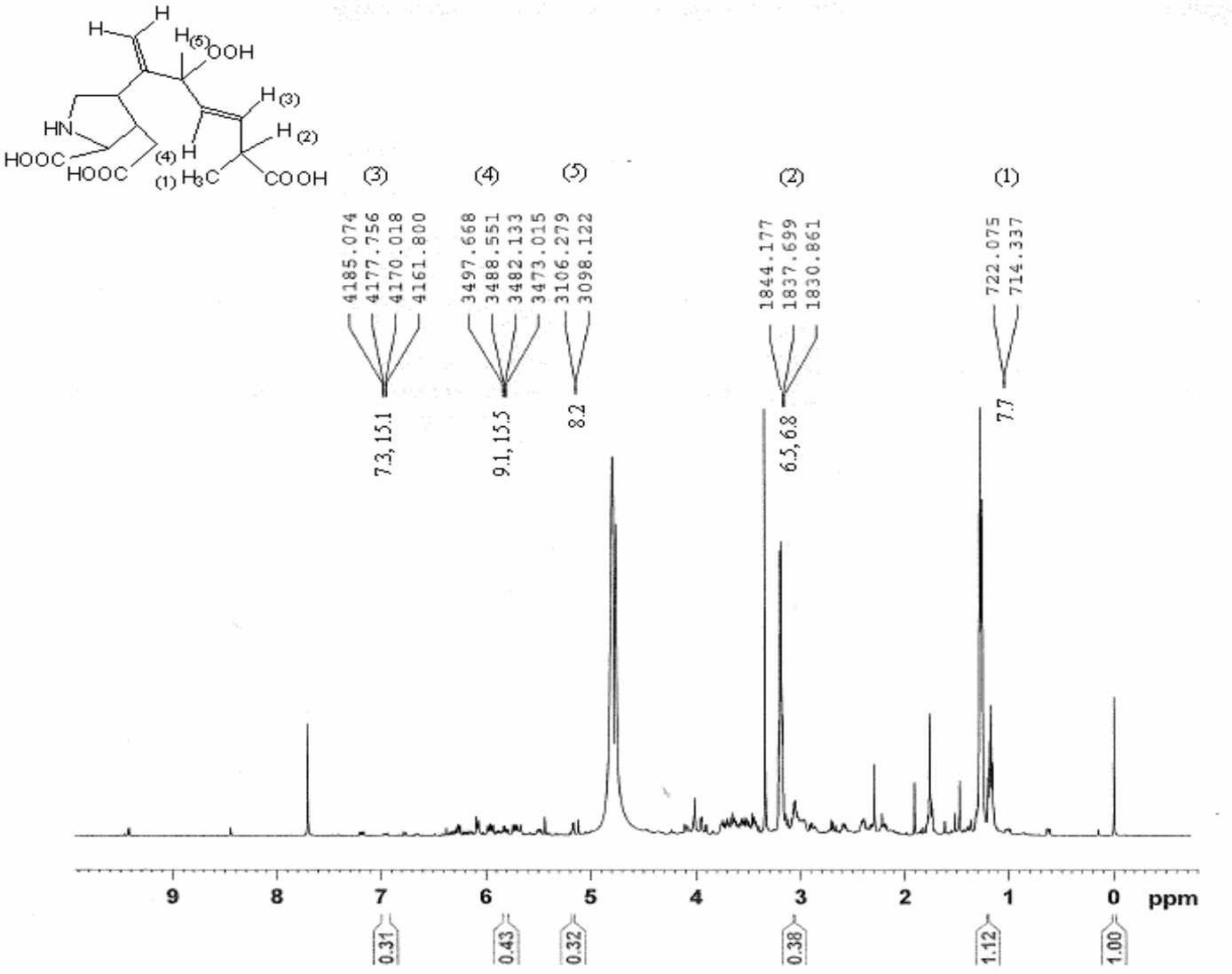

Figure 48 : ^{1}H NMR Showing DA Hydroperoxide Product Peaks

The next expected product which I tried to identify was the endoperoxide. The 4 + 2 product is an endoperoxide resulting from a Diels Alder reaction between DA and singlet oxygen as displayed in Figure 49. As singlet oxygen is able to attack either from the bottom or the top, a pair of diastereomeric products are expected. However, only one endoperoxide product has been identified using 1D and 2D NMR. Peak assignments have been finalized via COSY analysis as displayed in Figure 51 with all product peaks displayed in the ^{1}H NMR spectrum in Figure 52.

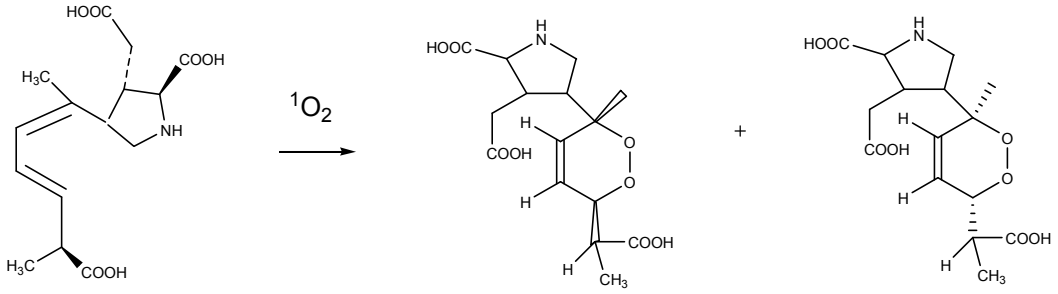

Figure 49: Diels-Alder Reaction between DA and Singlet Oxygen to Give an Endoperoxide

Assignments for the endoperoxide peak were made using both 1D and 2D NMR. Peak assignments have been made relative to the endoperoxide structure depicted in Figure 50.

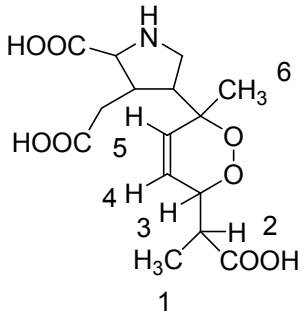

Figure 50: Endoperoxide Structure with Numerically Assigned Protons

For the endoperoxide product, the peak present at 1.17 is indicative of a methyl group and represents H1. With a coupling constant of 6.8 Hz a reasonable assumption can be made in regards with H1 coupling to a methine proton. Through the COSY H1 is seen to couple to a peak at 2.73 ppm assigned as H2. The coupling constant for H2 is 6.2 Hz which is in good agreement for coupling to an aliphatic proton. As with the hydroperoxide product further confirmation of peak assignments can be made using integration values. Having an integration ratio of 0.89/0.23 for H1/H2 the ratio is consistent with the expected ratio of 3/1. H2 couples to a peak found at 4.24 ppm which represents H3. The coupling constants for H3 are found to be 6.7 Hz and 9.5 Hz have been determined indicating coupling with a methine proton and the olefinic proton respectively. The ratio of H2/H3, 0.23/0.32 falls close to the expected 1/1 ratio. H3 couples to a peak at 6.87 ppm representative of the H4 proton having coupling constants of 7.3 Hz and 15.7 Hz. The value of 7.3 Hz represents coupling to the methine proton H3. Although the value isn't exactly 9.5 Hz as expected it is near proximity and may be difficult to discern exactly due to overlap. The integration ratio of 0.32/0.27 for H3/H4 lies close to the expected ratio of 1/1 for these protons. Through the COSY it is seen that

H4 couples to a peak at 6.71 ppm which may assigned to H5. The coupling constant for H5 is 15.8 Hz which is consistent with the coupling constant found for H4. The integration ratio of H4/H5 is 0.27/0.23 which lies near the expected 1/1 ratio. These values have been summarized in Table 7.

Table 7: ^{1}H NMR Chemical Shifts, Coupling Constants, and Integration Values for the DA Endoperoxide Product

Postion	1H, δ (ppm)	J (Hz)	Integration
1	1.17	6.8	0.89
2	2.73	6.2	0.23
3	4.24	6.7, 9.5	0.32
4	6.87	7.3, 15.7	0.27
5	6.71	15.8	0.23

**Coupling constants and integration values for all peaks could not be determined due to overlap of peaks.*

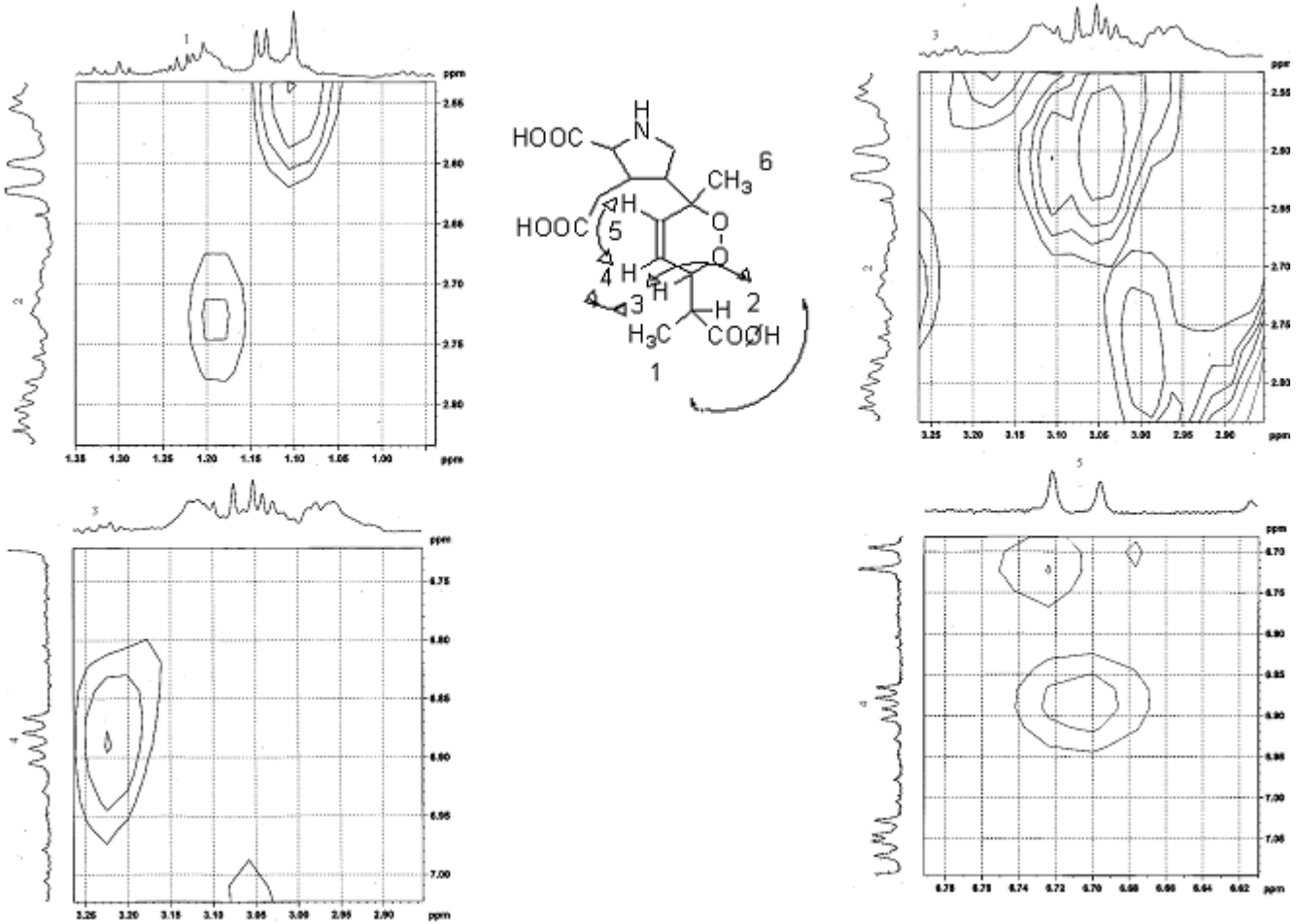

Figure 51 : COSY for DA Endoperoxide Product

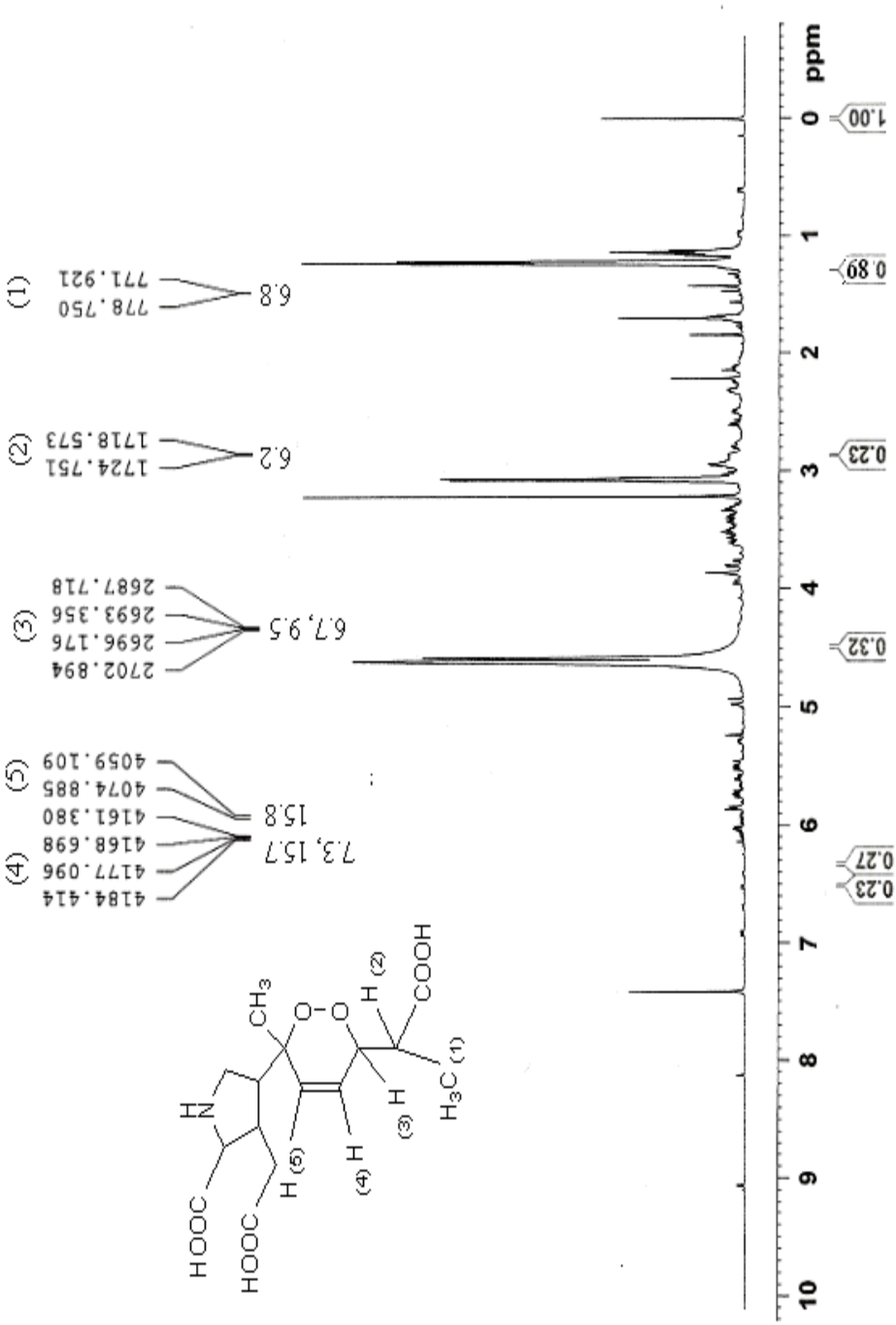

Figure 52: ^{1}H NMR of DA Endoperoxide Product

3.4 Conclusions

Based on my findings SA is confirmed to be a good model compound for studying photooxidation reactions between DA and singlet oxygen. The reactions between both DA and SA and singlet oxygen include the Diels-Alder reaction, the ene reaction and the 2 + 2 addition. In the case of the Diels-Alder an endoperoxide product is produced which is the major product in the case of SA but is only the second major product during photooxidation of DA. As for the ene reaction, the resulting hydroperoxide is the second major product for SA while is the leading product for DA. In both cases, the 2 + 2 addition products are minor constituents in the reaction mixture for both compounds. The difference in the quantity of the endoperoxide versus hydroperoxide product for DA and SA photooxidation may be due to the substitution in the conjugated diene moiety for both compounds. Possessing a greater electron density the trisubstituted olefin closer to the pyrrole ring is more likely to react with singlet oxygen than the olefin located further away from the ring thus giving an increased potential of occurrence of the ene reaction. However in the case of SA since both olefins are di-substituted the case of reaction seems equal despite the electron withdrawing acid group. In addition, the prominence of the ene product for the photooxidation of DA may also be due to rate of conformer production of DA versus SA. For SA the s-cis conformer may be produced at a higher rate than for DA due to the repulsion caused by the large pyrrole ring structure held by DA. Thus the Diels-Alder reaction seems more significant in SA than DA therefore leading to a greater production of the endoperoxide product in SA compared to DA.

3.5 Future Directions

To gain a better understanding of DA photooxidation HPLC will be employed to assess the formation of expected products at different reaction times. Such a method will allow for greater information on product confirmation. Once characterized, the products may be isolated by different chemical methods and the toxicity of the products tested using ELISA. Also for DA and SA the rate of photooxidation will be monitored using HPLC. The technique of HPLC may also prove fruitful for isolation of the SA hydroperoxide product so that it may be fully characterized. Other methods used to generate singlet oxygen such as TiO_2 photocatalysis may also be employed to compare the products found for photooxidation for both SA and DA. The research in this study offers many possible avenues that may be explored allowing one to gain greater insight on the topic of water treatment.

REFERENCES

Afanasev, I.; Afanas'ev, I. Superoxide Ion: Chemistry and Biological Implications, Volume 2. CRC Press, Boca Raton, **1991**, 232 pages.

Allen, W., **1934**. The Primary Food Supply of the Sea. *The Quaterly Review of Biology*, 9, 161-180.

Allen, W., **1936**. Occurrence of Marine Plankton Diatoms in a Ten Year Series of Daily Catches in Southern California. *Amer. J. of Biology*, 23, 60-63.

Anderson, D. "The Ecology and Oceanography of Harmful Algal Blooms." Brunn Memorial Lectures: Paris, **2005**.

Anderson, J; Whiting, M., **2003**. Total Synthesis of (±)-Kainic Acid with an Aza-[2,3]-Wittig Sigmatropic Rearrangement as the Key Stereochemical Determining Step. *J. Org. Chem*., 68 (16), 6160–6163.

Anslyn, E.; Dougherty, D. Modern Physical Organic Chemistry; University Science Books, **2006**, 1095 pages.

Avner, E.; Harmon, W.; Niaudet, P.; Yoshikawa, N. Pediatric Nephrology. Springer, **2009**, 2035 pages.

Backer, L.; McGillicuddy, D., **2006**. Harmful Algal Blooms at the Interface Between Coastal Oceanography and Human Health. *Oceangr.,* 19 (2), 94–106.

Balci, M. Basic 1H- and 13C-NMR Spectroscopy. Elsevier, **2005**, 430 pages.

Bandala , E.; Brito, L.; Pelaez, M., **2009**. Degradation of Domoic Acid Toxin by UV-Promoted Fenton-Like Processes in Seawater. *Desalination*, 245 (1–3), 135–145.

Bates, S. S., Garrison D. L., & Horner R. A., **1998**. Bloom Dynamics and Physiology of Domoic-Acid-Producing *Pseudonitzschia* Species. *Physiological Ecology of Harmful Algal Blooms*, 41, 267-292.

Beani, L.; Bianchi, C.; Guerrini, F.; Marani, L.; Pistocchi, R.; Tomasini, M.; Ceredi, A.; Milandri, A.; Poletti, R.; Boni, L., **2000**. High Sensitivity Bioassay of Paralytic (PSP) and Amnesic (ASP) Algal Toxins Based on the Fluorimetric Detection of $Ca2^{+}$ in Rat Cortical Primary Cultures. *Toxicon*., 38, 1283−1297.

Bell, A., **2003**. Nonprotein Amino Acids of Plants: Significance in Medicine Nutrition, and Agriculture. *J. Agric. Food Chem*., 51 (10), 2854–2865.

Beltran A.; Palafox-Uribe M.; Grajales-Montiel, J.; Cruz-Villacorta, A.; Ochoa, J., **1997**. Sea Bird Mortality at Cabo San Lucas, Mexico: Evidence That Toxic Diatom Blooms Are Spreading. *Toxicon*., 35, 447–553.

Berman, F.; Murray, T., **1997**. Domoic Acid Neurotoxicity in Cultured Cerebellar Granule Neurons is Mediated Predominantly by NMDA Receptors That Are Activated as a Consequence of Excitatory Amino Acid Release. *J. Neurochem*., 69, 693−703.

Botana, L. "Seafood and Freshwater Toxins: Pharmacology, Physiology, and Detection." CRC Press, **2008**.

Bouillon, R.; Kieber, R.; Skrabal, T.; Wright, J., **2008**. Photochemistry and Identification of Photodegradation Products of the Marine Toxin Domoic Acid. *Marine Chemistry*, 110 (1-2), 18-27.

Bouillon, R.; Knierim, T.; Kieber, R.; Skrabal, S.; Wright, J., **2006**. Photodegradation of the Algal Toxin Domoic Acid in Natural Water Matrices. *Limnol. Oceanogr*., 51, 321–330.

Brand, L.; Sunda, W.; Guillard, R.,**1986**. Reduction of Marine Phytoplankton Reproduction Rates by Copper and Cadmium. *J. of Experimental Marine Biology and Ecology*, 96, (3), 225-50.

Burlage, R. Principles of Public Health Microbiology. Jones & Bartlett Publishers, **2011**, 417 pages.

Burns, J.; Schock, T.; Hsia, T.; Moeller, P.; Ferry, J., **2007**. Photostability of Kainic Acid in Seawater. *J. Agric. Food Chem*., 55 (24), 9951–9955.

Calzavara-Pinton, P.; Szeimies, R.; Ortel, B. Photodynamic Therapy and Fluorescence Diagnosis in Dermatology. Elsevier, **2001**, 372 pages.

Chandler, D., **1940** Limnological Studies of Western Lake Erie III. Phytoplankton and Physical-Chemical Data from Novermber, 1939 to November, 1940. *Ohio J. Sci*., 42, 291-336.

Chen, Y.; Tang, X.; Zhan, L. "Advances in Environmental Geotechnics: Proceedings of the International Symposium on Geoenvironmental Engineering in Hangzhou, China 2009." **2010**, 964 pages.

Cholnoky, B. Die Okologie der Diatomeen in Binnengewassern. Cramer-Lehre. **1968**, 699 pages.

Cigic, K.; Plavec, J.; Smole Možina, S.; Zupančič-Kralj L., **2001**. Characterisation of Sorbate Geometrical Isomers. *J. of Chromatography A*, 905, (1–2, 5), 359–366.

Clayden, J.; Read, B.; Hebditch, K., **2005**. Chemistry of Domoic Acid, Isodomoic Acids, and Their Analogues. *Tetrahedron*., 61 (24), 5713–5724.

Combes, R.D., **2003**. The Mouse Bioassay for Diarrhetic Shellfish Poisoning: a Gross Misuse of Laboratory Animals and of Scientific Methodology. *Altern. Lab. Anim.,* 31*,* 595-610.

Conley, D.; Paerl, H.; Howarth, R.; Boesch, D.; Seitzinger, S.; Havens, K.; Lancelot, C.; Likens, G., **2009**. Controlling Eutrophication: Nitrogen and Phosphorus. *Science,* 323 (5917), 1014-1015.

Dai, P.; Dussault, P. H.; Trullinger, T. K., **2004**. Magnesium/Methanol: An Effective Reducing Agent for Peroxides and Ozonides *J. Org. Chem., 69*, 2851.

Davidson, P.; Sofos, J.; Branen, A. Antimicrobials in Food. CRC Press, Boca Raton, **2005**, 706 pages.

DeRosa, M.; Crutchley, R., **2002**. Photosensitized Singlet Oxygen and its Applications. *Coordination Chemistry Reviews*, 233-234, 351-371.

Dewick, P. Essentials of Organic Chemistry: For Students of Pharmacy, Medicinal Chemistry and Biological Chemistry. John Wiley & Sons: England, **2006**, 710 pages.

Djaoued, Y.; Thibodeau, M.; Robichaud, J.; Balaji, S.;Priya, S.; Tchoukanova, Bates, S., **2008**. Photocatalytic Degradation of Domoic Acid using Nanocrystalline TiO_2 Thin Films. *J. Photochemistry and Photobiology A: Chem*., 193 (2–3), 271–283.

Drago, R., **1977**. Synthesis of Sesquiterpene Antitumor Lactones I a Facile Synthesis of Cis-Fused-a-Ring in Vernolepin and Vernomenin. *Tetrahedron Lett*., 18 (8), 703–706.

Duxbury, M., **2000**. Liquid Chromatographic Determination of Amnesic Shellfish Poison in Mussels. *Journal of Chemical Education*, 77, 1319-1320.

Egmond, H.; van Apeldoorn, M.; Speijers, G. Marine Biotoxins: Issue 80. Food and Agriculture Organization of the United Nations, **2004**, 278 pages.

Falk, M.; Ping, S.; Walter J., **1991**. Solubility of Domoic Acid in Water and in Non-Aqueous Solvents. *An. J. Chem*., 69, 1740-1744.

Falkowski, P.; Knoll, A. Producers in the Sea. Eds Boston, Elsevier, 37-53.

Fennema, O. Food Chemistry. CRC Press, **1996**, 1069 pages.

Fisher; Malone; Giattina. "Coastal Monitoring Through Partnerships." Kluwer Academic Publishers: Netherlands, **2002**.

Fisher, J., Reese, J.; Pellechia, P.; Moeller, P.; Ferry, J., **2006**. Role of Fe(III), Phosphate, Dissolved Organic Matter, and Nitrate During the Photodegradation of Domoic Acid in the Marine Environment. *Environ. Sci. Technol*., 40, 2200–2205.

Fox, M.; Whitesell, J. Organic Chemistry: Third Edition. Jones & Bartlett Learning: Canada, **2004**, 1140 pages.

Fritz, L.; Quilliam, M..; Wright, J.; Beale, A;Work, T., **1992**. An Outbreak of Domoic Acid Poisoning Attributed to the Pennate Diatom *Pseudonitzschia Australis*. *J. Phycol*. 28, 439-442.

Garthwaite I.; Ross K.; Miles C.; Hansen R.; Foster, D.; Wilkins, A.; Towers N., 1998. Polyclonal Antibodies to Domoic Acid, and Their Use in Immunoassays for Domoic Acid in Sea Water and Shellfish. *Nat. Toxins*, 6, 93-104.

Glibert, P.; Anderson, D.; Gentien, P.; Graneli, E.; Sellner, K., **2005**. The Global, Complex Phenomena of Harmful Algal Blooms. *Oceanography*,18 (2), 136-147.

Giordano, G.; White, C.; McConnachie, L.; Fernandez, C.; Kavanagh, T.; Costa, L., **2006**. Neurotoxicity of Domoic Acid in Cerebellar Granule Neurons in a Genetic Model of Glutathione Deficiency. *Mol. Pharmacol*., 70, 2116–2126.

Giordano, G.; White, C.; Mohar, I.; Kavanagh, T.; Costa, L., **2007**. Glutathione Levels Modulate Domoic Acid-Induced Apoptosis in Mouse Cerebellar Granule Cells. *Toxicol. Sci*., 100, 433–444.

Graham, P. Instant Notes Organic Chemistry. Garland Science: Abingdon, **2004**, 357 pages.

Graneli, E.; Sakshaug, E.; Pallon, J.; Luckas, B.; Martinez, R.; Maestrini, S. , **2000.** Effect of Nutrient Ratios on Harmful Phytoplankton and Their Toxin Production Sea: NUTOX. *EurOCEAN 2000*, 1, 76-81.

Graneli, E.; Turner, T. Ecology of Harmful Algae. Springer, Ed. **2006**, 413 pages.

Graneli, E.; Turner, T. Ecology of Harmful Algae. Springer, Ed. **2007**, 416 pages.

Grebel J.; Pignatello, J.; Mitch, W., **2011**. Sorbic Acid as a Quantitative Probe for the Formation, Scavenging and Steady-State Concentrations of the Triplet-Excited State of Organic Compounds. *Water Research*, 45 (19), 6535–6544.

Gregory, E., **1892**. What are Diatoms? *Popular Sci*., 41 (13), 200-205.

Grove, A.; Weisleder, D., **1973**. Hydrolysis Products of 4-Acetamido-4-hydroxy-2-butenoic Acid y-Lactone. *J. Org. Chem*., 38 (4), 815- 816.

Gulland, F. "Domoic Acid Toxicity in California Sea Lions Stranded Along the Central California Coast, May–October 1998." U.S.Department of Commerce, **1999**.

Hampson, D.; Huang, X.; Wells, J.; Walter, J.; Wright, J., **1992**. Interaction of Domoic Acid and Several Derivatives with Kainic Acid and AMPA Binding Sites in Rat Brain. Euro. *J. Pharmacol*., 218, 1–8.

Hart, H.; Hart, D.; Craine, L.; Hadad, C. Organic Chemistry: A Short Course. Brooks Cole/ Cengage Learning: Belmont, **2011**, 608 pages.

Hasle, G.; Syvertsen E. Identifying Marine Phytoplankton. Academic Press, **1997**, 5-385.

He, Y; Fekete, A.; Chen, G; Harir, M.; Zhang, L.; Tong, P.; Schmitt-Kopplin, P., **2010**. Analytical Approaches for an Important Shellfish Poisoning Agent: Domoic Acid. *J. Agric. Food Chem*., 58 (22), 11525–11533.

Hedges, B.; Kumar, S. The Timetree of Life. Oxford University Press, **2009**, 572 pages.

Hesp, B.; Harrison, J.; Selwood, A.; Holland, P.; Kerr, P., **2005**. Detection of Domoic Acid in Rat Serum and Brain by Direct Competitive Enzyme-Linked Immunosorbent Assay (cELISA). *Anal. and Bioanalytical Chem*., 383 (5), 783-786.

Hess, P.; Gallacher, S.; Bates, L. A.; Brown, N.; Quilliam, M., **2001**. Determination and Confirmation of the Amnesic Shellfish Poisoning Toxin, Domoic Acid, in Shellfish from Scotland by Liquid Chromatography and Mass Spectrometry. *J. AOAC Int*., 84 (5) 1657– 1667.

Holland, P. Seafood and Freshwater Toxins Pharmacology, Physiology, and Detection, Second Edition. CRC Press, **2008**, 21–49.

Holland, P.; McNabb, P.; Rhodes, L.; Selwood, A.; Neil, T. "Amnesic Shellfish Poisoning Toxins in New Zealand Shellfish: Detection of an Unusual Domoic Acid Isomer Using a Newly Validated LC-MS/MS Method". Xanta de Galicia and IOC of UNESCO, **2004**, 29-42.

Horner, R. A., Hanson, L., Hatfield, C. L. & Newton, J. A. Domoic acid in Hood Canal, Washington, USA. Harmful and Toxic Algal Blooms. Intergovernmental Oceanographic Commission of UNESCO, **1996**, 127–129.

Hornsey, I. The Chemistry and Biology of Winemaking. Royal Society of Chemistry: England, **2007**, 457 pages.

Houdy, P.; Lahmani, M.; Marano, F. Nanoethics and Nanotoxicology. Springer, **2011**, 620 pages.

Isobe, M.; Iio, H.; Kawai, T.; Goto, T., **1977**. Synthesis of Sesquiterpene Antitumor Lactones I a Facile Synthesis of Cis-Fused-a-Ring in Vernolepin and Vernomenin. *Tetrahedron Lett*., 18, (8), 703–706.

John, D. The Freshwater Algal Flora of the British Isles: An Identification Guide to Freshwater and Terrestrial Algae. Cambridge University Press, **2002**, 714 pages.

Jones, K.; Cooper, W.; Mezyk, S., **2009**. Bimolecular Rate Constant Determination for the Reaction of Hydroxyl Radicals with Domoic and Kainic Acid in Aqueous Solution. *Environ. Sci. Technol*., 43 (17), 6764–6768.

Kadish, K.; Smith, K.; Guilard, R. The Porphyrin Handbook: Applications of Phthalocyanines, Volume 19. Elsevier, **2003**.

Kalluri, S. A Web-based Modeling Approach for Tracking Algal Blooms in Lower Great Lakes. Springer, **2007**, 416 pages.

Keller, L.; Lichter, J.; San Miguel, L. Laboratory Manual Organic Chemistry I & II. Hayden McNeil, **2010**.

Kleivdal, H.; Kristiansen, S.; Nilsen, M.; Briggs, L., **2007**. Single-Laboratory Validation of the Biosense Direct Competitive Enzyme-Linked Immunosorbent Assay (ELISA) for Determination of Domoic Acid Toxins in Shellfish. *J. of AOAC Int.*, 90 (4), 1000-1010.

Kohn, T.; Nelson, K., **2007**. Article Sunlight-Mediated Inactivation of MS2 Coliphage via Exogenous Singlet Oxygen Produced by Sensitizers in Natural Waters. *Environ. Sci. Technol*., 41 (1) 192–197.

Kondo, T.; Matsumoto, M.; Tanimoto, M., **1978**. Microwave and NMR Studies of the Structure and the Conformational Isomerization of 3,6-dihydro-1,2-dioxin. *Tetrahedron Lett.*, 19 (40), 3819–3822.

Kotaki, Y.; Koike, K.; Sato, S.; Ogata, T.; Fukuyo, Y.; Kodama, M.., **1996**. Confirmation of Domoic Acid Production of *Pseudonitzschia multiseries* Isolated from Ofunato Bay, Japan. *Toxicon.,* 37 (4), 677–682.

Kruk, I. Environmental Toxicology and Chemistry of Oxygen Species: The Handbook of Environmental Chemistry. Springer, **1998**, 277 pages.

Kürti, L.; Czakó, B. Strategic Applications of Named Reactions in Organic Synthesis: Background and Detailed Mechanisms. Focal Press, **2005**, 758 pages.

Lamberts, J.; Schumacher, D.; Neckers, D., **1984**. Novel Rose Bengal Derivatives: Synthesis and Quantum Yield Studies. *J. Am. Chem. Soc*., 106, 5879-5883.

Lawrence, J.; Menard, C., **1991**. Confirmation of Domoic Acid in Shellfish Using Butyl Isothiocyanate and Reversed-Phase Liquid Chromatography. *J. Chromatogr. A*, 550 (1-2), 595-601.

Lefebvre, K.; Bargu, S.; Kieckhefer, T.; Silver, M, **2002**. From Sanddabs to Blue Whales: the Pervasiveness of Domoic Acid. *Toxicon*., 40, 971–977.

Lefebvre, K.; Powell, C.; Busman, M.; Doucette, G.; Moeller, P.; Silver, J.; Miller, P.; Hughes, J.; Singaram, S.; Silver M.; Tjeerdema, R., **1999**. Detection of Domoic Acid in Northern Anchovies and California Sea Lions Associated with an Unusual Mortality Event. *Natural Toxins*, 7, 85–92.

Lowe, R. Environmental Requirements and Pollution Tolerance of Freshwater Diatoms. Envir. Prot. Agency, EPA-670/4-74-005. **1974**, 334 pages.

Luck E., **1990**. Food Applications of Sorbic Acid and its Salts. *Food Additives and Contaminants,* 7(5), 711-715.

Lundholm, N., & Moestrup, O., **2002**. The Marine Diatom *Pseudonitzschia Galaxiae* sp. nov. (*Bacillariophyceae*): Morphology and Phylogenetic Relationships. *Phycologia*., 41, 594-605.

Lundholm, N.; Moestrup, O.; Hasle G.; Hoef-Emden, K., **2003**. A Study of the *Pseudo-nitzschia pseudodelicatissima/cuspidata* Complex (*Bacillariophyceae*): What is P. pseudodelicatissima?. *Journal of Phycology*., 39, 797-813.

Macomber, R. Organic Chemistry, Volume 2. University Science Books: Sausilito, **1996**, 410 pages.

Maga, J.; Tu, A. Food Additive Toxicology. CRC Press, **1994**, 552 pages.

Matysik, J.; Bhalu, A.; Mohanty, P., **2002**. Molecular Mechanisms of Quenching of Reactive Oxygen Species by Proline Under Stress in Plants. *Curr. Sci*., 82, 525–532.

Maucher, J.; Ramsdell, J., **2005**. Ultrasensitive Detection of Domoic Acid in Mouse Blood by Competitive ELISA Using Blood Collection Cards. *Toxicon.*, 45 (5), 607–613.

McLellan, W.; Moeller, P.; Powell, C.; Rowles, T.; Silvagni, P.; Silver, M.; Spraker, T.; Trainer, V., **2000**. Mortality of Sea Lions Along the Central California Coast Linked to a Toxic Diatom Bloom. *Nature*, 403, 80–84.

McMurray, J. Organic Chemistry, Volume 1. Cengage Learning: Canada, **2009**, 546 pages.

Melzian, B.; Engle, V.; McAlister, M.; Sandhu, S. Coastal Monitoring Through Partnerships. **2003**, 420 pages.

Mendeleyev, D.; Kamensky, G.; Lawson, T. The Principles of Chemistry, Volume 4. American Home Library: New York, **1902**.

Metin, B. Basic 1H and 13C-NMR Spectroscopy. Elsevier, **2005**, 427 pages.

Miguez, A.; Fernandez, M. L.; Fraga, S. "First Detection of Domoic Acid in *Galicia* (NW Spain)". *UNESCO: Paris, France*, **1996**; 143− 145.

Millar, J.; Haynes, K. Chemical Methods. Kluwer Academic Publishers: Norwell, **1998**, 390 pages.

Mok, J.; Lee, T.; Oh, E.; Son, K.; Hwang, H.; Kim, J., **2009**. Stability of Domoic Acid at Different Temperature, pH and Light. *J. of the Korean Fisheries Soc*., .42 (1), 8-14.

Morse, H. Exercises in Quantitative Chemistry. Ginn and Company: Boston, **1905**, 556 pages.

Mos, L., **2001.** Domoic Acid: A Fascinating Marine Toxin. *Environ. Toxicol. Pharmacol.,* 9, 79−85.

Naidu, A. Natural Food Antimicrobial Systems. CRC Press: Boca Raton, **2000**, 818 pages.

National Research Council. "Clean Coastal Waters: Understanding and Reducing the Effects of Nutrient Pollution." National Academy Press: Washington, DC, **2000.**

Neckers, D.C.; Blossey, E.C.; Schaap, A. P. U.S. Patent 4 315998.

Neckers, D.; Gupta, S., **1987**. Spectral Properties of Rose Bengal Derivatives in Polar and Nonpolar Solvents. *J. Org. Chem*., 52 (5), 936-938.

Nemoto, K.; Kubo, T.; Nomachi, M.; Sano, T.; Matsumoto, T.; Hosoya, K.; Hattori, T; Kaya, K., **2007**. Simple and Effective 3D Recognition of Domoic Acid Using a Molecularly Imprinted Polymer. *J. Am. Chem. Soc*., 129 (44), 3626–3632.

Nyokong, T.; Ahsen, V. Photosensitizers in Medicine, Environment, and Security. Springer, **2012**, 662 pages.

Olah, G.; Molnár, A. Hydrocarbon Chemistry. John Wiley & Sons: Hoboken, **2003**, 871 pages.

O'Shea, K.; Foote, C., **1988**. Quantitative Rearrangement of Monocyclic Endoperoxides to Furans Catalyzed by Co(II). *J. Org. Chem*., 54, 3475.

Paczkowski, J.; Neckers, D., **1985**. Photochemical Properties of Rose Bengal. 11. Fundamental Studies in Heterogeneous Energy Transfer. *Macromolecules,* 18 (12), 2412-2418.

Paerl, H.; Scott, J., **2010**. Throwing Fuel on the Fire: Synergistic Effects of Excessive Nitrogen Inputs and Global Warmingon Harmful Algal Blooms. *Environ. Sci. Technol.,* 44, 7756–7758.

Pande, N. "Interactions Between the Toxic Alga, Alexandrium Fundyense, and Its Bacterial Associates: Stimulation, Inhibition, and Specificity of Bacterial Effects on Alexandrium Growth." ProQuest, **2008**, 67 pages.

Patrick, G. Instant Notes on Organic Chemistry. Taylor & Francis, **2004**, 328 pages.

Pattenden, G. General and Synthetic Methods. Royal Society of Chemistry: England, **1980**, 396 pages.

Pavia, D.; Lampman, G.; Kriz, G. Introduction to Spectrscopy: Third Edition. Brooks Cole: United States, **2001**.

Pawley, J. Handbook of Biological Confocal Microscopy. Springer: Madison, **2006**, 985 pages.

Pearson, A.; Gillett, T. Processed Meats. Springer: New York, **1996**, 448 pages.

Pennock, J.; Greene, R.; Fisher, W.; Villarea, T.; Simons, J.; Dortch, Q.; Moncreiff, C.; Steidinger, K.; Ors, T.; Stumpf, R.; Gallegos, S. "HABSOS An Integrated Case Study for the Gulf of Mexico Final Report July 2004." USEPA: Gulf of Mexico, **2004**.

Prisholm, K., Moestrup, O .;Lundholm N., **2002**. Taxonomic Notes on the Marine Diatom Genus Pseudonitzschia in the Andaman Sea Near the Island of Phuket, Thailand, with a Description of Pseudonitzschia Micropora sp. nov. *Diatom Research*, 17, 153-175.

Puschner, B.; Tor, E.; St. Leger, J.; Millar, M.; Jessup, D.; Whitehead, W. 2002 Annual Report: California Animal Health & Food Safety Laboratory System. Univ. of Ca, Davis, **2002**, 62 pages.

Quillam, M..; Wright, J., **1989**. The Amnesic Shellfish Poisoning Mystery. *Anal Chem.,* 61, 1053-1060.

Ramamurthy, V.; Schanze, K. Understanding and Manipulating Excited-State Processes. CRC Press, Boca Raton, **2001**, 757 pages.

Ramsdell, J.; Zabka, T., **2008**. In Utero Domoic Acid Toxicity: A Fetal Basis to Adult Disease in the California Sea Lion (*Zalophus californianus*). *Mar Drugs*, 6, 262–290.

Rappoport, Z. The Chemistry of Peroxides, Volume 2. John Wiley & Sons, **2007**, 1518 pages.

Rhodes, C. Toxicology of the Human Environment: The Critical Role of Free Radicals. CRC Press, **2000**, 494 pages.

Rhodes, L.; White, D.; Syhrb, M.; Atinkson, M. Pseudonitzschia Species Isolated from New Zealand Coastal Waters: Domoic Acid Production in vitro and Links with Shellfish Toxicity, Intcrgov. Oceanogr. Comm UNESCO, **1996**, 155-158.

Round, F. The Ecology of Algae. Press Syndicate of the University of Cambridge: Great Britain, **1984**, 664 pages.

Round, F.; Crawford, R.; Mann, D. Diatoms: Biology and Morphology of the Genera. Cambridge University Press, **1990**, 758 pages

Rue, E.; Bruland, K., **2001**. Domoic Acid Binds Iron and Copper: A Possible Role for the Toxin Produced by the Marine Diatom *Pseudonitzschia*. *Mar. Chem.,* 76, 127-134.

Sauer, U., **2005**. Animal vs. Non-Animal Tests for the Monitoring of Marine Biotoxins in the E.U. *ALTEX*, 22, 19.

Sawant, P.; Tyndall, J.; Holland, P.; Peake, B.; Mountfort, D.; Kerr, D., **2010**. In vivo Seizure Induction and Affinity Studies of Domoic Acid and Isodomoic Acids-D, -E and –F. *Neuropharmacology*, 59 (3), 129–138.

Scallet , A.; Schmued, L.; Johannessen, J, **2005**. Neurohistochemical Biomarkers of the Marine Neurotoxicant, Domoic Acid. *Neurotoxicology and Teratology,* 27, 745–752.

Scharf, H.; Janus, J. **1978**. Preparation of Fumaraldehydic Acid and Some of its Derivatives. *Chemische Berichte*, 111 (7), 2741–2744.

Schiaffo, C.; Dussault, P., **2008**. Ozonolysis in Solvent Water Mixtures: Direct Conversion of Alkenes to Aldehydes and Ketones. *J. Org. Chem*., 73, 4688-4690.

Schmidt, T.; Schaechter, M. Topics in Ecological and Environmental Microbiology. Academic Press, **2011**, 480 pages.

Scholin, C.; Gulland, F., **2000**. Mortality of Sea Lions Along the Central California Coast Linked to a Toxic Diatom Bloom. *Nature*, 403, 80-84.

Seckbach, J.; Kociolek, P. The Diatom World. Springer, **2011**, 534 pages.

Sigma-Aldrich. 2012. Sigma-Aldrich Co. LLC. 15 Jan. **2012.** <http://www.sigmaaldrich.com/united-states.html>.

Silvagni P.; Lowenstine, L.; Spraker, T.; Lipscomb, T.; Gulland, F., **2005**. Pathology of Domoic Acid Toxicity in California Sea Lions (*Zalophus californianus*). *Vet Pathol*., 42, 184–191.

Silverstein, R. Spectrometric Identification of Organic Compounds, 7th Edition. John Wiley and Sons Ltd, **2001**, 512 pages.

Sims, D. Advances In Marine Biology, Volume 56. Academic Press: London, **2009**, 408 pages.

Smayda, T., **1997**. What is a Bloom? A Commentary. *Limnol. Oceangr.,* 42, 1132-1136.

Smith, D.; Kitts, D., **1994**. A Competitive Enzyme-Linked Immunoassay for Domoic Acid Determination in Human Body Fluids. *Food and Chemical Tox.*, 32 (12), 1147–1154.

Smith, D.; Kitts, D., **1995**. Enzyme Immunoassay for the Determination of Domoic Acid in Mussel Extracts. *J. Agric. Food Chem*., 43, 367-371.

Smol, J.; Stoermer, E. The Diatoms: Applications for the Environmental and Earth Sciences. Cambridge University Press, **2010**, 686 pages.

Soderberg, T. Organic Chemistry with a Biological Emphasis. Lulu, **2012**.

Soumya, J.; Sekhar, K.; Mandal N., Kanagaraj M., **2012**. Marine Toxicity and its Implications on Human Health. *International Res. J. of Pharmacy,* 3 (3), 39-42.

Stewart, J.; Marks, L.; Gilgan, M.; Pfeifer, E.; Zwicker, B., **1998**. Microbial Utilization of the Neurotoxin Domoic Acid: Blue Mussels (*Mytilus edulis*) and Soft Shell Clams (*Mya arenaria*) as Sources of the Microorganisms. *Can. J. Microbiol*., 44, 456–464.

Stoermer, E.; Julius, M. "Centric Diatoms". Academic Press, **2003**. 918 pages

Sugiura, Y.; Tanaka, H., **1981**. Structure, Properties, and Transport Mechanism of Iron (III) Complex of Mugineic Acid, a Possible Phytosiderophore. *J. Am. Chem. Soc*., 103, 6979-6982.

Summer, A.; Dindal, A.; Wilenberg, Z.; Riggs, K.; Smith, W.; Wood, K. "Environmental Technology Verification Report." Battelle: Ohio, **2005**.

Sun, J.; Hutchins, D.; Feng, Y.; Seubert, E.; Caron, D.; Fu, F., **2011**. Effects of Changing pCO2 and Phosphate Availability on Domoic Acid Production and Physiology of the Marine Harmful Bloom Diatom *Pseudonitzschia Multiseries*. *Limnol*. *Oceanogr.*, 56 (3), 829–840.

Sun, T.; Wong, W., **1999**. Determination of Domoic Acid in Phytoplankton by High-Performance Liquid Chromatography of the 6-Aminoquinolyl-N-hydroxysuccinimidyl Carbamate Derivative. *J. Agric. Food Chem*., 47 (11), 4678-4681.

Takagi, S. Production of Phytosiderophores in Iron Chelation in Plants and Soil Microorganisms. Academic Press: California, **1993**.

Teitelbaum, J.; Zatorre, R.; Carpenter, S.; Gendron, D.; Evans, A.; Gjedde, A.; Cashman, N., **1990**. Neurologic Sequelae of Domoic Acid Intoxication Due to Ingestion of Contaminated Mussels, New Engl. *J. Med*., 322, 1781–1787.

The Committee on Environmental and Natural Resources (CENR). "Integrated Assessment of Hypoxia in the Northern Gulf of Mexico." NSTC & CENR, **2000**.

Thessen, A.; Stoecker D., **2008**. Distribution, Abundance and Domoic Acid Analysis of the Toxic Diatom Genus *Pseudonitzschia* from the Chesapeake Bay. *Estuaries and Coasts*, 31, 664-672.

Tiedeken J.; Ramsdell, J., **2010**. Zebrafish Seizure Model Identifies p,p'- DDE as the Dominant Contaminant of Fetal California Sea Lions That Accounts for Synergistic Activity With Domoic Acid. *Environ Health Perspect.,* 118, 545–551.

Todd, E., **1993**. Domoic Acid and Amnesic Shellfish Poisoning: A Review. *Journal of Food Protection*, 56(1), 69-83.

Tomas, C. Identifying Marine Phytoplankton. Academic Press, **1997**, 858 pages.

Tor, E.; Puschner, B.;Whitehead, W., **2003**. Rapid Determination of Domoic Acid in Serum and Urine by Liquid Chromatography−Electrospray Tandem Mass Spectrometry. *J. Agric. Food Chem*., 51 (7), 1791–1796.

Truelove, J.; Iverson, F., **1994**. Serum Domoic Acid Clearance and Clinical Observations in the Cynomolgus Monkey and Sprague-Dawley Rat Following a Single IV Dose. Contam. *Toxicol.,* 52, 479-486.

Tsao, Z.; Liao, Y.; Liu, B.; Su, B.; Yu, F., **2007**. Development of a Monoclonal Antibody against Domoic Acid and Its Application in Enzyme-Linked Immunosorbent Assay and Colloidal Gold Immunostrip. *J. Agric. Food Chem.*, *55* (13), 4921–4927.

Vale P., Sampayo M., Quilliam M. DSP Complex Toxin Profiles Relation with spp. Occurrence and Domoic Acid Confirmation by LC-MS in Portuguese Bivalves. Xunta de Galicia and Intergovernmental Oceanographic Commission of UNESCO, **1998**, 503-506.

Van Dolah, F.; Leighfield, T.; Haynes, B.; Hampson, D.; Ramsdell, J., **1997**. A Microplate Receptor Assay for the Amnesic Shellfish Poisoning Toxin, Domoic Acid, Utilizing a Cloned Glutamate Receptor. *Anal. Biochem*., 245, 102−105.

Vosmaer, A. Ozone, its Manufacture, Properties and Uses. D. Van Nostrand Co.: New York, **1916**, 197 pages.

Wainwright, M. Photosensitisers in Biomedicine. John Wiley and Sons: England, **2009**, 288 pages.

Waldron, K.; Jianjun, L., **1996**. Investigation of a Pulsed-Laser Thermo-Optical Absorbance Detector for the Determination of Food Preservatives Separated by Capillary Electrophoresis. *J Chromatogr B Biomed Appl.,* 683(1), 47-54.

Wang, Z.; King, K.; Ramsdell, J.; Doucette, G., **2007**. Determination of Domoic Acid in Seawater and Phytoplankton by Liquid Chromatography-Tandem Mass Spectrometry. *J Chromatogr. A*, 1163 (1-2), 169-176.

Wells, M.; Trick, C.; Cochlan, W.; Hughes, M.; Trainer, V., **2005**. Domoic Acid: The Synergy of Iron, Copper, and the Toxicity of Diatoms. *Limnol. and Oceanogr*., 50, 1908-1917.

Whitaker, M. Calcium in Living Cells. Academic Press: Burlington, **2010**, 316 pages.

Wilson, I.; Adlard, E.; Cooke, M.; Poole, C. Encyclopedia of Separation Science, Volume 7. Academic Press, **2000**, 4954 pages.

Wilson, W.; Heitz, J., **1984**. Oxygen Consumption during Photobleaching of Aqueous Solutions of Rose Bengal. *J. Agric. Food Chem*., 32, 615-617.

Wong, J.; Lee, H.; Harrison, P., **2009**. Forecasting of Environmental Risk Maps of Coastal Algal Blooms. *Harmful Algae*, 8 (3), 407–420.

Work, T.; Barr, B.; Beale, A.; Fritz, L., **1993**. Epidemiology of Domoic Acid Poisoning in Brown Pelicans (*Pelecanus Occidentalis*) and Brandt's Cormorants (*Phalacrocorax penicillatus*) in California. *J. Zoo and Wildlife Medicine,* 24 (1), 54-62.

Wright, J., **1995**. Dealing with Seafood Toxins: Present Approaches and Future Options. *Food Research International*, 28, (4), 347–358.

Wright, J.; Boyd, R.; Defreitas, A.; Falk, M.; Foxall, R.; Jamieson, W.; Laycock, M.; Mc Mulloch, A.; Mc Innes, A.; Odense, P., Pathak, V.; Quilliam, M.; Ragen.; Sim P.; Thibault, P.;Walter J.; Gilgan, M.; Richard, D.; Dewar D., **1989**. Identification of Domoic Acid, a Neuroexcitatory Amino Acid, in Toxic Mussels from Eastern P.E.I. *Harmful Algae Nitzschia pungens Can. J. Fish. Aquat. Sci.,* 67, 481-490.

Wright, J, Falk, M.; McInnes, A.; Walter, J., **1990**. Identification of Isodomoic acid D and Two New Geometrical Isomers of Domoic Acid in Toxic Mussels. *Can. J. Chem*., 68, 22–25.

Wright, J.; Quilliam, M., Methods for Domoic Acid, the Amnesic Shellfish Poisoning (ASP) Toxin. In Manual on Harmful Marine Microalgae. UNESCO: Paris, France, **1995**, 115− 135.

Xiang, T.; Anderson, B., **1998**. Influence of Chain Ordering on the Selectivity of Dipalmitoylphosphatidylcholine Bilayer Membranes for Permanent Size and Shape. *Biophysical J*., 75 (6), 2658-267.

Yu, F.; Liu, B.; Wu, T.; Chi, T.; Su, M., **2004**. Development of a Sensitive Enzyme-Linked Immunosorbent Assay for the Determination of Domoic Acid in Shellfish. *J. Agric. Food Chem*., 52 (17), 5334–5339.

Zhao, J.; Thibault, P.; Quilliam, M., **1997**. Analysis of Domoic Acid and Isomers in ‘Seafood by Capillary Electrophoresis. *Electrophoresis*, 18, 268-216.